MICROGEL BASED MATERIALS FOR CONTROLLED MACROMOLECULE DELIVERY

A Thesis
Presented to
The Academic Faculty

by

Christine M. Nolan

In Partial Fulfillment
of the Requirements for the Degree
Doctor of Philosophy in the
School of Chemistry and Biochemistry

Georgia Institute of Technology
February 2005

MICROGEL BASED MATERIALS FOR
CONTROLLED MACROMOLECULE DELIVERY

Approved by:

Dr. L. Andrew Lyon, Advisor
School of Chemistry and Biochemistry
Georgia Institute of Technology

Dr. Boris Mizaikoff
School of Chemistry and Biochemistry
Georgia Institute of Technology

Dr. Mostafa El-Sayed
School of Chemistry and Biochemistry
Georgia Institute of Technology

Dr. Lawrence Bottomley
School of Chemistry and Biochemistry
Georgia Institute of Technology

Dr. Haskell Beckham
School of Polymer, Textile and Fiber Engineering
Georgia Institute of Technology

February 25, 2005

ACKNOWLEDGEMENTS

First, I would like to sincerely thank my advisor, Dr. L. Andrew Lyon, for taking me into his research group and giving me a chance to work in his laboratory. He took a chance on me by letting me join his group so late in my Ph. D. career. I am extremely grateful to have had the fortunate opportunity to participate in such interesting and rewarding science. He was always passionate and enthusiastic about his research projects, was very open to new ideas and showed me how exciting research can be. Next, I would like to thank my parents and siblings for all of their love and support. I would especially like to thank my father for always telling me, ever since I was a little girl that I could be anything I wanted to be. That has instilled me with a sense of confidence that has brought me to where I am today. I would also like to thank all of the Lyon group members (present and past) for all of their help, ideas and collaborations. Finally, I would like to thank all of my dear friends (Eva, Tiffany, Catrena, Caroline, Ashlee, Stella, Jon, Victor, Amy Jill and Maritza) for all of their love and support, without which I would be lost.

TABLE OF CONTENTS

LIST OF TABLES

LIST OF FIGURES

LIST OF ABBREVIATIONS

AAc	Acrylic Acid
APS	Ammonium Persulfate
APTMS	3-Aminopropyltrimethoxysilane
BIS	*N, N'*-Methylene(bisacrylamide)
Con-A	Concanavalin A
CPS	Counts Per Second
DCl	Deuterated Hydrochloric Acid
DLS	Dynamic Light Scattering
DNA	Deoxyribose Nucleic Acid
DOH	Deuterated Sodium Hydroxide
D_2O	Deuterium Oxide
FITC-BSA	Fluorescein Isothiocyanate labeled Bovine Serum Albumin
FITC-dextran	Fluorescein Isothiocyanate labeled dextran
FITC-insulin	Fluorescein Isothiocyanate labeled insulin
GnRH	Gonodotropic Releasing Hormone
HCl	Hydrochloric Acid
KH_2PO_4	Potassium Phosphate
LbL	Layer-by-Layer
LCST	Lower Critical Solution Temperature
MW	Molecular Weight
MWCO	Molecular Weight Cut Off

NaCl	Sodium Chloride
Na_2HPO_4	Sodium Hydrogen Phosphate
NaOH	Sodium Hydroxide
NIPAm	*N*-Isopropylacrylamide
NMR	Nuclear Magnetic Resonance
PAH	Poly(Allylamine Hydrochloride)
PBA	Phenyl Boronic Acid
PBS	Phosphate Buffered Saline
PEG	Poly(Ethylene Glycol)
PEO	Poly(Ethylene Oxide)
pI	Isoelectric Point
pNIPAm	Poly(*N*-Isopropylacrylamide)
pNIPAm-co-AAc	Poly(*N*-Isopropylacrylamide-*co*-Acrylic Acid)
pNIPAm-MAAc	Poly(*N*-Isopropylacrylamide-Methacrylic Acid)
PSS	Poly(Styrene Sulfonate)
SDS	Sodium Dodecyl Sulfate
VPT	Volume Phase Transition

SUMMARY

This dissertation focuses on utilization of pNIPAm based mirogels for regulated macromolecule drug delivery applications. There is particular emphasis on incorporation of stimuli responsive materials into multi-layer thin film constructs with the main goal being fabrication of highly functional materials with tunable release characteristics. Chapter 1 gives a broad overview of hydrogel and microgel materials focusing on fundamental properties of pNIPAm derived materials. Chapter 2 illustrates the progression of controlled macromolecule release from hydrogel and microgel materials and sets up the scope of this thesis work. Chapter 3 details studies on thermally modulated insulin release from microgel thin films where extended pulsatile release capabilities are shown. Chapters 4 and 5 focus on more fundamental synthesis and characterization studies of PEG and acrylic acid modified pNIPAm microgels that could ultimately lead to the design of protein loaded microgel films with tunable release characteristics. Chapter 6 illustrates fundamental macromolecule loading strategies, which could also prove useful in future protein drug delivery design using stimuli responsive networks. Chapter 7 concentrates on direct insulin release studies that probe the interaction between entrapped and freely diffusing protein and microgels. These model experiments could prove useful in design of tunable macromolecule drug release from functionally modified microgels and could aid in the tailored design of peptide-loaded microgel thin films. Chapter 8 discusses the future outlook of controlled macromolecule release from microgel based materials.

CHAPTER 1

INTRODUCTION

This chapter gives a broad overview of hydrogel and microgel based materials. It pays particular attention to networks fabricated from the thermoresponsive monomer, *N*-Isopropylacrylamide (NIPAm). It focuses on synthesis, characterization and properties of these unique sets of materials.

1.1 Hydrogel Materials

1.1.1 Definition and Classification of Hydrogels

Hydrogels, by definition, are three-dimensional cross-linked polymeric networks that can imbibe large amounts of water.[1-4] These materials are generally classified into one of two categories based on their cross-linking chemistry.[5] The first category entails physical gels which are defined as polymeric networks that are bound together via polymer chain entanglement and/or non-covalent interactions that exist between polymer chains.[1,3,6,7] The attractive forces holding these networks together are typically based on hydrogen bonding, electrostatic or hydrophobic interactions and thus, the gels can be reversibly dissolved under certain conditions that would weaken these attractive forces, i.e. a change in pH.

In contrast to these weak physically cross-linked networks, the other general class of hydrogels is chemically cross-linked gels. These hydrogels exhibit improved stability due to the formation of covalent bonds between different polymer chains throughout the networks and display endurance with respect to network structure.[1,5,8] These gels are

commonly formed through monomer polymerization in the presence of a cross-linking agent, which is typically a monomer with at least two polymerizable functional moieties.

Beyond this simple classification of hydrogel materials based on cross-linking chemistry, these networks can also be categorized on the basis of their responsivity or lack thereof. Non-responsive gels are simple polymeric networks that dramatically swell upon exposure to water. Responsive gels, on the other hand, have added functionality and display changes in solvation in response to certain stimuli such as temperature,[9] pH,[10,11] ionic strength,[12-14] light,[15-19] and electric field.[20] Hence, this effect has broad implications in many arenas including biotechnology and biomedicine.[21] Reversible volume changes (sometimes as large as several hundred times the original volume) in response to minute changes in external environmental conditions have been thoroughly reported for a variety of gels derived from polymeric networks.[20,22,23]

Yet another area in which hydrogel materials can be categorized is based on gel dimensions. Typically, hydrogels can be categorized as either macrogels or microgels. Macrogels are bulk, monolithic networks that typically range in size from millimeters or greater.[9,23-26] Microgels, on the other hand, are defined as colloidally stable, water swellable polymeric networks whose diameter typically ranges from 100 nm to 1 μm.[10,27-34] While microgels internally have the same gel structure as their macroscopic version, microgels and macrogels are physically different. Microgel particles have surface to volume ratios that are several orders of magnitude larger than those existing in bulk gels.[35] The synthesis of microgel particles typically involves a nucleation, aggregation and growth mechanism that ultimately results in a non-uniform distribution

of polymer chains throughout the network.[35,36] Macrogels, on the other hand are typically prepared under conditions that result in fairly homogenous structures.[35]

1.1.2 Poly(N-Isopropylacrylamide) Hydrogels

As previously described, hydrogels are cross-linked polymeric networks that can take up immense quantities of solvent. Poly (*N*-alkyl acrylamides) have been extensively studied with respect to their thermoresponsivity[27,37,38] with poly(*N*-isopropylacrylamide) (pNIPAm) being one of the most strongly explored temperature sensitive hydrogels within this group.[8,27,38-41] The main incentive behind studies of pNIPAm has been its unique thermal behavior in aqueous solution that manifests itself in inverse solubility upon heating.[42]

The behavior of a polymer in aqueous media is a delicate balance between polymer-polymer versus polymer-solvent interactions where the solvent-solvent interactions that exist in water are especially strong, thus causing them to have some ordered structure.[42,43] When pNIPAm is solvated in water, there is ordering of the water molecules that results from hydrogen bonding. This ordering is quite important when the water molecules must reorient themselves around nonpolar areas, resulting in what is known as the hydrophobic effect.[42,43] This hydrophobic effect is what causes these unique systems to experience a reversible volume phase transition (VPT) at a lower critical solution temperature (LCST) where the hydrogel backbone collapses upon itself, thereby expelling water in an entropically favored fashion. Isopropyl groups in the pNIPAm sidechains play an important role in this temperature dependent phase separation above the LCST.[41] The temperature at which this coil-to-globule transition occurs is

approximately 31 °C,[27,44-46] with this temperature being dependent on the identity of the *N*-alkyl group. Below the LCST, the gel is swollen, hydrated and hydrophilic.[47] In this state, the powerful hydrogen bonding between water molecules and the hydrophilic amide groups exceeds the unfavorable free energy related to exposure of hydrophobic isopropyl groups to water.[35,48] Above the LCST, the gel becomes collapsed, dehydrated and hydrophobic[47] due to disruption of the water-polymer hydrogen bonding, allowing for intra- and inter-chain hydrogen bonding and attractive hydrophobic interactions to dominate.[35,48] This leads to entropically driven phase separation[48] where the entropy term dominates the enthalpy of hydrogen bonding between polar polymer groups and water.[42] The diminished rotational freedom of the polymer chains is compensated for by an entropic gain accomplished by release of structured water surrounding polymer hydrophobic groups.[48] Above the LCST, the overall free energy change becomes positive upon mixing and phase separation occurs.[42] A diagram depicting this phase transition event can be seen in Figure 1-1. The phase transition behavior of pNIPAm hydrogel networks has been investigated using a variety of detection modes including UV/vis spectroscopy, light scattering, differential scanning calorimetry, viscometry and fluorescence spectroscopy.[44-46,49-54]

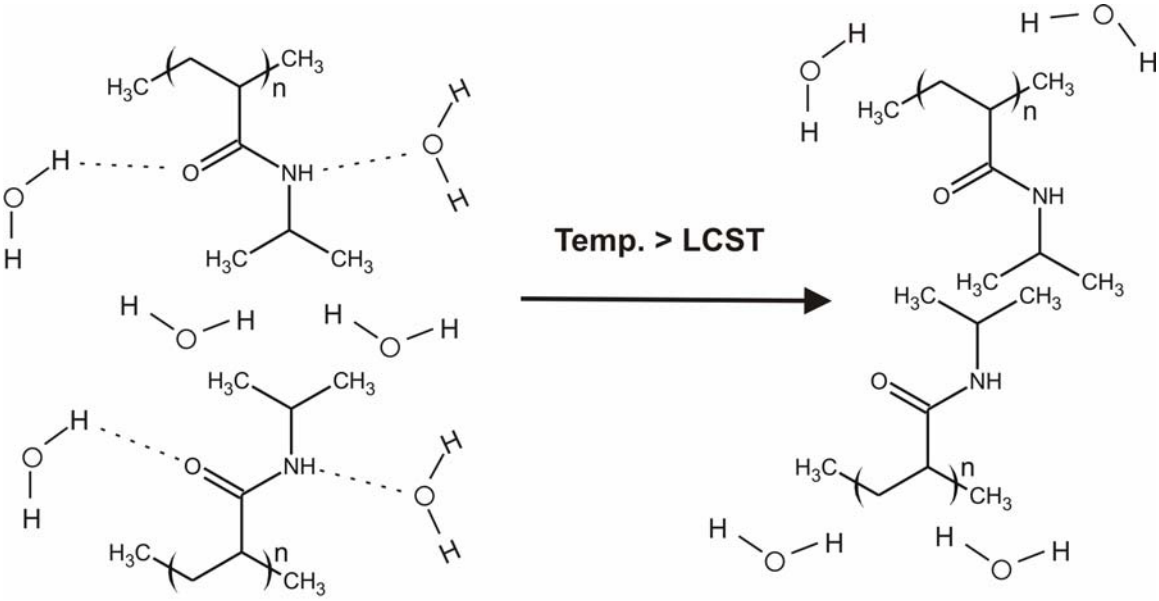

Figure 1-1. Diagram depicting the water dissociation process that occurs when pNIPAm hydrogel networks deswell. At temperatures below the LCST value of pNIPAm, water acts as a good solvent for the polymer chains forming hydrogen bonds with the amide hydrogens. When the temperature is raised above the LCST value, however, polymer-polymer interactions become dominant expelling water in an entropically favored fashion.

1.1.3 Macroscopic Poly(N-isopropylacrylamide) Hydrogels

Macroscopic bulk pNIPAm based hydrogels have been extensively studied over the past few decades due to the fact that these gels adopt the inherent thermoresponsive nature of the parent polymer that they are fabricated from. The dimensions of these networks typically fall within the millimeter scale. The thermosensitivity of these monolithic networks can be modulated based on cross-linker content and/or identity and also by the addition of hydrophilic and/or hydrophobic comonomers. Extensive work has been reported by Tanaka et al. that investigated the deswelling kinetics of such gels.[9,20,23-

[26] In particular, they have shown that the rate at which these networks collapse is inversely proportional to the square of the smallest dimension of the gel.[9,55] Due to this relationship, bulk gels can take up to hours or even days to fully collapse. One reason for this slow response is that when a swollen pNIPAm gel is subjected to temperatures above the LCST, deswelling immediately starts at the surface of the network, thus forming a dense skin layer.[56,57] This layer acts as a barrier retarding the diffusion of water out of the collapsed network. This dependence of deswelling rate on gel size and skin layer effect limits the applications of these macroscopic gels if fast deswelling rates are desired.

Incorporation of functional moieties within hydrogel materials that alter the hydrophilic/hydrophobic balance is another area that has been heavily explored. Typically, addition of hydrophobic comonomers decreases the LCST while incorporation of hydrophilic comonomers elevates the LCST of thermoresponsive hydrogels due to changes in the free energy of mixing.[48] It is well-known that cross-linked polymeric networks that bear weakly ionizable pendant groups absorb water in a pH dependent fashion.[47] pH sensitive hydrogels are typically prepared by copolymerization of weakly ionizable electrolytes into the polymer networks.[58] Variations in solution pH induce modulation of overall network ionization which causes significant differences in swelling behavior.[59] Typically, if a gel contains acidic groups, the swelling increases as the solution pH increases.[60,61] Conversely, a gel containing weak basic moieties decreases in size as the pH is elevated.[62] A commonly studied incorporated comonomer has been acrylic acid.[63] The effect of pH modulation on the swelling properties of these acid modified pNIPAm based systems has been studied in great detail.[21,35,47,64-66] Use of dually responsive temperature and pH sensitive hydrogel materials for controlled drug delivery

applications has also been increasingly examined.[67-69] Typically these doubly responsive networks exhibit controlled deswelling kinetics and a variety of release profiles can be obtained based on the ability to turn on and turn off release in response to the squeezing ability of these gels.[67] Studies on acid-incorporated and poly(ethylene glycol) (PEG)-modified systems have also been performed[56] and are also highly applicable for drug release devices.[69,70]

1.2 Microgel Materials

In contrast to slowly responding macrogels, discrete microgels are colloidally stable cross-linked polymeric networks on the size scale of nanometers to micrometers.[27] As previously discussed, the deswelling process is controlled by diffusion where the rate of collapse is strongly correlated to the gel dimension.[66] Tanaka and Fillmore (TF) developed a theory on deswelling kinetics that was based on the concept of cooperative diffusion.[55] According to the TF theory,

$$\tau \approx R^2/D \qquad (1)$$

where τ, R and D are the time of gel swelling or collapse, gel size and cooperative diffusion coefficient, respectively. According to this relation, the most obvious way to achieve faster response rates is to decrease the size of the gel.[66] Microgels, therefore, because of their significantly decreased size, deswell at rates much faster than bulk gels. The deswelling rates of temperature induced microgel collapse are typically on the microseconds timescale.[71]

1.2.1 Poly(N-isopropylacrylamide) Microgels

Microgel networks, just like macrogels, are extremely solvent swollen (approximately 95 % by volume) in their hydrated state and contain approximately 20 % solvent in their deswollen state.[27] An example of the typical volume phase transition behavior of pNIPAm based microgels can be seen in Figure 1-2. At low temperatures

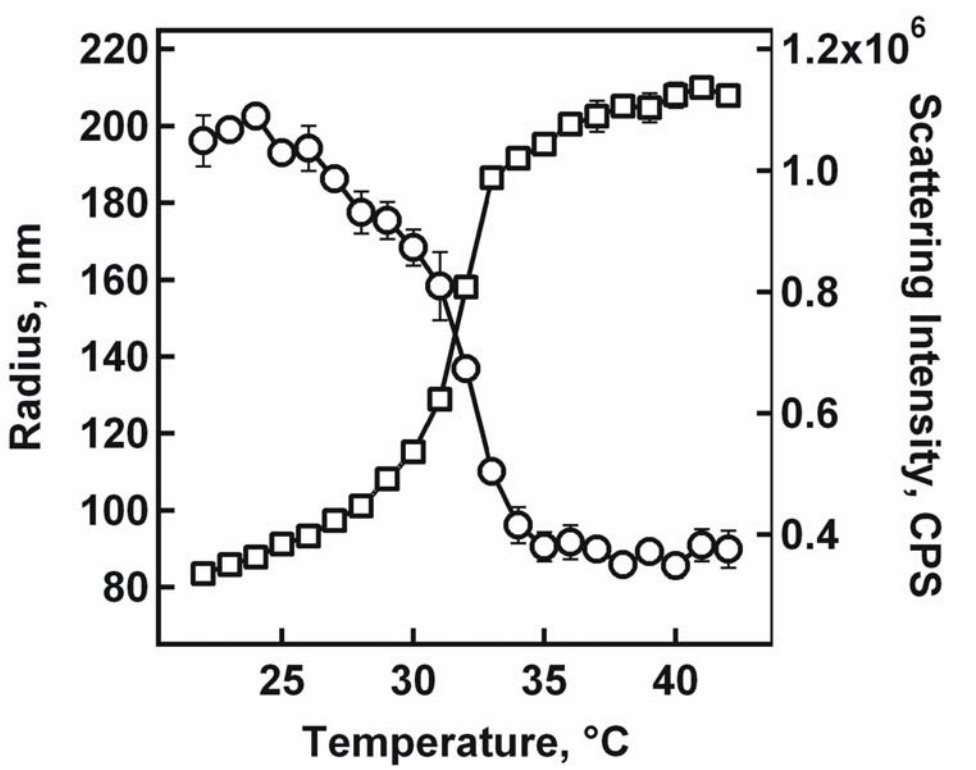

Figure 1-2. Example of a volume phase transition curve obtained via DLS. At low temperatures (below the characteristic LCST value of 31 °C), the microgels display an average hydrodynamic radius of approximately 200 nm. At temperatures above the LCST, the microgels deswell to approximately 90 nm in radius. The corresponding light scattering profile shows that when the microgels are swollen at low temperatures, little scattered light is detected but upon particle collapse, the microgels deswell into dense globules, thereby increasing the refractive index contrast. This results in a dramatic increase in detected scattered light.

(below the characteristic LCST value of 31 °C), the microgels display an average hydrodynamic radius of approximately 200 nm. At temperatures above the LCST, however, the microgels deswell and dramatically decrease in size to approximately 90 nm in radius. The corresponding light scattering profile illustrates that when the microgels are swollen at low temperatures, little scattered light is detected. This is due to the fact that in this highly hydrated state, the network is highly index matched to its environment. But, upon particle collapse, the microgels become dense globules, thereby increasing the refractive index contrast. This results in a dramatic increase in detected scattered light.

The versatility of pNIPAm microgels has been realized in modulation of the volume phase transition behavior through adjustment of the cross-linker identity and/or concentration, as well as incorporation of various comonomers. Many studies of pNIPAm based microgels have utilized the well-known cross-linker *N, N'*-Methylene(bisacrylamide) (BIS).[10,31-35,72-76] The overbearing choice for this cross-linker is most likely due to its structural resemblance to NIPAm along with its sustained precedence in polyacrylamide gels used in electrophoresis.[42] Work done in our group and by others has focused on fundamental synthesis and characterization of BIS cross-linked pNIPAm microgels[10,35] where it has been shown that there exists a cross-linking density gradient that radially decreases from the microgel interior outwards.[77]

Incorporation of functional moieties within pNIPAm based microgel materials that alter the hydrophilic/hydrophobic balance as well as swelling capacity is another area that has been widely explored where the main application has been drug delivery.[64,69,78,79] Work performed earlier in our group investigated tunable swelling kinetics of hydrophobically modified core/shell hydrogel nanoparticles.[31] Other studies done

previously in our group focused on incorporation of acrylic acid as a pH sensitive comonomer in core/shell materials that resulted in pH induced swelling phenomena.[10] These acrylic acid modified systems also proved useful for polyelectrolyte deposition onto charged substrates via electrostatics[75] which found employment in controlled uptake and release of various model drug compounds.[74,76]

1.2.2 PNIPAm Based Microgel Synthesis

Microgel particles composed primarily of pNIPAm can be synthesized using a variety of techniques including emulsion polymerization[80,81] and thermally induced free-radical precipitation polymerization.[10,27,31-33,73,75] The synthetic route by which all of the microgels discussed in this work have been fabricated is precipitation polymerization. In all of the syntheses performed, NIPAm served as the main monomer. Two different types of cross-linkers were explored. The first was BIS, a relatively short and rigid cross-linker, while the second was a more flexible oligomeric cross-linker, PEG diacrylate. Acrylic acid comonomer was also employed in certain cases to allow for pH sensitivity. The chemical structures of all of these monomers can be seen in Figure 1-3.

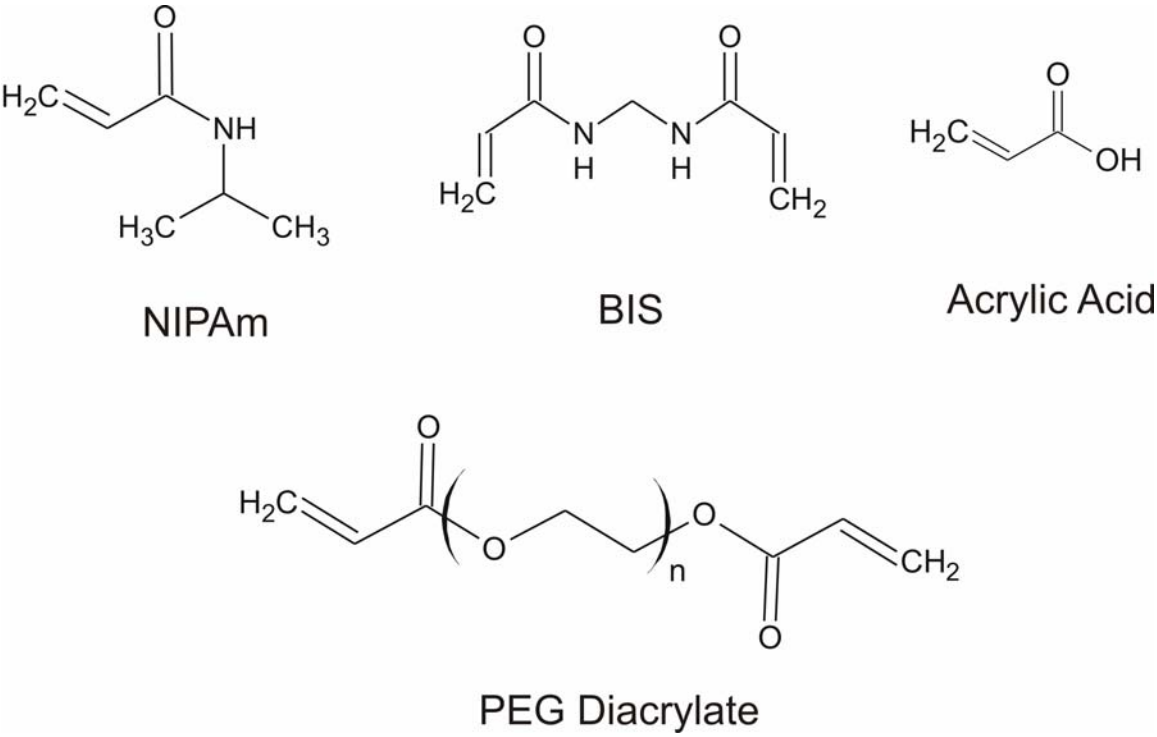

Figure 1-3. Chemical structures for *N*-isopropylacrylamide (NIPAm), *N*, *N'*-Methylene(bisacrylamide) (BIS), acrylic acid and poly(ethylene glycol) (PEG) diacrylate. These are the monomers utilized throughout this thesis work.

The details of temperature induced free-radical precipitation polymerization used in these studies are as follows. Sodium dodecyl sulfate (SDS) was used as the stabilizing surfactant while ammonium persulfate (APS) was used as the free radical initiator. The NIPAm monomer, cross-linker and surfactant were dissolved in nanopure water and then filtered through a 0.2 μm nylon membrane filter to remove any large particulate matter that could act as unwanted nuclei in the reaction. This dissolved solution was continuously stirred in a three-neck, 250 mL round-bottom flask. This solution was heated to 70 ºC while being purged with N_2 gas. This purging was necessary to remove any dissolved oxygen that could act as a free-radical scavenger that may interfere with

the polymerization process. Approximately one hour later, the temperature of the solution was stable at 70 ºC. Fifteen minutes later, the reaction was initiated by adding a hot (70 ºC) solution of APS. The solution turned turbid within 10 minutes, indicating successful initiation. The reaction proceeded for approximately 6 hours under a constant stream of nitrogen gas. Following synthesis, the microgels were cooled and filtered using a P2 Whatman filter paper. They were then dialyzed (using 10, 000 MWCO) for 2 weeks against nanopure water with a daily exchange of fresh water. For the synthesis of pH sensitive microgels, acrylic acid was added approximately 15 minutes prior to the addition of the initiator. A scheme depicting microgel synthesis using this technique is illustrated in Figure 1-4. This synthetic process results in the fabrication of monodisperse microgel particles.

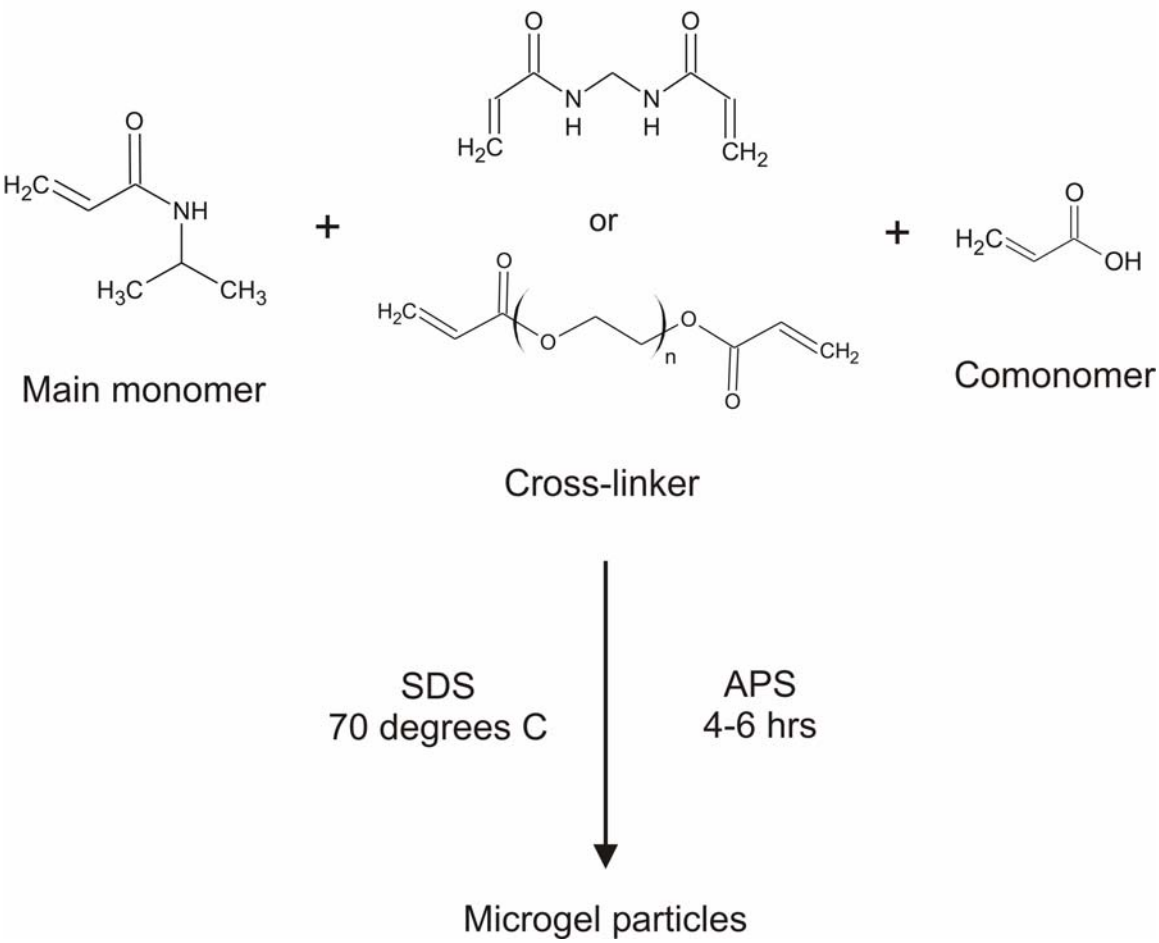

Figure 1-4. Synthesis scheme for pNIPAm based microgel particles. The monomers and surfactant (SDS) are all dissolved in water and this solution is heated to 70 °C. The polymerization is then initiated by addition of the free-radical initiator (APS). For pH sensitive microgel synthesis, the comonomer acrylic acid can be incorporated.

The route by which these microgels grow in solution is a typical nucleation, aggregation and growth mechanism.[27] An illustration of this mechanism is shown in Figure 1-5. It is important to note that all of these syntheses are carried out at 70 °C, which is a temperature well above the LCST of the polymer. This high temperature allows the thermal free-radical initiator (APS) to act effectively. It also aids in the nucleation process. Once the free-radical initiator is added to the heated monomer solution, growing oligoradical chains are formed immediately. These chains keep growing until a critical chain length is reached, after which these chains hydrophobically collapse upon themselves forming precursor particles. The reason for this collapse is because the polymer phase separates at temperatures above its LCST. It is onto these precursor particles that other growing oligoradical chains can attach, thereby forming

Figure 1-5. Schematic depicting the mechanism by which pNIPAm based microgel particles grow during free-radical precipitation polymerization. Once initiator is added to the heated monomer solution, growing oligoradicals form in solution. Once these growing chains reach a critical chain length, the chain collapses and forms precursor particles. To these precursor particles, other growing oligoradicals can attach until all monomer is exhausted, resulting in the formation of colloidally stable microgel particles.

growing particles that keep maturing until all of the monomer has been exhausted. The size of these microgel particles can be tuned by modulating the concentration of stabilizing surfactant as well as initiator. Typically, higher surfactant concentration results in smaller microgels and vice versa. Previous work done in our group has focused on expanding upon this fundamental synthetic technique whereby various functionalities have been spatially localized in pNIPAm core/shell microgels.[10,31-34,72]

1.2.3 PNIPAm Based Microgel Characterization

Characterization of pNIPAm based microgels can be achieved with a variety of techniques,[27] including dynamic light scattering,[82-85] differential scanning calorimetry[14] and neutron scattering.[86-89] In this dissertation, dynamic light scattering (DLS) has been the most commonly used technique to characterize the phase transition behavior of the microgel particles. This detection mode will hence be discussed in detail.

For all of the DLS experiments performed in this work, a Protein Solutions DynaPro-MS/X system was utilized. A schematic of this setup is illustrated in Figure 1-6. The laser source uses a wavelength of 784.8 nm. This light hits the ultradilute microgel dispersion and scattered light at 90 °C with respect to the incident light is detected by an avalanche photodiode detector. This signal is then sent to an autocorrelator board which relays the signal to a CPU. DLS monitors fluctuations in scattered light intensity and these fluctuations are analyzed in terms of correlation functions. From the autocorrelation function, a relaxation rate can be determined which is directly proportional to the translational diffusion coefficient. With the assumption of random Brownian motion, the

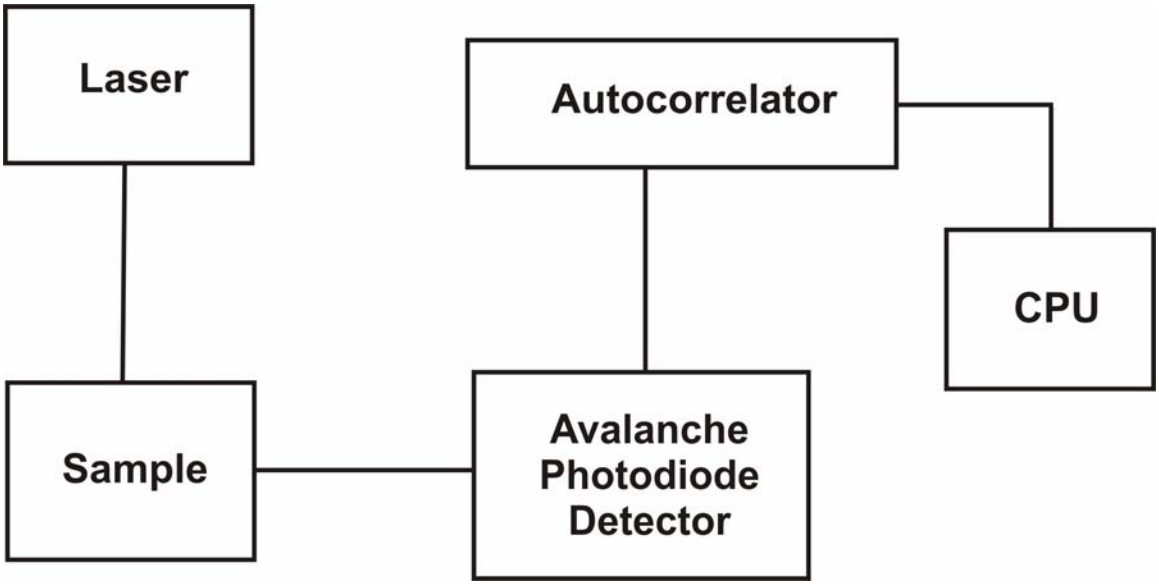

Figure 1-6. Schematic of Dynamic Light Scattering (DLS) setup. An ultradilute colloid dispersion is placed in the sample cuvette and scattered light is detected at 90 °C with respect to the incident light. The detected signal goes to the autocorrelator, an autocorrelation function is calculated, from which translational diffusion coefficients of the particles in solution are derived.

hydrodynamic radius of the dispersed microgels can be calculated using the Stokes-Einstein equation

$$R_h = k_b T / 6\pi\eta D \qquad (2)$$

where R_h is the hydrodynamic radius, k_b is the Boltzman constant, T is the temperature, η is the viscosity and D is the diffusion coefficient.

This chapter gave a broad overview of synthesis, characterization and unique properties of hydrogel and microgel based materials. This sets up the next chapter which focuses on controlled macromolecule release from such responsive systems. The next

chapter deals with the progression of advancements made in the field of modulated biomolecule delivery devices and sets the overall scope of this thesis work.

1.3 References

(1) Hoffman, A. S. *Adv. Drug Delivery Rev.* **2002**, *54*, 3-12.

(2) Drury, J. L.; Mooney, D. J. *Biomaterials* **2003**, *24*, 4337-4351.

(3) DeRossi, D.; Kajiwara, K.; Osada, Y.; Yamauchi, A. *Polymer Gels: Fundamentals and Biomedical Applications*; Plenum Press: New York, 1991.

(4) Dhara, D.; Nisha, C. K.; Chatterji, P. R. *J. Macromol. Sci., Pure Appl. Chem.* **1999**, *A36*, 197-210.

(5) Hennink, W. E. *Adv. Drug Delivery Rev.* **2002**, *54*, 13-36.

(6) Akiyoshi, K.; Kang, E. C.; Kurumada, S.; Sunamoto, J.; Principi, T.; Winnik, F. M. *Macromolecules* **2000**, *33*, 3244-3249.

(7) Collier, J. H.; Hu, B. H.; Ruberti, J. W.; Zhang, J.; Shum, P.; Thompson, D. H.; Messersmith, P. B. *J. Am. Chem. Soc.* **2001**, *123*, 9463-9464.

(8) Eddington, D. T.; Beebe, D. J. *Adv. Drug Delivery Rev.* **2004**, *56*, 199-210.

(9) Li, Y.; Tanaka, K. *J. Chem. Phys.* **1990**, *92*, 1365-1371.

(10) Jones, C. D.; Lyon, L. A. *Macromolecules* **2000**, *33*, 8301-8306.

(11) Moselhy, J.; Wu, X. Y.; Nicholov, R.; Kodaria, K. *J. Biomater. Sci., Polym. Ed.* **2000**, *11*, 123-147.

(12) Duracher, D.; Sauzedde, F.; Elaiessari, A.; Perrin, A.; Pichot, C. *Colloid Polym. Sci.* **1998**, *276*, 219-231.

(13) Duracher, D.; Sauzedde, F.; Elaiessari, A.; Pichot, C. *Colloid Polym. Sci.* **1998**, *276*, 920-929.

(14) Snowden, M. J.; Chowdhry, B. Z.; Vincent, B.; Morris, G. E. *J. Chem. Soc.-Faraday Trans.* **1996**, *92*, 5013-5016.

(15) Sershen, S. R.; Westcott, S. L.; Halas, N. J.; West, J. L. *J. Biomed. Mater. Res.* **2000**, *51*, 293-298.

(16) Sershen, S. R.; Westcott, S. L.; West, J. L.; Halas, N. J. *Appl. Phys. B* **2001**, *73*, 379-381.

(17) Sershen, S. R.; Westcott, S. L.; Halas, N. J.; West, J. L. *Applied Physics Letters* **2002**, *80*, 4609-4611.

(18) Suzuki, A.; Tanaka, T. *Nature* **1990**, *346*, 345-347.

(19) Suzuki, A.; Ishii, T.; Maruyama, Y. *J. Appl. Phys.* **1996**, *80*, 131-136.

(20) Tanaka, T.; Nishio, I.; Sun, S. T.; Ueno-Nishio, S. *Science* **1982**, *218*, 467-469.

(21) Kishi, R.; Miura, T.; Kihara, H.; Asano, T.; Shibata, M.; Yosomiya, R. *J. Appl. Polym. Sci.* **2003**, *89*, 75-84.

(22) Tanaka, T. *Phys. Rev. Lett.* **1978**, *40*, 820-823.

(23) Tanaka, T.; Fillmore, D. J.; Sun, S. T.; Nishio, I.; Swislow, G.; Shah, A. *Phys. Rev. Lett.* **1980**, *45*, 1636-1639.

(24) Li, Y.; Tanaka, K. *J. Chem. Phys.* **1989**, *90*, 5161-5166.

(25) Tanaka, T. *Physica A* **1986**, *140A*, 261-268.

(26) Tanaka, T.; Wang, C.; Pande, V.; Grosberg, A. Y.; English, A.; Masamune, S.; Gold, H.; Levy, R.; King, K. *Faraday Discuss.* **1995**, *101*, 201-206.

(27) Pelton, R. H. *Adv. Colloid. Interface Sci.* **2000**, *85*, 1-33.

(28) Saunders, B. R.; Vincent, B. *Adv. Colloid. Interface Sci.* **1999**, *80*, 1-25.

(29) Kawaguchi, H. *Prog. Polym. Sci.* **2000**, *25*, 1171-1210.

(30) Gilanyi, T.; Varga, I.; Meszaros, R.; Filipcsei, G.; Zrinyi, M. *Phys. Chem. Chem. Phys.* **2000**, *2*, 1973-1977.

(31) Gan, D.; Lyon, L. A. *J. Am. Chem. Soc.* **2001**, *123*, 7511-7517.

(32) Gan, D.; Lyon, L. A. *J. Am. Chem. Soc.* **2001**, *123*, 8203-8209.

(33) Gan, D.; Lyon, L. A. *Macromolecules* **2002**, *35*, 9634-9639.

(34) Jones, C. D.; Lyon, L. A. *Macromolecules* **2003**, *36*, 1988-1993.

(35) Saunders, B. R.; Crowther, H. M.; Morris, G. E.; Mears, S. J.; Cosgrove, T.; Vincent, B. *Colloids Surf. A* **1999**, *149*, 57-64.

(36) Wu, X.; Pelton, R. H.; Hamielec, A. E.; Woods, D. R.; McPhee, W. *Colloid Polym. Sci.* **1994**, *272*, 467-477.

(37) Shibayama, M.; Tanaka, T. *Adv. Polym. Sci.* **1993**, *109*, 1-62.

(38) Inomata, H.; Goto, S.; Saito, S. *Macromolecules* **1990**, *23*, 4887-4888.

(39) Wu, X. S.; Hoffman, A. S.; Yager, P. *J. Polym. Sci., Part A: Polym. Chem.* **1992**, *30*, 2121-2129.

(40) Chen, J.; Park, H.; Park, K. *Polym. Mater. Sci. Eng.* **1998**, *79*, 236-237.

(41) Kaneko, Y.; Nakamura, S.; Sakai, K.; Aoyagi, T.; Kikuchi, A.; Sakurai, Y.; Okano, T. *Macromolecules* **1998**, *31*, 6099-6105.

(42) Schild, H. G. *Prog. Polym. Sci.* **1992**, *17*, 163-249.

(43) Ben-Naim. *Hydrophobic Interactions*; Plenum Press: New York, 1980.

(44) Wu, C.; Wang, X. *Phys. Rev. Lett.* **1998**, *80*, 4092-4094.

(45) Wu, C.; Zhou, S. *Macromolecules* **1995**, *28*, 8381-8387.

(46) Wu, C.; Zhou, S. *Macromolecules* **1995**, *28*, 5388-5390.

(47) Yoo, M. K.; Sung, Y. K.; Lee, Y. M.; Cho, C. S. *Polymer* **2000**, *41*, 5713-5719.

(48) Feil, H.; Bae, Y. H.; Feijen, J.; Kim, S. W. *Macromolecules* **1993**, *26*, 2496-2500.

(49) Winnik, F. M. *Macromolecules* **1990**, *23*, 1647-1649.

(50) Winnik, F. M. *Langmuir* **1990**, *6*, 522-524.

(51) Winnik, F. M. *Macromolecules* **1990**, *23*, 233-242.

(52) Wu, C.; Zhou, S. *Macromolecules* **1996**, *29*, 1574-1578.

(53) Wu, C. *Polymer* **1998**, *39*, 4609-4619.

(54) Wu, C.; Qiu, X. *Phys. Rev. Lett.* **1998**, *80*, 620-622.

(55) Tanaka, T.; Fillmore, D. J. *J. Chem. Phys.* **1979**, *70*, 1214-1218.

(56) Lee, W.-F.; Chiu, R.-J. *J. Appl. Polym. Sci.* **2003**, *90*, 2214-2223.

(57) Okano, T.; Bae, Y. H.; Jacobs, H.; Kim, S. W. *J. Controlled Release* **1990**, *11*, 255-265.

(58) Siegel, R. A.; Falamarzian, M.; Firestone, B. A.; Moxley, B. C. *J. Controlled Release* **1988**, *8*, 179-182.

(59) Beltran, S.; Baker, J. P.; Hooper, H. H.; Blanch, H.; Prausnitz, J. M. *Macromolecules* **1991**, *24*, 549-551.

(60) Cussler, E. L.; Stokar, M. R.; Varberg, J. E. *AIChE J.* **1984**, *30*, 578-582.

(61) Grignon, J.; Scallan, A. M. *J. Appl. Polym. Sci.* **1980**, *25*, 2829-2843.

(62) Kost, J.; Horbett, T. A.; Ratner, B. D.; Singh, M. J. *Biomed. Mater. Res.* **1985**, *19*, 1117-1133.

(63) Plunkett, K. N.; Kraft, M. L.; Yu, Q.; Moore, J. S. *Macromolecules* **2003**, *36*, 3960-3966.

(64) Dowding, P. J.; Vincent, B.; Williams, E. *J. Colloid Interface Sci.* **2000**, *221*, 268-272.

(65) Aoyagi, T.; Ebara, M.; Sakai, K.; Sakurai, Y.; Okano, T. *J. Biomater. Sci., Polym. Ed.* **2000**, *11*, 101-110.

(66) Hirose, H.; Shibayama, M. *Macromolecules* **1998**, *31*, 5336-5342.

(67) Gutowska, A.; Bark, J. S.; Kwon, I. C.; Bae, Y. H.; Cha, Y.; Kim, S. W. *J. Controlled Release* **1997**, *48*, 141-148.

(68) Kubota, N.; Matsubara, T.; Eguchi, Y. *J. Appl. Polym. Sci.* **1998**, *70*, 1027-1034.

(69) Bromberg, L.; Temchenko, M.; Hatton, T. A. *Langmuir* **2002**, *18*, 4944-4952.

(70) Torres-Lugo, M.; Peppas, N. A. *Macromolecules* **1999**, *32*, 6646-6651.

(71) Wang, J.; Gan, D.; Lyon, L. A.; El-Sayed, M. A. *J. Am. Chem. Soc.* **2001**, *124*, 11284-11289.

(72) Jones, C. D.; Lyon, L. A. *Langmuir* **2003**, *19*, 4544-4547.

(73) Nayak, S.; Lyon, L. A. *Chem. Mater.* **2004**, *16*, 2623-2327.

(74) Nolan, C. M.; Serpe, M. J.; Lyon, L. A. *Biomacromolecules* **2004**, *5*, 1940-1946.

(75) Serpe, M. J.; Jones, C. D.; Lyon, L. A. *Langmuir* **2003**, *19*, 8759-8764.

(76) Serpe, M. J.; Yarmey, K. A.; Nolan, C.; Lyon, L. A. *Biomacromolecules* **2005**, *6*, 408-413.

(77) Guillermo, A.; Cohen Addad, J. P.; Bazile, J. P.; Duracher, D.; Elaissari, A.; Pichot, C. *J. Polym. Sci., Part B: Polym. Phys.* **2000**, *38*, 889-898.

(78) Lynn, D. M.; Mansoor, M. A.; Langer, R. *Angew. Chem. Int. Ed.* **2001**, *40*, 1707-1710.

(79) Kim, I.-S.; Jeong, Y.-I.; Cho, C. S.; Kim, S.-H. *Int. J. Pharm.* **2000**, *211*, 1-8.

(80) Pelton, R. H.; Chibante, P. *Colloids Surf.* **1986**, *20*, 247-256.

(81) Wu, J.; Zhou, B.; Hu, Z. *Phys. Rev. Lett.* **2003**, *90*, 1-4.

(82) Crowther, H. M.; Vincent, B. *Colloid Polym. Sci.* **1998**, *276*, 46-51.

(83) Bouillot, P.; Vincent, B. *Colloid Polym. Sci.* **2000**, *278*, 74-79.

(84) Weeks, J. R.; Van Duijneveldt, J. S.; Vincent, B. *J. Phys.: Condens. Matter* **2000**, *12*, 3605-3614.

(85) Kratz, K.; Hellweg, T.; Eimer, W. *Colloid Surf. A* **2000**, *170*, 137-149.

(86) Kratz, K.; Hellweg, T.; Eimer, W. *Ber. Bunsenges. Phys. Chem.* **1998**, *102*, 1603-1608.

(87) Crowther, H. M.; Saunders, B. R.; Mears, S. J.; Cosgrove, T.; Vincent, B.; King, S. M.; Yu, G. E. *Colloid Surf. A* **1999**, *152*, 327-333.

(88) Kratz, K.; Lapp, A.; Eimer, W.; Hellweg, T. *Colloid Surf. A* **2002**, *197*, 55-67.

(89) Hellweg, T.; Kratz, K.; Pouget, S.; Eimer, W. *Colloid Surf. A* **2002**, *202*, 223-232.

CHAPTER 2

CONTROLLED MACROMOLECULE RELEASE FROM HYDROGEL MATERIALS

Given the broad overview of hydrogel and microgel materials discussed in the previous chapter, this chapter delves into the specific application of regulated macromolecule drug delivery from both sets of materials. This chapter serves to illustrate the progression of macromolecular release devices studied within the past decade and ultimately casts the purpose of this thesis work.

2.1 Drug Delivery from Hydrogel Based Materials

Over the past decade, great strides have been made in the fields of controlled and targeted drug delivery. As discussed previously, hydrogels are three-dimensional polymeric networks that can imbibe large amounts of water. Thus, they have been extensively studied as a vehicle for controlled drug release systems due to their high water content, soft tissue-like consistency, and potential biocompatibility.[1-5] Stimuli-responsive hydrogels, which experience changes in swelling in response to perturbations in external conditions, have found great use as novel materials in controlled drug delivery applications.[6-11] Poly(*N*-isopropylacrylamide) (pNIPAm), one of the most commonly utilized temperature sensitive hydrogels, displays reversible volume phase transition behavior at the characteristic lower critical solution temperature (LCST) value of 31 °C.[12] During this deswelling event the polymer goes from a highly solvated swollen state to a

collapsed dehydrated globule. This squeezing phenomenon has been utilized as a mechanism to control uptake and release of various model drug compounds. Microgels, discrete sub-micron sized spherical hydrogel networks,[12-14] are another subclass of hydrogels that have also been extensively pursued for drug release studies,[15-20] considering the fact that they display the same stimuli responsive nature that the parent polymer exhibits but, at a faster rate.

2.2 Macromolecule Release from Hydrogels

Advances in the development of protein therapeutic agents[9] has created the need for design of controlled drug delivery vehicles, driven by a number of components.[21] For instance, these devices when used *in vivo* help to protect the protein from harsh enzymes that may cause denaturation.[22] Furthermore, many of these macromolecularly based therapeutic agents are extremely potent and thus, the carrier can act to target the drug to its desired location in the body, thereby diminishing any unwanted systemic side effects.[22] Among the types of materials explored in these type of applications, polymer-based devices have been heavily pursued[22] with hydrogels playing a major role.[21,23,24] Due to its temperature dependent responsivity, cross-linked pNIPAm hydrogels have been increasingly investigated for drug delivery systems.[6-11,25] Early work done by Hoffman and coworkers focused on uptake and release of model enzymes and macromolecules using pNIPAm hydrogel materials.[26-33] They then investigated macromolecule release from pH sensitive and thermoresponsive networks.[34-36]

Temperature sensitive hydrogel materials that are also responsive to pH can generally be fabricated by copolymerization of pNIPAm with an array of hydrophilic and

hydrophobic comonomers. This results in the production of positive and negative, or on and off, pulsatile drug release profiles in reaction to temperature changes across the LCST value.[37] Significant progress in this area has been made by Peppas et al. where they have fabricated pH sensitive copolymer hydrogels capable of preserving a peptide while it is transported through the harsh environment of the stomach. Early studies focused on optimizing protein loading and release from ionic hydrogels.[34,38] They then showed that poly(methacrylic-*g*-ethylene glycol) hydrogels display reversible pH dependent swelling behavior and have proposed these systems be utilized mainly for oral protein delivery applications. Under low pH conditions, the hydrogels are collapsed and protect the encapsulated peptide from denaturing enzymes present in the stomach. But, as the loaded vehicle passes to the upper small intestine, the pH becomes more basic thereby inducing protein release due to dramatic swelling of the hydrogel.[39,40] Modified release of peptide agents has also been achieved by exploring ionized amphiphilic hydrogel networks.[41]

Since insulin is endogenously released in a cyclical manner,[42] methods to achieve pulsatile release of this protein from hydrogel materials have also been vigorously pursued.[43] Park and coworkers utilized dually responsive pH and temperature sensitive hydrogels to achieve controlled insulin release from pNIPAm hydrogels copolymerized with *N, N'*-diethylaminopropyl methacrylamide that exhibited swelling changes at pH 7.4.[44] Further advances in self-regulated insulin delivery were made with studies focusing on glucose sensitive hydrogels that utilize entrapped glucose oxidase[45,46] or phenylborate moieties[47] as a mechanism to switch pH, causing reversible hydrogel swelling. This resulted in subsequent regulated insulin delivery. Studies on modulated insulin release

from biodegradable dextran hydrogels have been pursued as well[48,49] where investigations performed by Yui and coworkers utilized PEG containing dextran gels to preferentially load the protein.[49,50]

Regulated protein release by use of degradable hydrogel drug delivery devices has been yet another area heavily explored. Work done by McBride and coworkers illustrated enhanced loading and activity retention of bioactive proteins using dextran gels.[51] Investigations conducted by Hubbell et al. examined controlled protein release from degradable PEG hydrogels[52] while Langer and coworkers studied protein release from biodegradable poly(lactic acid) containing gels.[53] Extensive work has been performed by Hennink and coworkers who focused on using physically cross-linked dextran based hydrogels as biocompatible and biodegradable macromolecule release devices.[54-58] Work from Park et al. also investigated the use of enzyme digestible dextran hydrogels for regulated protein delivery.[59-62]

While all of these studies are significant advances in the field of modulated macromolecule release, bulk hydrogels have the inherent disadvantage of slow response due to their large dimensions. Thus, use of smaller, faster responding microgel networks for controlled protein delivery has seen much more precedence recently.

2.3 Macromolecule Release from Microgels

As previously illustrated with macrogels, there have also been significant advances made in the design of controlled macromolecule release devices involving microgel materials.[18,22,63-65] Encapsulation of protein drugs into microspheres has been widely explored in recent years due to the fact that these carriers provide longer

circulatory half-lives and better stability of their cargo.[66] In the late 1980's and early 1990's, significant progress in the field of protein drug delivery was made with use of polysaccharide hydrogels. These systems have the advantages of being non-toxic, biocompatible, biodegradable and abundant.[66] Many of these early studies focused on insulin delivery via a nasal route using starch microspheres.[67-71] Enhanced bioavailability of the peptide was reported and was attributed to the mucoadhesive properties of the polymers. Work done by Langer et al. has focused on controlled macromolecule release using ionotropic hydrogels.[72] They have also investigated hydrogel nanoparticle carriers for protein nasal administration[73] and DNA encapsulation and release.[74] The use of microgel particles composed of other hydrogel materials for controlled insulin delivery has also found great precedence in the literature.[75-78]

As similarly seen with macrogels, incorporation of functional moieties within microgel materials that alter the hydrophilic/hydrophobic balance as well as swelling capacity has been heavily explored for development of biomolecule carriers. Early work done by Peppas et al. has concentrated on using pH sensitive bulk gels for controlled macromolecule release.[39,40] This work was then extended to include faster responding discrete microgel particles composed of the same pH responsive poly(methacrylic-*g*-ethylene glycol) polymer.[79,80] A particular focus on regulated oral insulin delivery was made.[77,81-86] They made further advances in these systems by investigating pulsatile release characteristics of glucose-oxidase immobilized microspheres.[83] When these networks are exposed to external glucose in solution, glucose oxidase turns into gluconic acid, thereby causing a decrease in pH.[87] This ultimately yields these networks pH sensitive and this switch can cleverly be used to trigger release of embedded proteins, i. e.

insulin. By using poly(diethylamino-ethyl methacrylate-*g*-ethylene glycol) microparticles, they were able to achieve pH induced swelling at pH values below 7.0. Thus, the pH responsivity of these networks was indicative of their response to external glucose levels and could be useful in cyclical insulin release.[83] Peppas et al. also made thorough studies focusing on transport mechanisms of macromolecules,[80] particularly insulin,[88-91] across cellular membranes where they observed enhanced transport when the protein was encapsulated in microgels.

Among the extensive studies focusing on microgels for controlled protein delivery, exploration of biodegradable networks has shown great promise.[92] Work done by Park and co-workers has focused on controlled protein release from degradable microspheres composed of lactic acid containing networks.[93-97] Work done by Hennink and coworkers has utilized dextran based networks that are both biocompatible and biodegradable.[98] Even further advances have been made by Frechet and co-workers regarding acid-labile cross-linked networks. Typically, most hydrogel networks are cross-linked using amide, ester or carbonate linkages that are degradable under basic pH conditions.[19] For targeted drug delivery applications, use of protein loaded networks that utilize acid degradable cross-links would be especially useful considering the fact that many targets needing therapeutics exist at slightly acidic pHs. These include tumors and inflammatory tissues.[99,100] Frechet et al. developed a novel acetal cross-linker that allows for protection from release under neutral pH conditions but pH dependent release of model macromolecules due to acid degradation under slightly acidic pH conditions of 5.0.[19] They have extended these studies to also include development of protein and DNA based vaccines where they take advantage of the pH differential between serum (pH 7.4)

and the lysosome (pH 5.0). Hence, once these loaded microgels are internalized in lysosomal components, the particles should degrade and expel the impregnated bioactive species.[18,20]

Advances in release of proteins in an oscillatory fashion have also been realized in recent years due to the fact that many hormones are known to be endogenously released in a pulsatile manner.[42,101-104] Among these are insulin and gonodotropic releasing hormone (GnRH).[105,106] Studies have shown that the efficacy of replacement therapy improves dramatically when the hormones are administered in a pulsatile manner.[107] Oscillatory insulin release from hydrogel systems has thus been explored.[50] Self-regulating insulin delivery systems that utilize pH responsivity as a means to respond to increases in free glucose concentration have been investigated.[45,108] Superporous hydrogel networks[109] and biodegradable hydrogel networks are yet another area of insulin release devices that have been researched.[48,49,110]

The fundamental challenges that remain for protein and DNA based therapeutic delivery are effective targeting to specific tissues and the subsequent intracellular release into the correct cellular components.[111] In this area, momentous advances have been made by Hoffman and coworkers who have developed polymer-biomolecule conjugates, or bioconjugates.[112] They have illustrated thermally triggered release of bound biotin from site-specific pNIPAm-streptavidin conjugates.[113,114] They have also prepared site-specific conjugates with pH and light sensitive polymers.[112,115] Furthermore, they have shown that the specific site for polymer conjugation can be spatially localized far away from, close to, or even within the active site in order to regulate the protein-ligand binding process as well as biological activity of the protein.[116,117] In the area of cellular

release, studies have shown that pH sensitive hydrogels can be molecularly engineered to efficiently disrupt eukaryotic membranes within narrow pH ranges[118-120] as well as significantly enhance gene expression levels while providing serum stability in cell culture models.[121] The function of these systems was expanded by the design and synthesis of a glutathione containing pH sensitive terpolymer. This novel design served to not only cause pH dependent endosomal membrane disruption and escape into the cytoplasm but, it also was cleverly designed to allow for drug release by reduction of disulfide linkages in the presence of glutathione (a highly abundant reducing agent present in most cells).[122] Hoffman et al. also developed polymeric carriers that target uptake and enhance intracellular delivery of oligonucleotides.[123]

2.4 Macromolecule Drug Delivery from Hydrogel Films, Implants and Through Hydrogel Membranes

Release of macromolecules from hydrogel films and implants is yet another mode of controlled drug delivery devices being heavily explored. Work done by Hoffman and coworkers investigated hormone release from hydrogel films made of chitosan[124] while Park et al. explored deposition of enzymes onto hydrogel contact lenses.[61,125] Investigations on extended insulin release from hydrogels implanted into mice have also been pursued.[126,127] Langer and coworkers made advances by investigating glucose-mediated insulin release from implantable polymers[128,129] while Ratner et al. looked at insulin transport through glucose sensitive membranes.[130] Tunable macromolecule release from erosion-controlled films has also been demonstrated.[131] Work done by Lynn and coworkers displayed sustained release of functional DNA from mutli-layer thin

films.[132] Yet even more recently, work has focused on a novel technique to encapsulate cells into hollow hydrogel particles.[133]

As previously mentioned, exploration of glucose sensitive hydrogel systems has seen much activity over the years in efforts to achieve self-regulating insulin release devices. One of the strategies pursued has involved the specific interaction between polymer-bound glucose and concanavalin A (Con-A). In these approaches, hydrogels can be cross-linked by binding of Con-A, which has four glucose binding sites, to the glucose-bound polymer. Early in these approaches, Hoffman and coworkers showed that interactions between glucose bound polymers and con-A resulted in precipitation[134,135] and glucose sensitivy.[136] Work done by Park et al. showed that such interactions could result in glucose dependent reversible gel transitions[137,138] and that that these responses could control the release of insulin through a hydrogel membrane.[139] This work done by Park et al. was later improved upon by PEGylating Con-A to improve solubility and stability which resulted in enhanced reproducibility[140] of modulated insulin delivery through the membrane.[108]

Significant advances in macromolecule delivery devices that achieve release in a pulsatile fashion have been made by Siegel and coworkers. They first proposed a novel strategy for open loop, sustained pulsatile drug release that does not need an external activation source.[107,141] They then showed that rhythmic delivery of the hormone GnRH was achievable due to the pH dependent swelling state of a polyelectrolyte pNIPAm-methacrylic acid (pNIPAm-MAAc) hydrogel membrane that displayed glucose sensitivity. They attributed oscillatory release to nonlinear feedback between the membrane and glucose oxidase.[142-144] Siegel and coworkers utilized the well-established

pH responsivity of the hydrogel network but, for the first time, cleverly used it in such a way that the rhythms were autonomous. That is, the hydrogel behaves rhythmically even at constant levels of glucose which is in contrast to previously reported glucose responsive systems.[145] They have also worked on further development of glucose responsive hydrogels using a phenylboronic acid (PBA) containing network that has been shown to bind to glucose and thus achieve a change in polymer charge, leading to tunable swelling and permeability to insulin.[146,147] This system has important implications in microfabricated glucose sensitive hydrogel based valve constructs.

Given all of the progress made within the field of regulated macromolecule release using hydrogel materials, a fundamental challenge that still remains in this arena is initial burst. Ways to reserve the encapsulated protein and achieve extended pulsatile delivery still need to be realized.[148] Along this note, formulations involving a multi-layer thin film construct may serve beneficial since these materials are inherently more stable than free carriers in solution. Furthermore, with the explosion of activity within the field of multi-layer thin films in recent years, there is great opportunity to finely tune the functionalities of these films at the molecular level. Thus, incorporation of stimuli responsive materials into these multi-layer thin films could conceivably allow for tunable release characteristics of highly functional materials. It is this rational that has been the main driving force behind the studies discussed in this dissertation, which lie at the interface between drug delivery and colloidal polymeric science. Chapter 3 details studies on thermally modulated insulin release from microgel thin films where extended pulsatile release capabilities are shown. Chapters 4 and 5 focus on more fundamental synthesis and characterization studies of PEG and acrylic acid modified microgels that could ultimately

lead to the design of protein loaded microgel films with tunable release characteristics. Chapter 6 illustrates fundamental macromolecule loading strategies, which could also prove useful in future protein drug delivery design using stimuli responsive networks. Chapter 7 focuses on direct insulin release studies that probe the interaction between entrapped and freely diffusing protein and microgels. These model experiments could prove useful in design of tunable macromolecule drug release from functionally modified microgels and could aid in the tailored design of peptide-loaded microgel thin films. Finally, Chapter 8 illustrates the general outlook of future research studies that could be pursued in this area.

2.5 References

(1) Peppas, N. A.; Bures, P.; Leobandung, W.; Ichikawa, H. *Eur. J. Pharm. Biopharm.* **2000**, *50*, 27-46.

(2) Peppas, N. A.; Mikos, A. G. *Hydrogels in Medicine and Pharmacy*; CRC Press: Boca Raton, 1986; Vol. 1.

(3) Brannon-Peppas, L. *Absorbent Polymer Technology*; Elseiver: Amsterdam, 1990.

(4) Peppas, N. A.; Langer, R. *Science* **1994**, *263*, 1715-1720.

(5) Peppas, N. A. *Curr. Opin. Colloid Interface Sci.* **1997**, *2*, 531-537.

(6) Peppas, N. A.; Leobandung, W. *J. Biomat. Sci., Poly. Ed.* **2004**, *15*, 125-144.

(7) Siegel, R. A.; Ziaie, B. *Adv. Drug Delivery Rev.* **2004**, *56*, 121-123.

(8) Kikuchi, A.; Okano, T. *Adv. Drug Delivery Rev.* **2002**, *54*, 53-77.

(9) Hoffman, A. S. *Adv. Drug Delivery Rev.* **2002**, *54*, 3-12.

(10) Qiu, Y.; Park, K. *Adv. Drug Delivery Rev.* **2001**, *53*, 321-339.

(11) Kopecek, J.; Kopeckova, P.; Minko, T.; Lu, Z. R.; Peterson, C. M. *J. Controlled Release* **2001**, *74*, 147-153.

(12) Pelton, R. H. *Adv. Colloid. Interface Sci.* **2000**, *85*, 1-33.

(13) Senff, H.; Richtering, W. *J. Chem. Phys.* **1999**, *111*, 1705-1711.

(14) Saunders, B. R.; Vincent, B. *Adv. Colloid. Interface Sci.* **1999**, *80*, 1-25.

(15) Kiser, P. F.; Wilson, G.; Needham, D. *J. Controlled Release* **2000**, *68*, 9-22.

(16) Lynn, D. M.; Mansoor, M. A.; Langer, R. *Angew. Chem. Int. Ed.* **2001**, *40*, 1707-1710.

(17) Kim, I.-S.; Jeong, Y.-I.; Cho, C. S.; Kim, S.-H. *Int. J. Pharm.* **2000**, *211*, 1-8.

(18) Murthy, N.; Xu, M.; Schuck, S.; Kunisawa, J.; Shastri, N.; Frechet, J. M. J. *Proc. Natl. Acad. Sci.* **2003**, *100*, 4995-5000.

(19) Murthy, N.; Thng, Y. X.; Schuck, S.; Xu, M. C.; Frechet, J. M. J. *J. Am. Chem. Soc.* **2002**, *124*, 12398-12399.

(20) Goh, S. L.; Murthy, N.; Xu, M.; Frechet, J. M. J. *Bioconj. Chem.* **2004**, *15*, 467-474.

(21) Langer, R. *Science* **1990**, *249*, 1527-1533.

(22) Mellott, M. B.; Searcy, K.; Pishko, M. V. *Biomaterials* **2001**, *22*, 929-941.

(23) Peppas, N. A.; Khare, A. R. *Adv. Drug Delivery Rev.* **1993**, *11*, 1-36.

(24) Ende, M. T.; Mikos, A. G. *Protein Delivery: Phys. Sys.* **1997**, 139-165.

(25) Hwang, S.-J.; Baek, N.; Park, H. *Drug Delivery Systems in Cancer Therapy* **2004**, 97-115.

(26) Dong, L.; Hoffman, A. S.; Yan, Q. *J. Biomat. Sci., Poly. Ed.* **1994**, *5*, 473-484.

(27) Park, T. G.; Hoffman, A. S. *Biotech. Progress* **1991**, *7*, 383-390.

(28) Park, T. G.; Hoffman, A. S. *J. Biomed. Mater. Res.* **1990**, *24*, 21-38.

(29) Park, T. G.; Hoffman, A. S. *Appl. Biochem. Biotech.* **1988**, *19*, 1-9.

(30) Hoffman, A. S.; Afrassiabi, A.; Dong, L. *J. Controlled Release* **1986**, *4*, 213-222.

(31) Afrassiabi, A.; Hoffman, A. S.; Cadwell, L. A. *J. Membr. Sci.* **1987**, *33*, 191-200.

(32) Nakamae, K.; Nizuka, T.; Miyata, T.; Furukawa, M.; Nishino, T.; Kato, K.; Inoue, T.; Hoffman, A. S.; Kanzaki, Y. *J. Biomat. Sci., Poly. Ed.* **1997**, *9*, 45-53.

(33) Hoffman, A. S.; Afrassiabi, A.; Dong, L. *J. Controlled Release* **1986**, *4*, 223-227.

(34) Dong, L.; Yan, Q.; Hoffman, A. S. *J. Controlled Release* **1992**, *19*, 171-177.

(35) Mumper, R. J.; Hoffman, A. S.; Puolakkainen, P. A.; Bouchard, L. S.; Gombotz, W. R. *J. Controlled Release* **1994**, *30*, 241-251.

(36) Inoue, T.; Chen, G.; Nakamae, K.; Hoffman, A. S. *J. Controlled Release* **1997**, *49*, 167-176.

(37) Bae, Y. H.; Okano, T.; Kim, S. W. *Macromol. Chem., Rapid Commun.* **1987**, *8*, 481-485.

(38) am Ende, M. T.; Hariharan, D.; Peppas, N. A. *Reactive Polymers* **1995**, *25*, 127-137.

(39) Lowman, A. M.; Peppas, N. A. *J. Biomater. Sci., Polym. Ed.* **1999**, *10*, 999-1009.

(40) Torres-Lugo, M.; Peppas, N. A. *Macromolecules* **1999**, *32*, 6646-6651.

(41) Yu, H.; Grainger, D. W. *J. Controlled Release* **1995**, *34*, 117-127.

(42) Chou, H. F.; Ipp, E. *Diabetes* **1990**, *39*, 112-117.

(43) Kagatani, S.; Shinoda, T.; Konno, Y.; Fukui, M.; Ohmura, T.; Osada, Y. *J. Pharm. Sci.* **1997**, *86*, 1273-1277.

(44) Park, T. G. *Biomaterials* **1999**, *20*, 517-521.

(45) Traitel, T.; Cohen, Y.; Kost, J. *Biomaterials* **2000**, *21*, 1679-1687.

(46) Guiseppi-Elie, A.; Brahim, S. I.; Narinesingh, D. *Adv. Mater. (Weinheim, Ger.)* **2002**, *14*, 743-746.

(47) Matsumoto, A.; Yoshida, R.; Kataoka, K. *Biomacromolecules* **2004**, *5*, 1038-1045.

(48) Zhang, Y.; Chu, C.-C. *J. Biomat. Appl.* **2002**, *16*, 305-325.

(49) Moriyama, K.; Yui, N. *J. Controlled Release* **1996**, *42*, 237-248.

(50) Moriyama, K.; Tooru, O.; Nobuhiko, Y. *J. Biomater. Sci., Polym. Ed.* **1999**, *10*, 1251-1264.

(51) Gehrke, S. H.; Uhden, L. H.; McBride, J. F. *J. Controlled Release* **1998**, *55*, 21-33.

(52) Elbert, D. L.; Pratt, A. B.; Lutolf, M. P.; Halstenberg, S.; Hubbell, J. A. *J. Controlled Release* **2001**, *76*, 11-25.

(53) Park, T. G.; Cohen, S.; Langer, R. *Macromolecules* **1992**, *25*, 116-122.

(54) Bos, G. W.; Jacobs, J. J. L.; Koten, J. W.; Van Tomme, S.; Veldhuid, T.; van Nostrum, C. F.; Den Otter, W.; Hennink, W. E. *Eur. J. Pharm. Sci.* **2004**, *21*, 561-567.

(55) Cadee, J. A.; de Groot, C. J.; Jiskoot, W.; Den Otter, W.; Hennink, W. E. *J. Controlled Release* **2002**, *78*, 1-13.

(56) de Jong, S. J.; van Eerdenbrugh, B.; van Nostrum, C. F.; Kettenes-van den Bosch, J. J.; Hennink, W. E. *J. Controlled Release* **2001**, *71*, 261-275.

(57) Hennink, W. E.; Franssen, O.; van DijkWolthius, W. N. E.; Talsma, H. *J. Controlled Release* **1997**, *48*, 107-114.

(58) Hennink, W. E.; de Jong, S. J.; Bos, G. W.; Veldhuis, T. F. J.; van Nostrum, C. F. *Int. J. Pharm.* **2004**, *277*, 99-104.

(59) Park, K.; Kamath, K. R.; Park, H. *Polym. Prepr. (Am. Chem. Soc., Div. Polym. Chem.)* **1993**, *34*, 844-845.

(60) Kamath, K. R.; Park, K. *ACS Symposium Series* **1994**, *545*, 55-65.

(61) Kamath, K. R.; Park, K. *Polymer Gels and Networks* **1995**, *3*, 243-254.

(62) Kamath, K. R.; Park, K. *Int. J. Pharm. Advances* **1996**, *1*, 258-268.

(63) Wang, N.; Wu, X. S.; Li, J. K. *Pharm. Res.* **1999**, *16*, 1430-1435.

(64) Slager, J.; Domb, A. J. *Biomaterials* **2002**, *23*, 4389-4396.

(65) Hanes, J.; Chiba, M.; Langer, R. *Biomaterials* **1998**, *19*, 163-172.

(66) Chen, J.; Jo, S.; Park, K. *Carbohydr. Polym.* **1995**, *28*, 69-76.

(67) Bjork, E.; Edman, P. *Int. J. Pharm.* **1988**, *47*, 233-238.

(68) Bjork, E.; Edman, P. *Int. J. Pharm.* **1990**, *62*, 187-192.

(69) Edman, P.; Bjork, E.; Ryden, L. *J. Controlled Release* **1992**, *21*, 165-172.

(70) Farraj, N. F.; Johansen, B. R.; Davis, S. S.; Illum, L. *J. Controlled Release* **1990**, *13*, 253-261.

(71) Illum, L.; Farraj, N. F.; Fisher, A. N.; Gill, I.; Miglietta, M.; Benedetti, L. M. *J. Controlled Release* **1994**, *29*, 133-141.

(72) Andrianov, A. K.; Cohen, S.; Visscher, K. B.; Payne, L. G.; Allcock, H. R.; Langer, R. *J. Controlled Release* **1993**, *27*, 69-77.

(73) M., T.; Gref, R.; Sanchez, A.; Langer, R.; Alonso, M. J. *Pharm. Res.* **1998**, *15*, 270-275.

(74) Hirosue, S.; Muller, B. G.; Mulligan, R. C.; Langer, R. *J. Controlled Release* **2001**, *70*, 231-242.

(75) Kwong, A. K.; Chou, S.; Sefton, M. V. *J. Controlled Release* **1986**, *4*, 47-62.

(76) Soriano, I.; Evora, C.; Llabres, M. *Int. J. Pharm.* **1996**, *142*, 135-142.

(77) Leobandung, W.; Ichikawa, H.; Fukumori, Y.; Peppas, N. A. *J. Controlled Release* **2002**, *80*, 357-363.

(78) Damge, C.; Vranckx, H.; Balschmidt, P.; Couvreur, P. *J. Pharm. Sci.* **1997**, *86*, 1403-1409.

(79) Torres-Lugo, M.; Garcia, M.; Record, R.; Peppas, N. A. *J. Controlled Release* **2002**, *80*, 197-205.

(80) Torres-Lugo, M.; Garcia, M.; Record, R.; Peppas, N. A. *Biotechnol. Prog.* **2002**, *18*, 612-616.

(81) Morishita, M.; Lowman, A. M.; Takayama, K.; Nagai, T.; Peppas, N. A. *J. Controlled Release* **2002**, *81*, 25-32.

(82) Lowman, A. M.; Morishita, M.; Kajita, M.; Nagai, T.; Peppas, N. A. *J. Pharm. Sci.* **1999**, *88*, 933-937.

(83) Podual, K.; Doyle III, F. J.; Peppas, N. A. *Biomaterials* **2000**, *21*, 1439-1450.

(84) Kim, B.; Peppas, N. A. *Int. J. Pharm.* **2003**, *266*, 29-37.

(85) Nakamura, K.; Murray, R. J.; Joseph, J. I.; Peppas, N. A. *J. Controlled Release* **2004**, *95*, 589-599.

(86) Foss, A. C.; Goto, T.; Morishita, M.; Peppas, N. A. *Eur. J. Pharm. Biopharm.* **2004**, *57*, 163-169.

(87) Podual, K.; Doyle III, F. J.; Peppas, N. A. *Polymer* **2000**, *41*, 3975-3983.

(88) Lopez, J. E.; Peppas, N. A. *J. Biomat. Sci., Poly. Ed.* **2004**, *15*, 385-396.

(89) Morishita, M.; Takahiro, G.; Peppas, N. A. *J. Controlled Release* **2004**, *97*, 115-124.

(90) Foss, A. C.; Peppas, N. A. *Eur. J. Pharm. Biopharm.* **2004**, *57*, 447-455.

(91) Ichikawa, H.; Peppas, N. A. *J. Biomed. Mater. Res.* **2003**, *67A*, 609-617.

(92) Maulding, H. *J. Controlled Release* **1987**, *6*, 167-176.

(93) Crotts, G.; Sah, H.; Park, T. G. *J. Controlled Release* **1997**, *47*, 101-111.

(94) Park, T. G. *J. Controlled Release* **1994**, *30*, 161-173.

(95) Crotts, G.; Park, T. G. *J. Controlled Release* **1997**, *44*, 123-134.

(96) Park, T. G.; Lee, H. Y.; Nam, Y. S. *J. Controlled Release* **1998**, *55*, 181-191.

(97) Cho, K.; Choi, S. H.; Kim, C. H.; Nam, Y. S.; Park, T. G.; Park, J. K. *J. Controlled Release* **2001**, *76*, 275-284.

(98) Franssen, O.; Vandervennet, L.; Roders, P.; Hennink, W. E. *J. Controlled Release* **1999**, *60*, 211-221.

(99) Helmlinger, G.; Sckell, A.; Dellian, M.; Forbes, N. S.; Rakesh, K. J. *Clin. Cancer Res.* **2002**, *8*, 1284-1291.

(100) Trevani, S.; Andonegui, G.; Giordano, M.; Lopez, D.; Gamberale, R.; Minucci, F.; Geffner, J. R. *J. Immunol.* **1999**, *162*, 4849-4857.

(101) Goodner, C. J.; Walike, B. C.; Koerker, D. J.; Ensinck, J. W.; Brown, A. C.; Chideckel, E. W.; Palmer, J.; Kalnasy, L. *Science* **1977**, *195*, 177-179.

(102) Hansen, B. C.; Jen, K. C.; Belbez, P. S.; Wolfe, R. A. *J. Clin. Endocrinol. Metab.* **1982**, *54*, 785-792.

(103) Lang, D. A.; Matthews, D. R.; Burnett, M.; Turner, R. C. *Diabetes* **1981**, *30*, 435-439.

(104) Porksen, N.; Munn, S.; Steers, J.; Vore, S.; Veldhuis, J.; Butler, P. *Am. J. Physiol.* **1995**, *269*, E478-E488.

(105) Matthews, D. R.; Naylor, B. A.; Jones, R. G.; Ward, G. M.; Turner, R. C. *Diabetes* **1983**, *32*, 617-621.

(106) Santoro, N.; Filicori, M.; Crowley, W. F. *Endocrine Revs.* **1986**, *7*, 11-23.

(107) Siegel, R. A.; Colin, G. P. *J. Controlled Release* **1995**, *33*, 173-188.

(108) Kim, J. J.; Park, K. *J. Controlled Release* **2001**, *77*, 39-47.

(109) Dorkoosh, F. A.; Verhoef, J. C.; Ambagts, M. H. C.; Rafiee-Tehrani, M.; Borchard, G.; Junginger, H. E. *Eur. J. Pharm. Sci.* **2002**, *15*, 433-439.

(110) Watnasirichaikul, S.; Davies, N. M.; Rades, T.; Tucker, I. G. *Pharm. Res.* **2000**, *17*, 684-689.

(111) Stayton, P.; Hoffman, A. S.; Murthy, N.; Lackey, C. A.; Cheung, C.; Tan, P.; Klumb, L. A.; Chilkoti, A.; Wilbur, F. S.; Press, O. *J. Controlled Release* **2000**, *65*, 203-220.

(112) Hoffman, A. S.; Stayton, P.; Bulmus, V.; Chen, G.; Chen, J.; Cheung, C.; Chilkoti, A.; Ding, Z.; Dong, L.; Fong, R.; Lackey, C. A.; Long, C.; Miura, M.; Morris, J. E.; Murthy, N.; Nabeshima, Y.; Park, T. G.; Press, O.; Shimoboji, T.; Shoemaker, S.; Yang, H. J.; Monji, N.; Nowinski, R. C.; Cole, C. A.; Priest, J. H.; Harris, J. M.; Nakamae, K.; Nishino, T.; Miyata, T. *J. Biomed. Mater. Res.* **2000**, *52*, 577-586.

(113) Ding, Z.; Long, C.; Hayashi, Y.; Bulmus, E. V.; Hoffman, A. S.; Stayton, P. *Bioconj. Chem.* **1999**, *10*, 395-400.

(114) Bulmus, V.; Ding, Z.; Long, C.; Stayton, P.; Hoffman, A. S. *Bioconj. Chem.* **2000**, *11*, 78-83.

(115) Kyriakides, T. R.; Cheung, C.; Murthy, N.; Bornstein, P.; Stayton, P.; Hoffman, A. S. *J. Controlled Release* **2002**, *78*, 295-303.

(116) Chilkoti, A.; Chen, G.; Stayton, P.; Hoffman, A. S. *Bioconj. Chem.* **1994**, *5*, 504-507.

(117) Stayton, P.; Shimoboji, T.; Long, C.; Chilkoti, A.; Chen, G.; Harris, J. M.; Hoffman, A. S. *Nature* **1995**, *378*, 472-474.

(118) Murthy, N.; Robichaud, J. R.; Tirrell, D. A.; Stayton, P.; Hoffman, A. S. *J. Controlled Release* **1999**, *61*, 137-143.

(119) Lackey, C. A.; Murthy, N.; Press, O.; Tirrell, D. A.; Hoffman, A. S.; Stayton, P. *Bioconj. Chem.* **1999**, *10*, 401-405.

(120) Lackey, C. A.; Press, O.; Hoffman, A. S.; Stayton, P. *Bioconj. Chem.* **2002**, *13*, 996-1001.

(121) Cheung, C.; Murthy, N.; Stayton, P.; Hoffman, A. S. *Bioconj. Chem.* **2001**, *12*, 906-910.

(122) Bulmus, V.; Woodward, M.; Lianne, L.; Murthy, N.; Stayton, P.; Hoffman, A. S. *J. Controlled Release* **2003**, *93*, 105-120.

(123) Murthy, N.; Campbell, J.; Fausto, N.; Hoffman, A. S.; Stayton, P. *J. Controlled Release* **2003**, *89*, 365-374.

(124) Brown, C. D.; Kreilgaard, L.; Nakakura, M.; Caram-Lelham, N.; Pettit, D. K.; Gombotz, W. R.; Hoffman, A. S. *J. Controlled Release* **2001**, *72*, 35-46.

(125) Kidane, A.; Sxabocsik, J. M.; Park, K. *Biomaterials* **1998**, *19*, 2051-2055.

(126) Caliceti, P.; Salmaso, S.; Lante, A.; Yoshida, M.; Katakai, R.; Martellini, F.; Mei, L. H. I.; Carneza, M. *J. Controlled Release* **2001**, *75*, 173-181.

(127) Kofuji, K.; Akamine, H.; Oshirabe, H.; Maeda, Y.; Murata, Y.; Kawashima, S. *J. Biomat. Sci., Poly. Ed.* **2003**, *14*, 1243-1253.

(128) Brown, L.; Edelman, E. R.; Fischel-Ghodsian, F.; Langer, R. *J. Pharm. Sci.* **1996**, *85*, 1341-1345.

(129) Edelman, E. R.; Brown, L.; Langer, R. *J. Pharm. Sci.* **1996**, *85*, 1271-1275.

(130) Albin, G.; Horbett, T. A.; Ratner, B. D. *J. Controlled Release* **1985**, *2*, 153-164.

(131) Tuovinen, L.; Peltonen, S.; Jarvinen, K. *J. Controlled Release* **2003**, *91*, 345-354.

(132) Zhang, J.; Chua, L. S.; Lynn, D. M. *Langmuir* **2004**, *20*, 8015-8021.

(133) Rabanel, J. M.; Hildgen, P. *J. Microencapsulation* **2004**, *21*, 413-431.

(134) Morris, J. E.; Hoffman, A. S.; Fisher, R. R. *Biotech. Bioeng.* **1993**, *41*, 991-997.

(135) Nakamae, K.; Miyata, T.; Jikihara, A.; Hoffman, A. S. *J. Biomater. Sci., Polym. Ed.* **1994**, *6*, 79-90.

(136) Miyata, T.; Jikihara, A.; Nakamae, K.; Hoffman, A. S. *Macromol. Chem. Phys.* **1996**, *197*, 1135-1146.

(137) Lee, S. J.; Park, K. *Polym. Prepr. (Am. Chem. Soc., Div. Polym. Chem.)* **1994**, *35*, 391-392.

(138) Obaidat, A. A.; Park, K. *Pharm. Res.* **1996**, *13*, 989-995.

(139) Obaidat, A. A.; Park, K. *Biomaterials* **1997**, *18*, 801-806.

(140) Kim, J. J.; Park, K. *Pharm. Res.* **2001**, *18*, 794-799.

(141) Zou, X.; Siegel, R. A. *J. Chem. Phys.* **1999**, *110*, 2267-2279.

(142) Dhanarajan, A. P.; Misra, G. P.; Siegel, R. A. *J. Phys. Chem. A* **2002**, *106*, 8835-8838.

(143) Misra, G. P.; Siegel, R. A. *J. Controlled Release* **2002**, *79*, 293-297.

(144) Dhanarajan, A. P.; Misra, G. P.; Siegel, R. A. *Polymer Preprints* **2002**, *43*, 808-809.

(145) Kost, J.; Horbett, T. A.; Ratner, B. D.; Singh, M. J. *Biomed. Mater. Res.* **1985**, *19*, 1117-1133.

(146) Kataoka, K.; Miyazaki, H. T.; Bunya, M.; Okano, T.; Sakurai, Y. *J. Am. Chem. Soc.* **1998**, *120*, 12694-12695.

(147) Siegel, R. A.; Gu, Y.; Bladi, A.; Ziaie, B. *Macromol. Symp.* **2004**, *207*, 249-256.

(148) Yeo, Y.; Park, K. *Arch. Pharm. Res.* **2004**, *27*, 1-12.

CHAPTER 3

THERMALLY MODULATED INSULIN RELEASE FROM MICROGEL THIN FILMS

In this chapter we present results on the construction and characterization of insulin impregnated microgel thin films for controlled pulsatile release applications. Our aim was to effectively load a model peptide, insulin, into poly(*N*-isopropylacrylamide-*co*-acrylic acid) (pNIPAm-*co*-AAc) microgels and then build up multi-layer thin films in a uniform manner through Layer-by-Layer (LbL) polyelectrolyte assembly. We hoped to achieve extended, cyclical release of the peptide while tunability over the quantity of macromolecule pulsed out was explored by controlling the release temperature and film thickness. We also rationalized the mechanism of release by studying the deswelling and delivery kinetics of these novel films. We hypothesize that film thermoresponsivity plays an important role in that subjection to many thermal cycles enables the embedded peptide to solubilize and subsequently partition through film layers. These insulin-impregnated films are extremely stable with the potential to release constant pulses of peptide for more than one month at a time. These studies indicate that these highly robust peptide loaded microgel thin films show great potential in future drug delivery design.

3.1 Introduction

As discussed previously, great strides have been made in the fields of controlled and targeted drug delivery utilizing hydrogel materials, with pNIPAm being one of the most heavily studied thermosensitive gels.[1] Because of their high water content, soft

tissue-like consistency, and potential biocompatibility[2-6] significant work has focused on using responsive gels as carriers for peptide delivery, among which many studies have focused on hydrogel insulin release systems.[7-12] Another field of research that has found great popularity in biotechnology is that of polyelectrolyte multi-layer thin films.

The buildup of multi-layer thin films is typically achieved through a Layer-by-Layer (LbL) assembly process, first introduced by Decher,[13] where oppositely charged polyelectrolytes are deposited in an alternating-charge fashion.[14] A schematic representing this protocol is shown in Figure 3-1. Traditionally, a substrate is functionalized with some polyelectrolyte to yield it multiply charged. In this case, it is positively charged and this can be achieved by exposure to 3-Aminopropyltrimethoxysilane (APTMS). In step 1, this charged substrate is exposed to a polyelectrolyte solution of opposite charge, which adsorbs to the surface via electrostatic attractive forces, resulting in charge reversal. This step is key for true multi-layer buildup and relies upon the fact that the molecules in solution are multiply charged. In step 2, the substrate is once again exposed to an oppositely charged polyion solution. These steps can be repeated as many times as one desires to achieve as many layers as needed.[15] A well studied polycation has been poly(allylamine hydrochloride) (PAH) while a heavily explored polyanion has been poly(styrene sulfonate) (PSS).[15] A diagram illustrating the molecular structure of these common polyelectrolytes is shown in Figure 3-2.

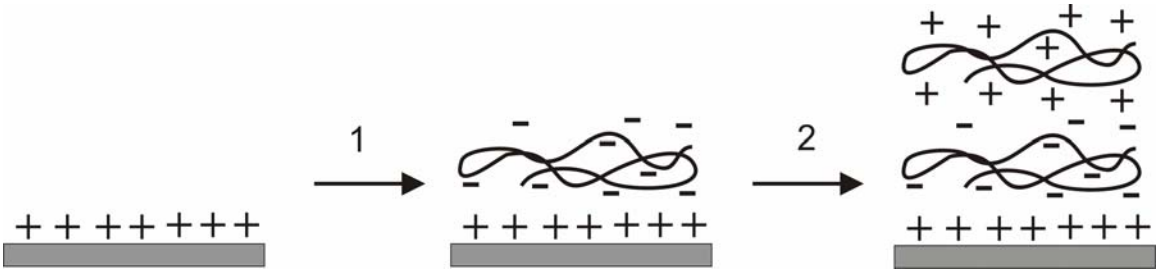

Figure 3-1. Schematic representing traditional Layer-by-Layer (LbL) assembly of electrostatically bound polyelectrolyte films. In step 1, a polyanionic species is deposited onto a positively charged substrate, resulting in charge reversal. In step 2, an oppositely charged polycationic species is deposited onto the negatively charged surface. These steps can be repeated as many times as desired to build up films of any desired thickness.

The advantages of this technology are numerous and include short preparation time, precise control over polycation–polyanion complexes at the molecular level, minimal sample volume and control over the composition, and surface functionality of these materials in three dimensions. Other advantages to this technique are that it is inexpensive, simple, and versatile.[16] Thus, this technique has been commonly explored for fabrication of various polymer based thin films.[17-24] Furthermore, it has found many applications in the biosciences including the work of Caruso and co-workers, wherein they have prepared hollow polyelectrolyte capsules by depositing oppositely charged polyelectrolytes onto a sacrificial core template.[25] These hollow capsules can in theory serve as drug containers for applications in drug or gene delivery. The use of polyelectrolyte multi-layer thin films for the uptake and release of small model drug compounds has also been successfully explored.[26,27] Deposition of biological species

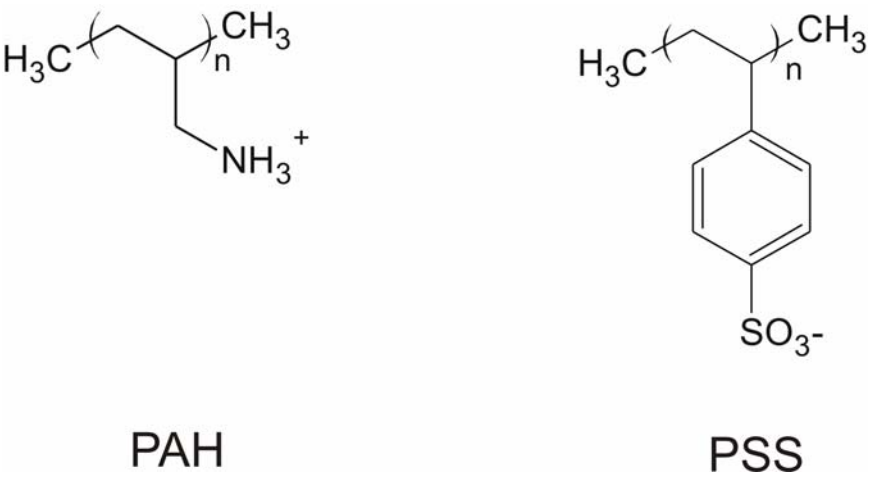

Figure 3-2. Chemical structures for commonly used polyelectrolytes. Poly(allylamine hydrochloride) (PAH) is a common cationic polyelectrolyte while poly(styrene sulfonate) (PSS) is a common anionic polyelectrolyte.

within thin films themselves has also been studied,[28-34] with the main proposed application being biosensing.[28] Direct encapsulation of bioactive species within polyelectrolyte shells has been pursued wherein oppositely charged polyelectrolyte layers are deposited onto charged core crystals.[35,36] Other work done by Sukhorukov et al. extended these studies to tuning the permeability of hollow polyelectrolyte shells to encapsulate macromolecular species based on pH-dependent changes in shell porosity.[37-39] The versatility of these systems can be enhanced by adding functionally modified materials to them and are not limited to polyelectrolytes alone. Inclusion of nano-objects such as inorganic and metal colloidal nanoparticles has been pursued.[40-44] Work done earlier in our group showed that incorporation of discrete thermoresponsive microgels could be achieved in order to build up thermosensitive polymeric thin films.[45] With this

knowledge, we wanted to add increased functionality to polymeric thin films and investigate their capabilities toward the regulation of macromolecule delivery.

3.2 Experimental Section

Materials

All chemicals were obtained from Sigma Aldrich unless otherwise stated. *N*-Isopropylacrylamide (NIPAm) was recrystallized from hexane (J. T. Baker) prior to use. *N*, *N*′-Methylene(bisacrylamide) (BIS), ammonium persulfate (APS), anhydrous acrylic acid (AAc; Fluka), hydrochloric acid (J. T. Baker), 95% ethanol, 200 proof anhydrous ethanol, sodium hydroxide (NaOH), formic acid (J. T. Baker), 70, 000 MW poly(allylamine hydrochloride) (PAH), fluorescein isothiocyanate labeled insulin (FITC-insulin) from bovine pancreas, sodium chloride, and potassium dihydrogenphosphate were used as received. 3-Aminopropyltrimethoxysilane (APTMS) was obtained from United Chemical Technologies. Anhydrous dibasic sodium phosphate was purchased from EM Science. Glass microscope coverslips (22 × 22 mm) were purchased from Fisher Scientific. 0.2 μm nylon membrane disks and Spectra/Por 10, 000 MWCO dialysis membrane were purchased from VWR. Water used in all experiments was distilled and then purified using a Barnstead E-Pure system operating at a resistance of 18 MΩ. A 0.2 μm filter was incorporated into this system to remove particulate matter.

Particle Synthesis

Microgels of 1 mole % BIS cross-linked pNIPAm-*co*-AAc (9:1) were synthesized by free-radical precipitation polymerization via a method slightly modified from that previously described.[46] The total monomer concentration was 100 mM, no surfactant was

used, and APS was used as the free radical initiator. The NIPAm monomer and BIS cross-linker were dissolved in 100 mL of nanopure water and then continuously stirred in a three-neck, 200 mL round-bottom flask. This solution was heated to 70 °C while being purged with N_2 gas. Approximately 1 hour later, the temperature of the solution was stable at 70 °C. To this hot solution, the acrylic acid comonomer was added. Fifteen minutes later, the reaction was initiated by adding a hot (70 °C) 35 mg/mL solution of APS (1 mM final concentration). The solution turned turbid within 10 minutes, indicating successful initiation. The reaction proceeded for 6 hours under a constant stream of nitrogen. Following synthesis, the microgels were filtered using a P2 Whatman filter paper and then dialyzed (using 10, 000 MWCO) for 2 weeks against nanopure water with a daily exchange of fresh water.

Dynamic Light Scattering (DLS)

Hydrodynamic radii and light scattering intensities were obtained by DLS (Protein Solutions, Inc.). The 10 mM solutions of pH 3.5, 4.3, and 6.5 were first prepared using the appropriate buffer systems (formate and phosphate). Prior to analysis, the purified microgels were diluted in filtered media (using 0.2 μm filters) until a count rate of 250 kCt/s was obtained. The suspensions were then held at each temperature for 10 minutes to achieve thermal equilibration before measurements were taken. Longer equilibration times did not result in variations of particle radius, polydispersity, or light scattering intensity. The data points presented here are an average of 25 measurements with a 5 second acquisition time and a signal-to-noise ratio threshold of 2.5. Hydrodynamic radii were calculated from the measured diffusion coefficients using the

Stokes–Einstein equation. All correlogram analyses were performed with manufacturer-supplied software (Dynamics v.5.25.44, Protein Solutions, Inc.).

Microgel Loading of FITC-insulin

A FITC-insulin stock solution was prepared by dissolving approximately 3 mg of FITC-insulin in 1.5 mL of 0.1 N HCl. This was done because insulin is most soluble under acidic conditions.[10] This stock solution was then mixed with 10 mL of the 1 mole % BIS cross-linked p(NIPAm-*co*-AAc) (9:1) microgels, and the pH was adjusted to 7.4 by slow addition of 0.1 M NaOH. This solution was left to stir in the refrigerator overnight in the dark. It should be noted that insulin and/or FITC-insulin can also be completely dissolved in 25 mM pH 3.5 formate buffer so milder, less harsh acidic conditions can be utilized.

Thin Film Deposition and Buildup Characterization

Spin coating was used to build up the multi-layer thin films. This technique was used, as opposed to passive adsorption, to achieve uniform films within a short time frame. Glass microscope slides were used as the substrates and were cleaned by placing in a plasma cleaner using argon gas (Harrick Plasma Cleaner/Sterilizer PDC-32G) for 10 minutes. After this treatment the slides were rinsed with 200 proof anhydrous ethyl alcohol. APTMS was then used to amine-functionalize the glass slides. The slides were immersed in a 0.4 % APTMS solution (in 200 proof ethanol) at room temperature for 2 hours, and were then rinsed with 95 % ethanol to remove excess/unreacted silane. The slides were stored in 95 % ethanol until use. Prior to spin coating, an amine-functionalized slide was rinsed well with nanopure water and then dried with nitrogen gas. The slide was positioned on the spin coater (Speedline Technologies, Spincoater,

P6700 Series) vacuum chuck as illustrated in Figure 3-3. The rotor speed was maintained at 3, 000 rpm during deposition.

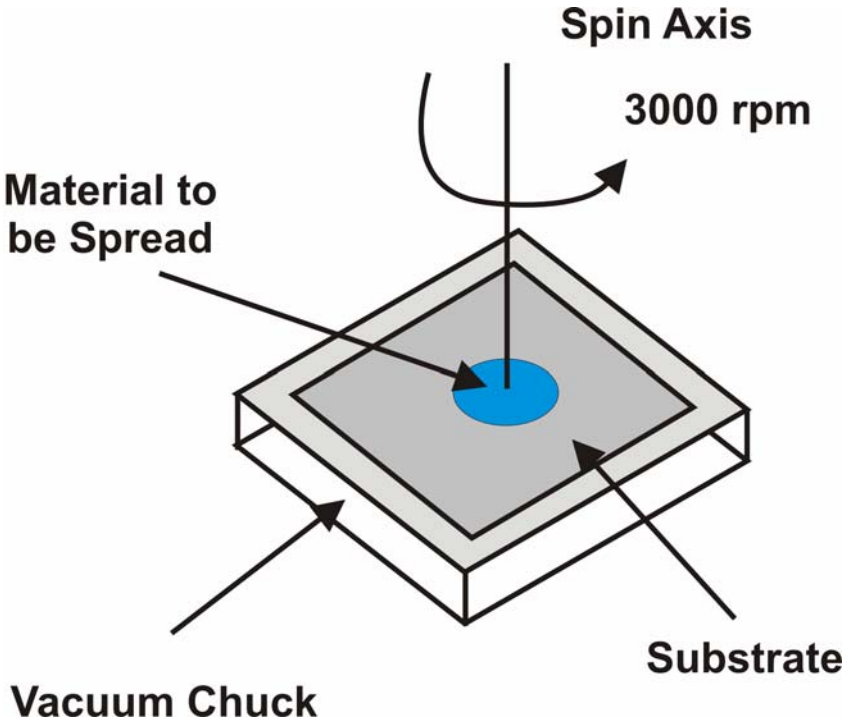

Figure 3-3. Schematic of the spin coating process. A substrate is placed on the vacuum chuck of the spin coater. While the substrate is rotating at high speed, the solution to be deposited is dropped on the center of the substrate. Upon impact at this high speed, the solution immediately spreads uniformly over the surface.

Deposition of one bilayer consisted of depositing 5 drops of the FITC-insulin loaded 1 mole % BIS cross-linked p(NIPAm-*co*-AAc) (9:1) microgels (pH 7.4), rinsing with nanopure water, depositing 5 drops of a 4.0×10^{-5} M PAH solution, and then rinsing with

water. After each step, 45 seconds was allowed to pass to ensure adequate removal of excess water. In this fashion, films made up of 3, 6, 9 and 30 layers were deposited. To achieve more uniform buildup, it was observed that after the 45 seconds passed, if the film was left spinning on the spin coater for two minutes before the next layer was deposited, enhanced linear buildup resulted. It was also noted that it was key to have the FITC-insulin loaded microgel solution, as well as the PAH solution, at equilibrated room temperature to ensure optimal deposition (no splattering of the solution off of the substrate). To monitor the buildup of these multi-layer thin films, UV/vis spectroscopy was employed. After each bilayer of a film was deposited, the absorbance of the film was taken in the wavelength range of 400-600 nm using a bare glass slide as a reference.

Optical Microscopy

To ascertain effective macromolecule loading into the microgels, as well as qualitative evaluation of peptide content after release cycles, fluorescence microscopic images of the FITC-insulin loaded films were taken using an Olympus IX-70 inverted microscope equipped with a mercury arc lamp. Images were captured using a color CCD camera (Pixel Fly, Cooke Corp.) and an Olympus 100x UplanFl 1.30 NA oil immersion objective. Scanning electron microscopy (SEM) images were also obtained for a 1 layer film with the aid of Dr. Michael Serpe.

Thermoresponsivity Light Scattering Studies

A steady state fluorescence spectrophotometer (Photon Technology International) equipped with a Model 814 PMT photon-counting detector was used to record scattered light at an angle of 90° as a function of temperature. The temperature was controlled using a PE 60 temperature controller Peltier stage (Linkam Scientific Instruments Ltd.,

Surrey, UK). A rectangular piece of the film was placed diagonally in the cuvette sitting inside the fluorimeter such that the film face was at a 45° angle with respect to both the source and the detector. A schematic representing this setup is shown in Figure 3-4.

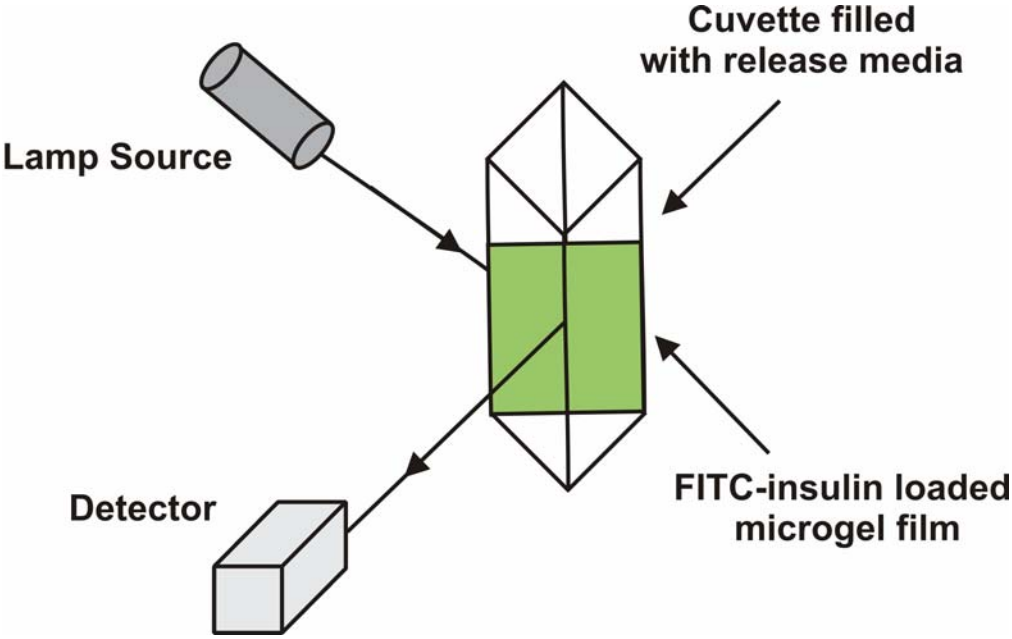

Figure 3-4. Schematic of light scattering setup for thermoresponsivity measurements of FITC-insulin loaded microgel thin films. The detected light is 90 ° from the incident light.

The cuvette was filled with 3.5 mL of 0.02 M PBS, and scattered light intensity of the film was monitored at the desired temperature until equilibration of the signal was reached. The slit widths were set to a bandwidth of 2 nm while the excitation and emission monochromators were each set to pass 600 nm light.

Drug Release Studies

For direct release investigations, a rectangular piece of an insulin-impregnated microgel thin film (10 × 22 mm) was carefully mounted to the side of the cuvette (as shown in Figure 3-5) that was filled with 1.35 mL of release medium (0.02 M PBS). This solution was constantly stirred at 220 rpm to maintain a homogeneous solution. The fluorescence emission of the release medium was monitored using an excitation wavelength of 473 nm and an emission wavelength of 512 nm. Thermally induced pulsatile release was monitored at 25, 37 and 40 °C.

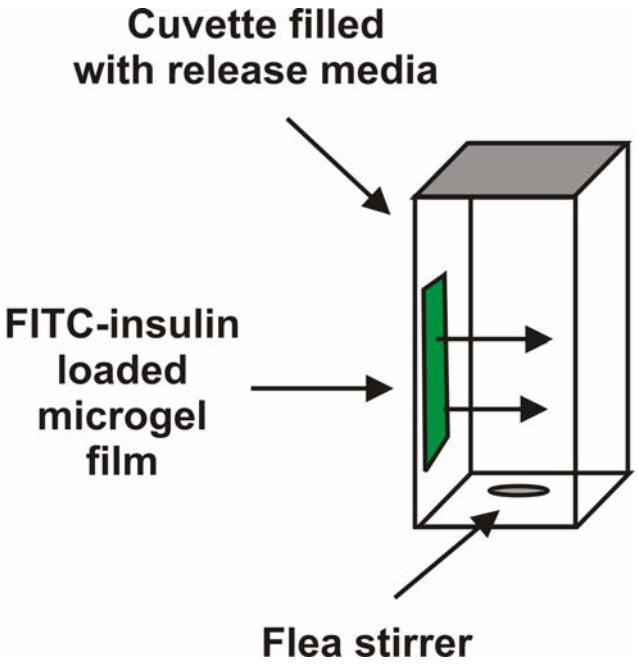

Figure 3-5. Experimental setup for direct detection of insulin release from microgel thin films via fluorescence spectroscopy.

To test the robustness of these films under extended release conditions, the FITC-insulin loaded films were placed in 4 mL of 0.02 M PBS. These films were left in the cold medium (25 °C) for 1 hour, the medium was then fully replaced, and the films were placed in a 40 °C hot bath for the same length of time; the cycle was then repeated. This was done every weekday for 1 month. The release medium samples were then analyzed via fluorescence spectroscopy using an excitation wavelength of 473 nm and an emission wavelength of 512 nm, to obtain cumulative release profiles.

3.3 Results and Discussion

Particle synthesis and characterization

As described above, p(NIPAm-*co*-AAc) (9:1) microgels containing 1 mole % BIS as the cross-linker were chosen for construction of the insulin-loaded films. The main monomer, NIPAm, imparts thermoresponsivity to these particles, while the comonomer, acrylic acid, imparts pH sensitivity and a negative charge to the microgels. Characterization of hydrodynamic radius as a function of pH and temperature was performed using DLS. Panel a of Figure 3-6 illustrates the volume phase transition behavior of these microgels at three different pH values. At pH 3.22 (open circles), the microgels have an average hydrodynamic radius of 280 nm at low temperatures, and then undergo a sharp volume phase transition at approximately 31 °C to a minimum hydrodynamic radius of 80 nm. This corresponds well with the LCST of typical pNIPAm microgels.[1] At this pH, the system is below the p*K*a of the acrylic acid groups, which is approximately 4.26, and almost all of the acid groups within the microgels are protonated. When the pH of the system is increased to the p*K*a (open squares),

approximately half of the acid groups are deprotonated, causing osmotic swelling as well as Coulombic repulsion between negatively charged groups in the particle. This results in a size increase to 405 nm at 25 °C. Under these conditions the system still deswells to about the same size that it did under pH 3.22 conditions upon increasing the temperature. The LCST, however, has been shifted to a higher temperature and the transition itself is somewhat broadened. This is due to the increased hydrophilicity of the system, resulting from an increased amount of negatively charged acid groups that can accommodate increased water solvation.[47-50] At a pH value of 6.15, well above the p*K*a (open triangles), almost all of the acid groups are deprotonated and hence there exists tremendous osmotic swelling and Coulombic repulsion between the negatively charged AAc moieties. This results in essentially no observable phase transition within the temperature range of 22–42 °C. This type of behavior, where greater swelling ratios result from increased hydrophilicity of the network, is common hydrogel behavior.[47-50] Panel b of Figure 3-6 shows the corresponding light scattering profiles of the same systems at different pH values. Under all three pH conditions, the microgels show very little scattered light intensity at low temperatures below the corresponding LCST values. This is due to the fact that these porous microgel networks are highly solvent swollen (approximately 95% water by volume) and are, therefore, nearly index matched to their environment. When the microgels collapse into dense globules at temperatures above the LCST, however, the microgels display a higher scattering cross section, and therefore, a dramatic increase in scattered light intensity is observed from the suspensions above the LCST.

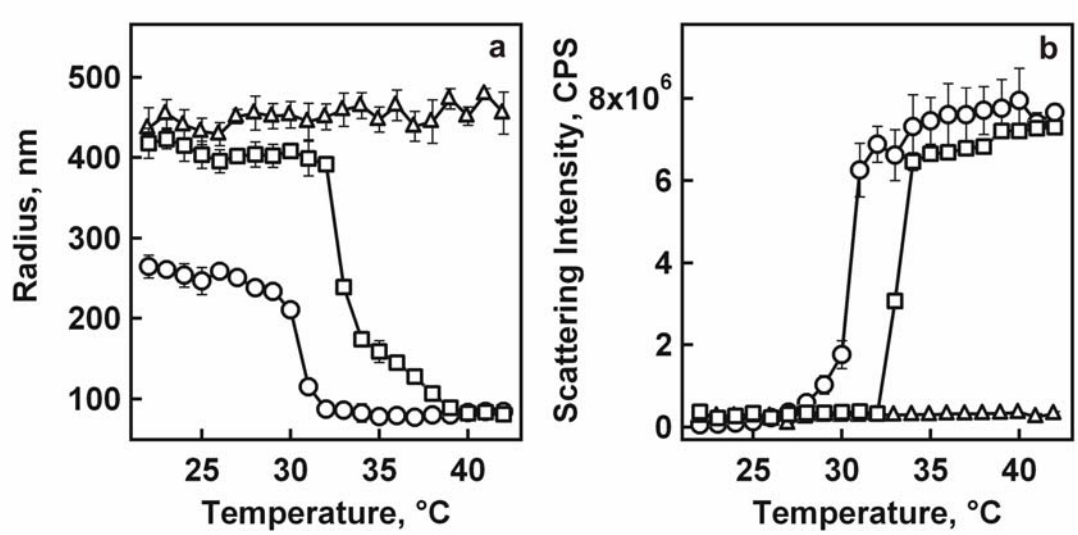

Figure 3-6. (a) Volume phase transition curves for 1 mole % BIS cross-linked p(NIPAm-*co*-AAc) (9:1) microgels and (b) light scattering profiles in pH 3.22 (open circles), pH 4.37 (open squares), and pH 6.15 (open triangles) 10 mM media.

Impregnation of Microgels with FITC-Insulin

These multi-responsive microgels were passively loaded with a concentrated solution of a therapeutic agent, FITC labeled insulin. The molecular formula of insulin is shown in Figure 3-7 below. It consists of 51 amino acids with 21 residues on the A chain, 30 residues on the B chain and includes two disulfide bridges. It has an overall molecular weight of 5, 800 Daltons, has an isoelectric point (pI) of 5.6 and hence, is zwitterionic.[51] In the loading procedure, we take advantage of the pH responsivity of these microgels as well as the pH-dependent solubility of insulin. Insulin is only sparingly soluble at neutral pH values but is quite soluble under acidic conditions. Thus, it was first dissolved in 0.1 N HCl to prepare the stock solution.[7] This solution was then

mixed with 10 mL of the microgel solution. Slow addition of NaOH was used to gradually increase the pH to 7.4. Upon increasing the pH of this solution, the microgels increase in size due to osmotic swelling and Coulombic repulsion between deprotonated acid groups. This pH switch allows for the microgels to become more porous as well as the insulin solubility in water to decrease. The overall effects that supposedly propel insulin partitioning into the microgel networks are an amalgamation of its low water solubility[52] as well as hydrophobic effects and electrostatic interactions (at pH 7 insulin is zwitterionic).[53] At pH 7.4, both the insulin and the microgels are overall negatively charged. This allows for the FITC-insulin loaded microgels to serve as a polyanion for polyelectrolyte multi-layer deposition.

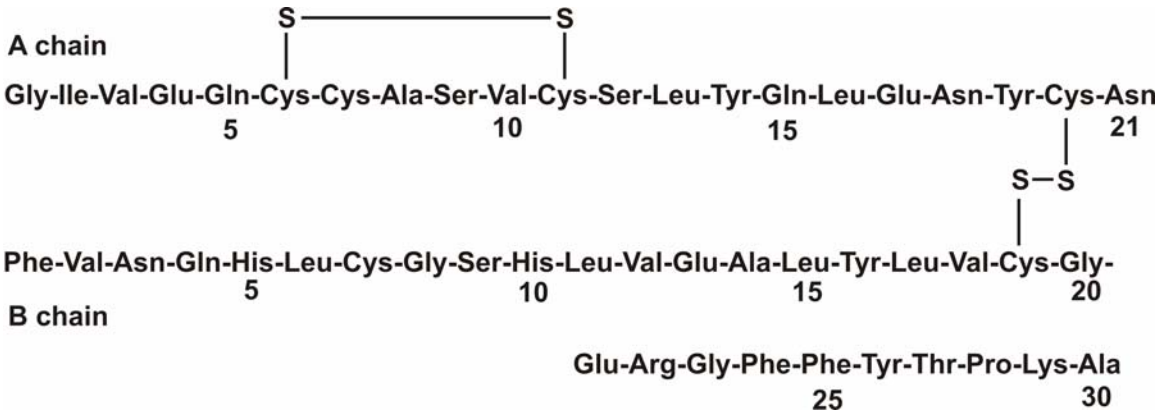

Figure 3-7. Primary structure of insulin.

Deposition and characterization of FITC-insulin loaded microgel thin films

To prepare the FITC-insulin loaded microgel thin films, the traditional charge-based alternate layer deposition protocol was followed. Glass substrates were first functionalized with 3-aminopropyltrimethoxysilane (APTMS) solution to make them cationic. Films were then deposited by spin coating as described above. Work done previously in our group has demonstrated that p(NIPAm-*co*-AAc) (9:1) particles can be used as the anionic component in film assembly.[45] Hence, negatively charged, insulin-impregnated microgels served as the polyanionic layer to which poly(allylamine hydrochloride) (PAH) was then deposited as a polycationic layer. A schematic depicting a 3 layer FITC-insulin loaded microgel film construct is shown below in Figure 3-8.

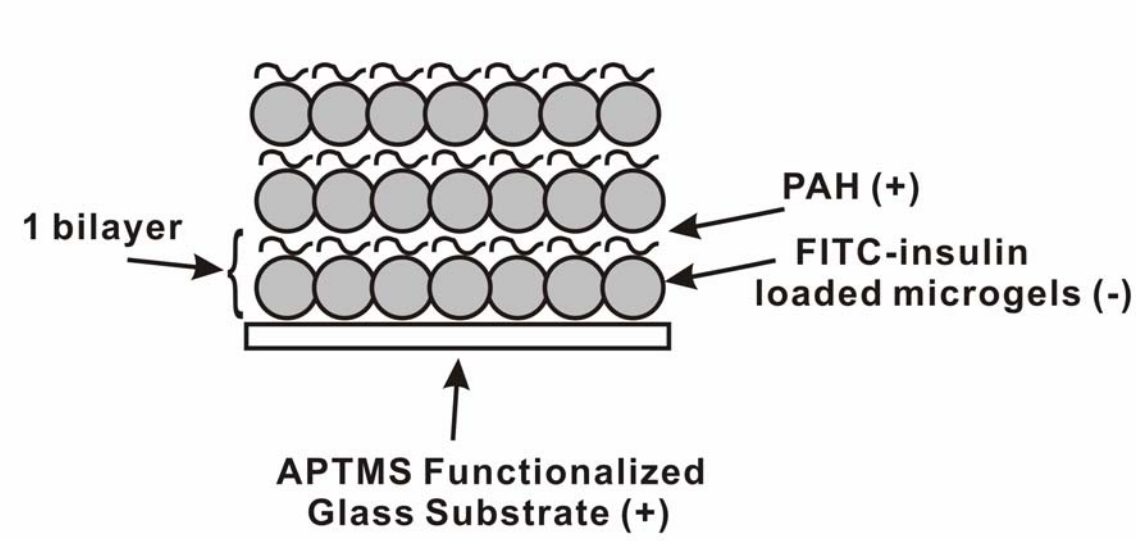

Figure 3-8. Schematic representation of the structure of a 3 layer film where 1 bilayer consists of negatively charged FITC-insulin loaded microgels alternated with positively charged PAH.

Figure 3-9, panel a, illustrates an SEM image obtained for a 1 layer film. What should be noted here is that the microgels (which are depicted by the dark circles) appear oblong in shape and somewhat flattened. This is to be expected considering that these soft spheres were deposited using a high impact technique such as spin coating. Panel b of Figure 3-9 shows a fluorescence microscopic image of a 1 layer film. The strong fluorescence of the microgels, along with decreased background fluorescence, indicates that the FITC-insulin is effectively impregnated within the microgels while high particle packing density indicates uniform layer deposition. This uniform deposition, even for a 1 layer film, is in contrast to results observed earlier in our group, where passive adsorption led to low surface coverages.[45]

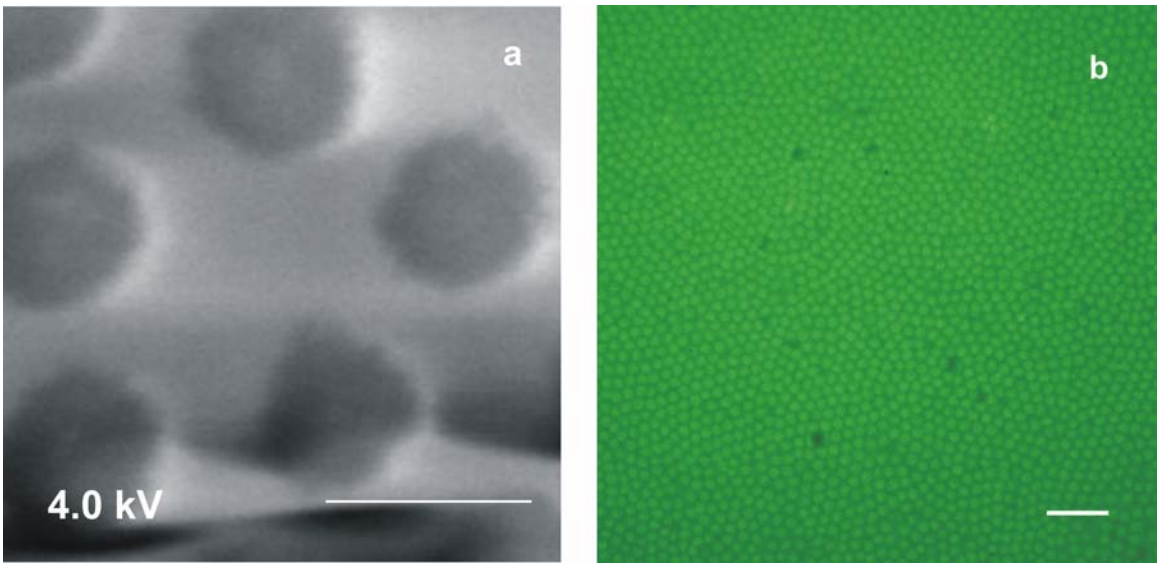

Figure 3-9. (a) SEM image and (b) fluorescence microscopic image of a 1 layer FITC-insulin loaded microgel thin film. The scale bars represent 1 μm and 10 μm for panels a and b, respectively.

Multi-layer Thin Film Buildup Confirmation

The linearity of film assembly was investigated using UV/vis spectroscopy. After one layer of a film was deposited, the absorbance of the film was taken in the wavelength range of 400–600 nm using a bare glass slide as a reference. Figure 3-10, panel a, shows a steady increase in film absorbance as the layer number increases. Panels b, c and d of Figure 3-10 confirm that this increase is linear as a function of film layer number for 3, 6 and 9 layer films, respectively. In this work, we chose to investigate the possibility of building up thicker films uniformly that could possibly release more effective amounts of insulin. The linearity of buildup for a thick 30 layer film was also probed using UV/vis spectroscopy and is shown in Figure 3-11. Panel a of Figure 3-11 again shows a monotonic growth in film absorbance as the layer number increases while panel b verifies that this increase is linear as a function of film layer number. These findings suggest that the FITC-insulin loaded microgel thin films are being built up in a uniform manner even for a 30 layer thick film.

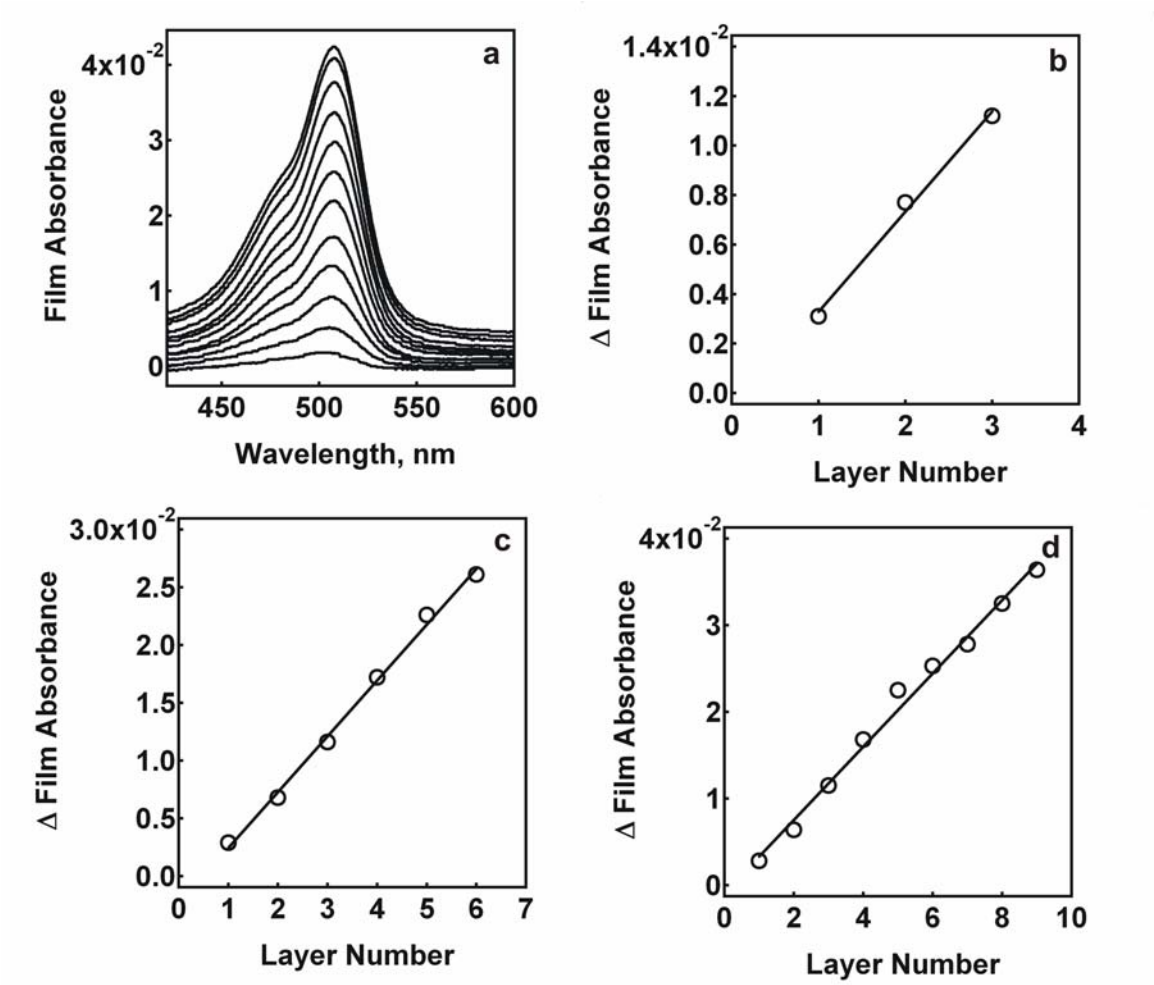

Figure 3-10. FITC-insulin loaded microgel thin film buildup confirmation. (a) Increase in film absorbance with increasing layer number. Plots of film absorbance versus layer number for a (b) 3 layer, (c) 6 layer and (d) 9 layer microgel thin film.

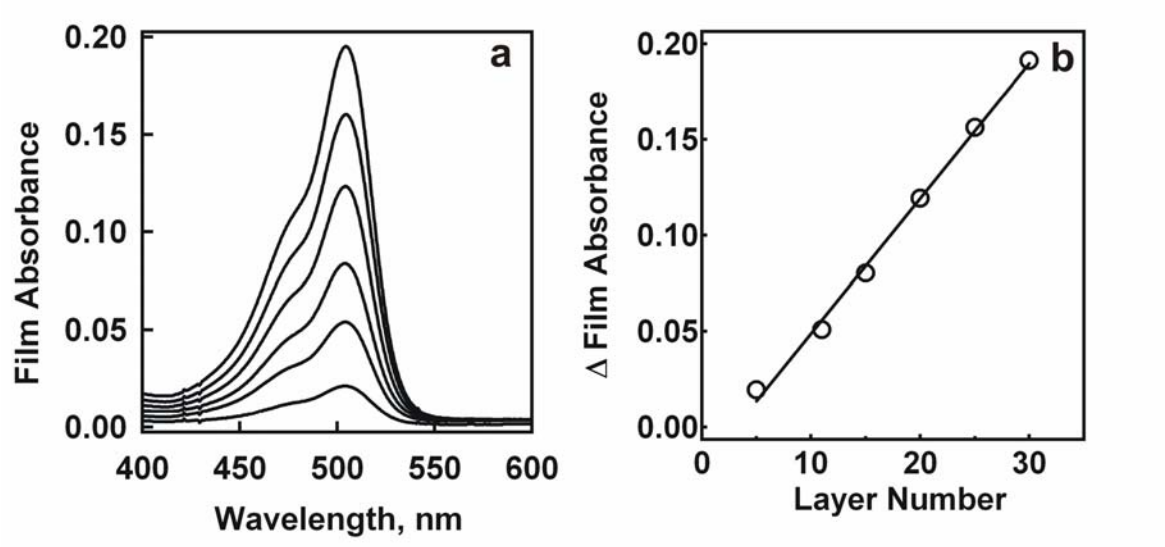

Figure 3-11. FITC-insulin loaded microgel thin film buildup confirmation for a 30 layer film. (a) Increase in film absorbance with increasing layer number. (b) Plot of film absorbance versus layer number.

Thermoresponsivity Studies of the Insulin Loaded Microgel Thin Films

The scope of this project relies on the hypothesis that release of macromolecule from microgel thin films can be controlled by utilizing the thermoresponsive nature of these films, considering the fact that these microgels are temperature sensitive in solution. Hence, thermoresponsivity of these films first needed to be proven. The setup for these experiments is detailed in the Experimental Section (see Figure 3-4). As described previously,[45] LbL films containing pNIPAm particles display a temperature-dependent opacity due to thermal deswelling of the component microgels at the LCST. To map out the phase transition behavior of these films, the scattered light intensity was measured as a function of bath temperature. Figure 3-12 illustrates the phase transition profiles

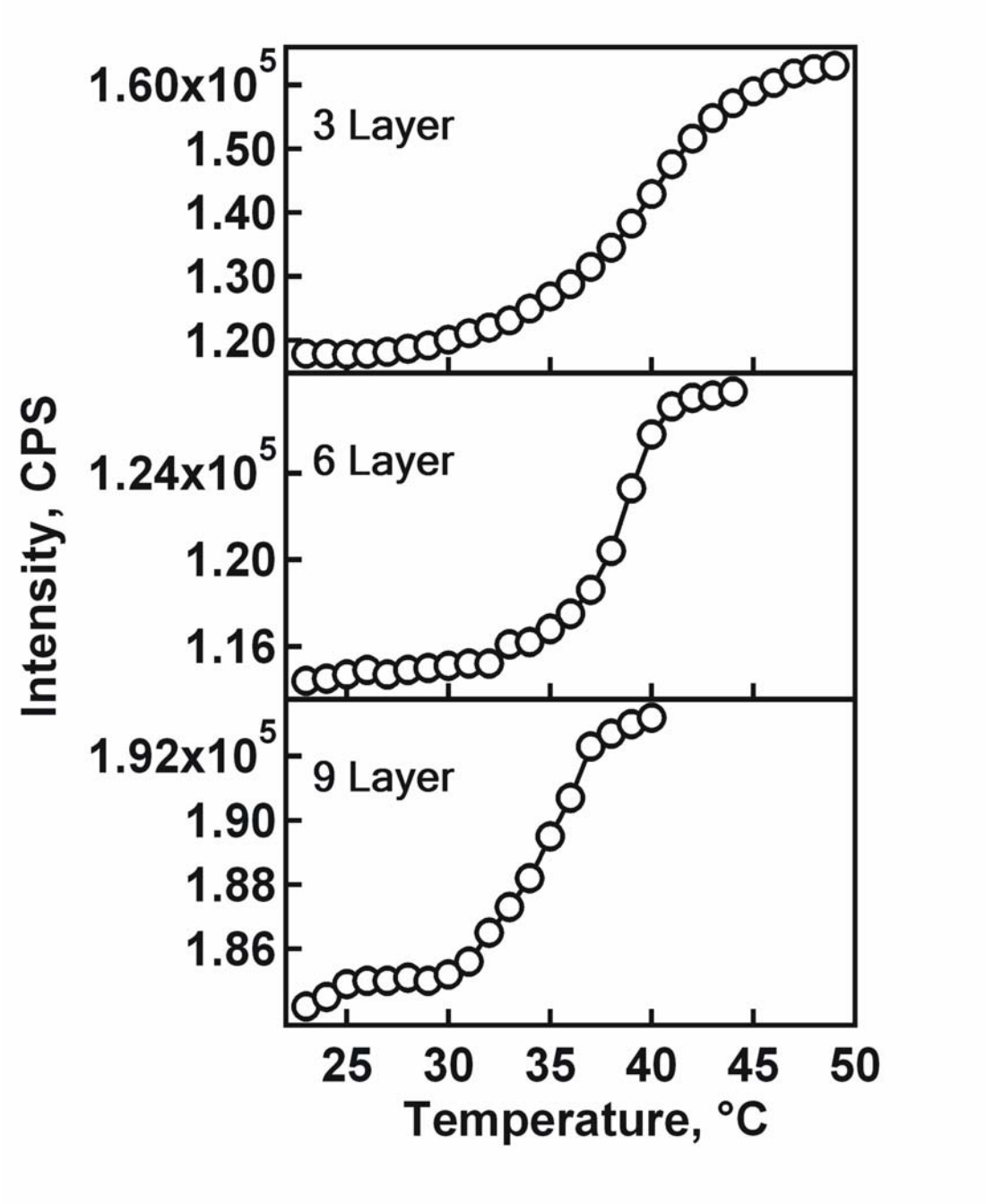

Figure 3-12. Phase transition curves for 3, 6 and 9 layer FITC-insulin loaded microgel thin films.

obtained for 3, 6, and 9 layer FITC-insulin loaded microgel thin films in 0.02 M PBS. In comparing the profiles shown in Figure 3-12, it is clear that the phase transition temperature (inflection point of the profile) decreases as the film layer number increases. Similar findings have been reported wherein the decreased phase transition temperatures for thicker films was ascribed to the relaxation of substrate effects on film behavior.[54] It is interesting to note that these films do indeed deswell at pH 7.4, despite the fact that the microgels themselves in high pH solution do not deswell within the temperature range of 22–42 °C (see Figure 3-6). We assume that the films collapse under these pH conditions due to partial or complete charge neutralization of the acrylic acid moieties within the microgels by the PAH chains.

To probe the possibility of these films to maintain thermally induced pulsatile release capabilities over many cycles, the thermoresponsivity of these films under these cyclical conditions was investigated by obtaining light scattering signals of the films in 0.02 M PBS at temperatures below and above the LCST of the microgels (25 and 40 °C). In panels a, b and c of Figure 3-13, the odd number cycles represent light scattering signals obtained at 25 °C while the even number cycles were values obtained at 40 °C. The values plotted represent equilibrated light scattering intensities. In all cases, the films show an increase in scattered light upon heating and a concurrent decrease in scattered light intensity upon film reswelling at 25 °C. These results indicate that these thermoresponsive films do show potential in thermally triggered pulsatile release. Furthermore, they suggest that they can potentially be used to effectively uptake media thereby, solubilizing the embedded drug and then can thermally pump out insulin in a regulated manner.

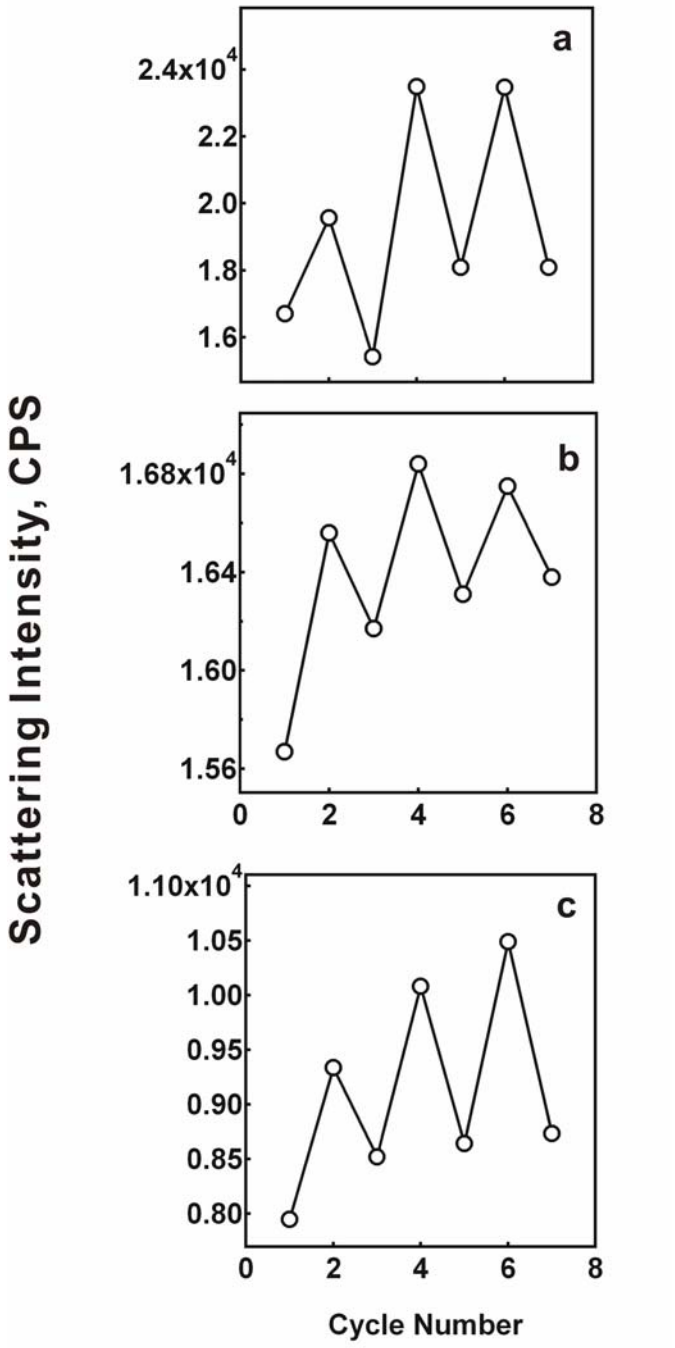

Figure 3-13. Light scattering thermoresponsivity plots for (a) 3 (b) 6 and (c) 9 layer FITC-insulin loaded microgel thin films in 0.02 M PBS with oscillating temperature. Odd cycle number = 25 °C, even cycle number = 40 °C.

Kinetic Studies

To probe the thermodynamic behavior of peptide release from these films, the correlation between film collapse and FITC-insulin pulsed release under hot conditions (40 °C) was investigated. Figure 3-14 shows plots of film light scattering intensity and insulin release versus time for 3 (panel a), 6 (panel b), and 9 layer (panel c) films. Some differences in film deswelling rates are observed as a function of thickness, with the six-layer film apparently deswelling more slowly than the three- and nine-layer films. However, it should be noted that measuring light scattering from the films is more correctly a measure of microstructure dimensions and refractive index contrast, as opposed to simply film dimension. Thus, there is some uncertainty as to the direct relationship between film thickness and scattering intensity. Nonetheless, the scattering changes give a semiquantitative picture of the changes in film morphology, and comparing these changes to the release kinetics offers some insight into the relationship between these two quantities. In all cases, the films deswell at a rate that is faster than the release of insulin. The slopes of the release profiles also appear to be somewhat linear during the initial stages of release. These results suggest that release of insulin from these films is not solely limited to the "pumping action" presumably associated with the collapse of the network, but is also regulated by solubility or partitioning effects. This type of permeability, governed by polymer hydration, has been previously observed for thermosensitive polymers.[55] In comparing the release profiles for the three-, six-, and nine-layer films, it is obvious that more FITC-insulin is released as the film increases in layer number. These findings suggest that the amount of peptide released can be tuned based on film layer thickness.

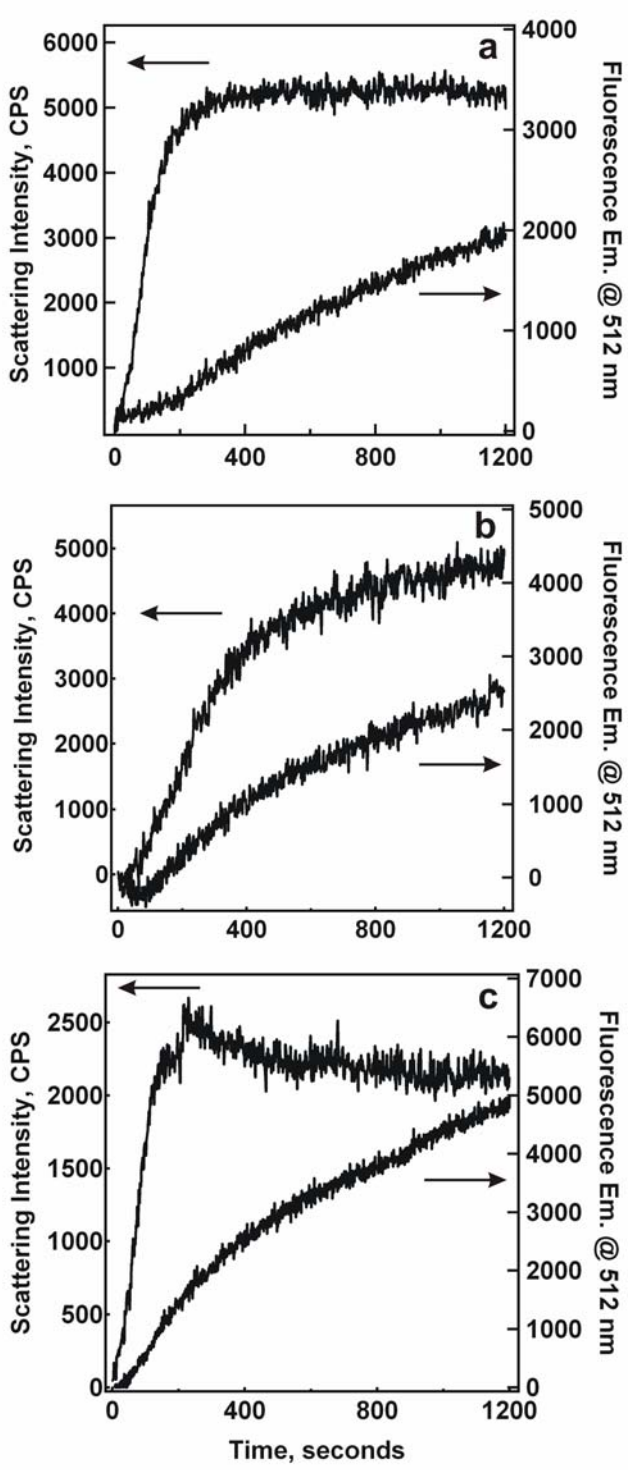

Figure 3-14. Profiles of deswelling (left axis) versus release (right axis) kinetics for (a) 3, (b) 6 and (c) 9 layer FITC-insulin loaded microgel thin films in 0.02 M PBS.

Investigation of Pulsatile Release Capabilities

To directly monitor the pulsatile release characteristics of these insulin-impregnated films, a rectangular piece of the film was mounted to the side of a fluorescence cuvette filled with 1.35 mL of 0.02 M PBS release medium. In this geometry, the film itself is located outside the beam path such that only the fluorescence of insulin released into the medium is detected (see Figure 3-5). The solution was constantly stirred at 220 rpm to maintain a homogeneous mixture. The fluorescence emission from the release medium was monitored at 512 nm as a function of time and temperature. Figure 3-15 shows the results obtained for direct release of FITC-insulin from a 9 layer film. The pink curves represent cold (25 °C) release, while the black curves represent hot (40 °C) release. At first, placing a freshly prepared dry film into cold media results in some insulin release, presumably from weakly adsorbed insulin molecules at the surface. However, after ramping the temperature to 40 °C, the amount of peptide released increases significantly. Upon full media replacement (indicated by dashed lines), the film displays almost zero insulin release upon reswelling at 25 °C. However, upon repeating the heating cycle, another fast burst of insulin is released. This thermal pulsing of insulin can be repeated over many cycles while the magnitude of release remains roughly constant. This ability to effectively turn off release under cold conditions and subsequently turn on release under hot conditions makes these model systems highly attractive.

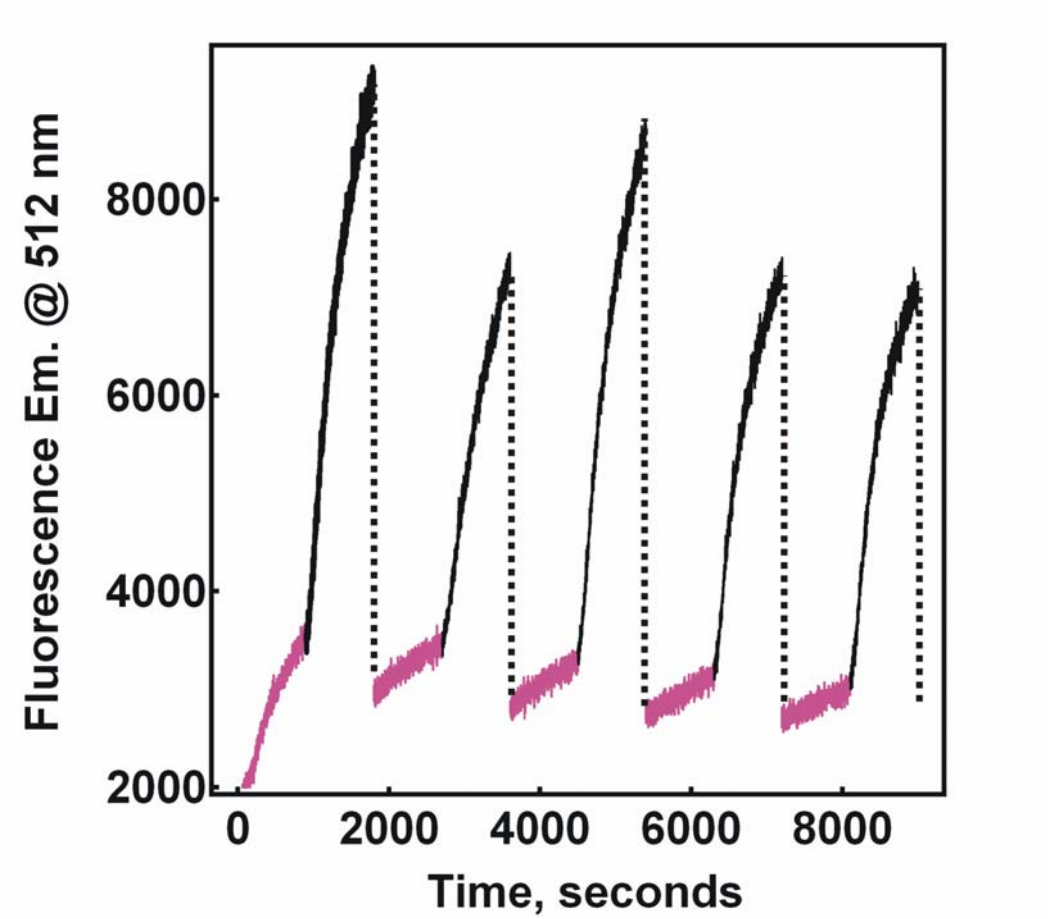

Figure 3-15. Direct release profiles of FITC-insulin from a 9 layer microgel thin film into 0.02 M PBS. The dashed lines indicate full media replacement.

These pulsatile release capabilities were also directly probed for a thicker 30 layer film to perhaps achieve more biologically relevant quantities of release. Figure 3-16 illustrates the direct release profiles obtained from this thicker peptide loaded film. Panel a represents the thermal pulses that the film is subjected to while panel b illustrates the actual oscillations in release. When the highly loaded film is initially placed into the cold release medium, not an insignificant amount of peptide is released presumably from

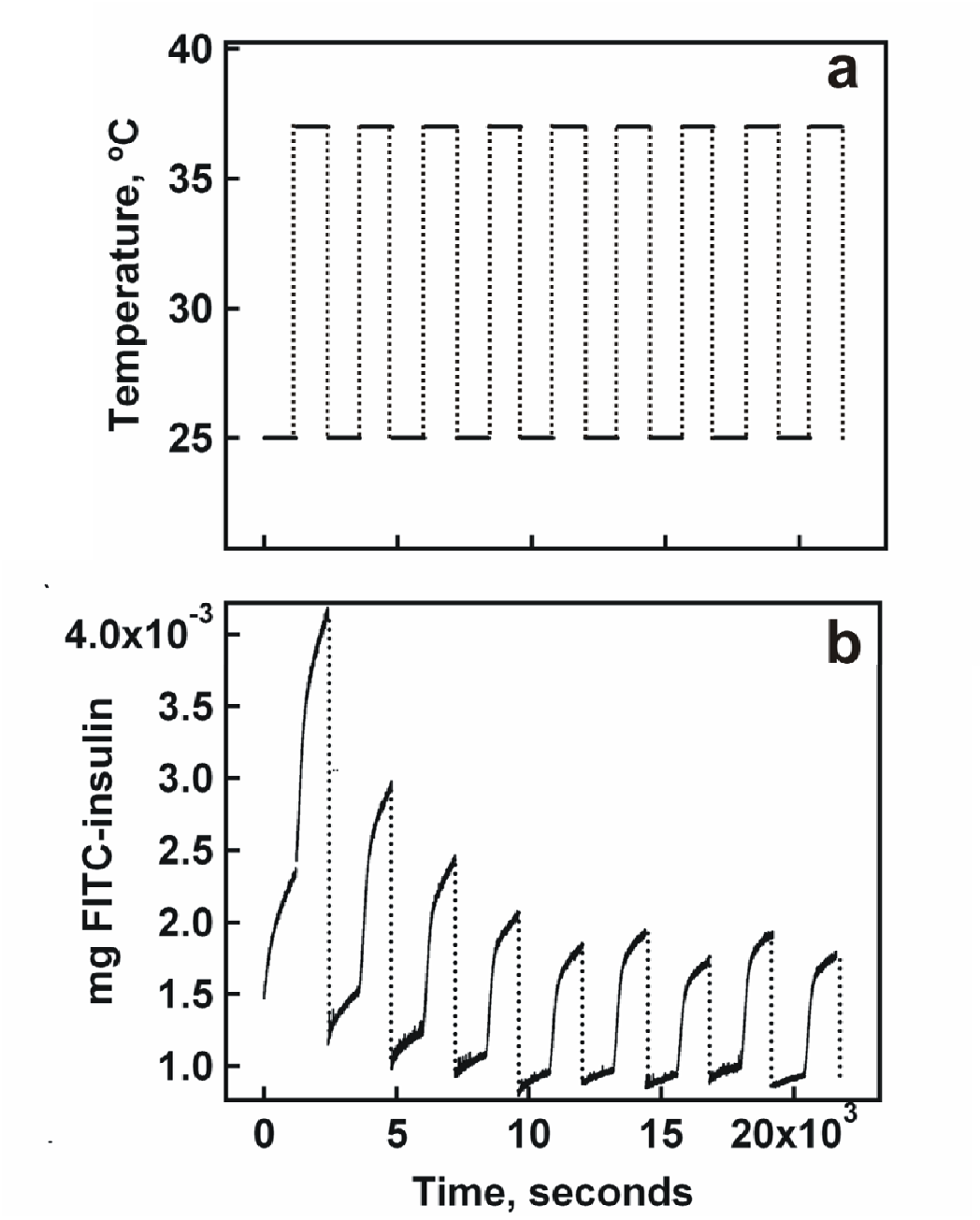

Figure 3-16. Direct pulsatile release profiles of FITC-insulin from a 30 layer microgel thin film into 0.02 M PBS. Panel a represents the thermal pulses that the film is subjected to while panel b illustrates the actual oscillations in release. The dashed lines indicate full media replacement.

weakly adsorbed insulin molecules at the film exterior. After ramping the temperature to 37 °C, the amount of peptide released increases significantly. Upon full media replacement (as indicated by dashed lines), the film displays significantly reduced insulin release upon reswelling at 25 °C. But, upon duplicating the thermal pulse, a second burst of insulin is quickly expelled from the film. The peptide can be repeatedly pulsed out in response to thermal modulation over many cycle times while the quantity released stays roughly consistent. This feature of thermally tuning the magnitude of insulin released makes these model thin film constructs highly attractive for macromolecule drug delivery applications.

Investigation of Extended Release Capabilities

To test the robustness of these thin films, extended release studies were performed wherein the drug loaded microgel thin films were placed in 4 mL of 0.02 M PBS release medium for 1 h at 25 °C. After this, the media was removed completely and replaced, after which the film was placed in a hot bath at 40 °C for the same length of time. This thermal cycling was repeated daily for 1 month. Panel a of Figure 3-17 shows cumulative release profiles for 3, 6 and 9 layer films subjected to these conditions. These profiles show a strong correlation between the amount of peptide released and the film thickness, confirming the earlier observation that the amount of insulin released is tunable. While the profile for the 3 layer film seems to have reached a plateau region toward the end of the month (perhaps indicating film depletion), the profiles for the 6 and 9 layer films are still increasing. As with the direct release studies, we find that the films effectively turn off release under cold conditions and turn on release under hot conditions as illustrated in panels b, c and d of Figure 3-17. These panels show an expansion of the curves in Figure

3-17a (cycles 10–22) for the 3, 6 and 9 layer films, where even numbers represent hot cycles and odd numbers represent cold cycles.

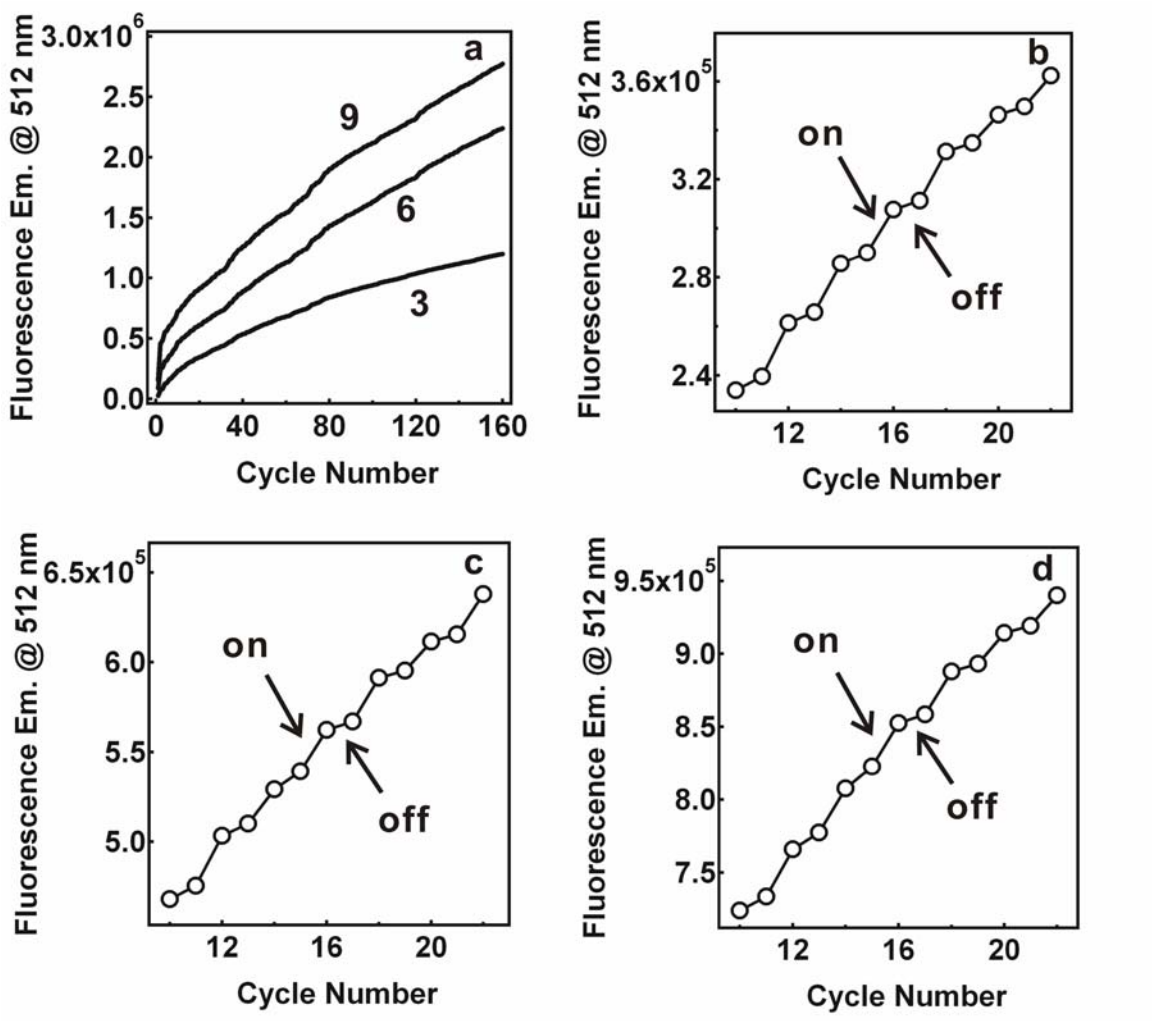

Figure 3-17. (a) Cumulative thermally induced release profiles for FITC-insulin loaded microgel thin films over 1 month (numbers indicate film layer number). Expanded view of cycles 10-22 for the (b) 3 layer, (c) 6 layer and (d) 9 layer films.

To ascertain how stable these films were against constant thermal cycling for an entire month, fluorescence microscopic images of the films after subjection to such conditions were obtained. Figure 3-18 shows these images for the corresponding 3 (panel a), 6 (panel b) and 9 (panel c) layer films after one month of pulsatile release. In all cases, the films still appear highly fluorescent. The image of the 3 layer film, however, shows areas with decreased fluorescence, supporting the earlier conclusion of some film depletion. These findings indicate that the films are still highly loaded with drug and can potentially keep releasing drug for much longer periods of time. These images also support the conclusion that these insulin impregnated films are extremely stable to excessive thermal cycling and hold great capacity to keep releasing therapeutic agents for extended periods of time.

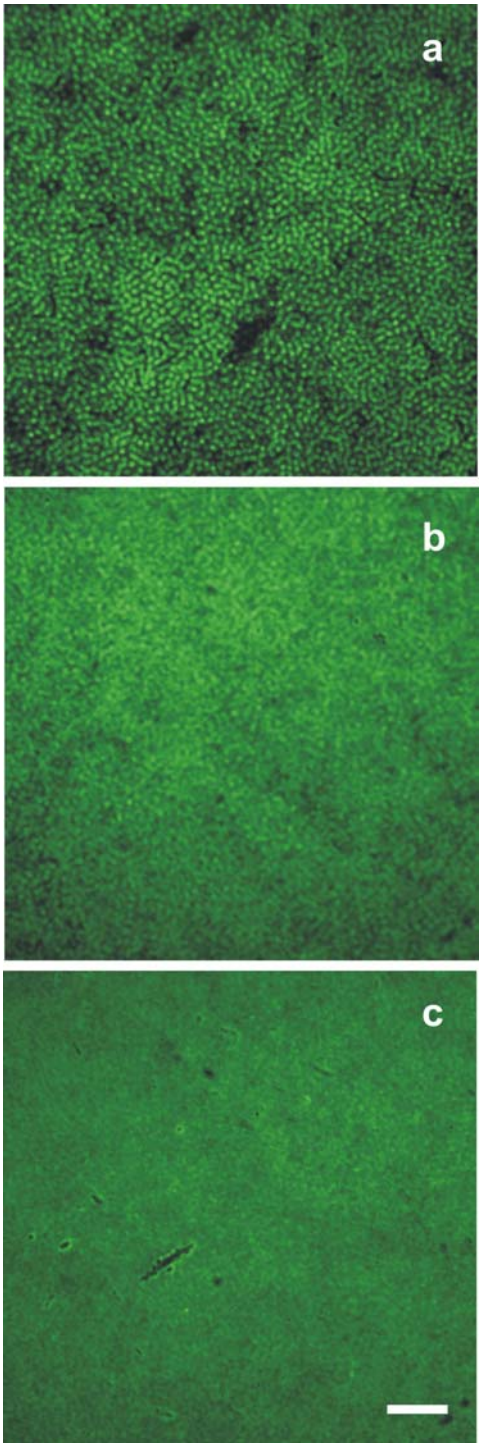

Figure 3-18. Fluorescence microscopic images of a (a) 3, (b) 6 and (c) 9 layer FITC-insulin loaded microgel thin film after one month of one hour thermal pulsing. Scale bar represents 20 μm.

3.4 Conclusions

Multifunctional microgels, successfully impregnated with a bioactive macromolecule, FITC-insulin, have been incorporated into multi-layer thin films that exhibit controlled release capabilities. These drug loaded thin films can be built up in a stepwise growth fashion allowing for uniform deposition of individual layers, even up to 30 layers. While the mechanism of release can mostly be attributed to partitioning effects, the fact that these films exhibit thermosensitivity is key in that it allows for solubilization of embedded drug material and subsequent thermally induced release. These films can successfully deliver fast bursts of FITC-insulin over many cycles and also prove to be extremely stable after extended continuous thermal pumping. Hence, these novel macromolecule loaded microgel thin films may prove quite useful for drug delivery devices.

3.5 References

(1) Pelton, R. H. *Adv. Colloid. Interface Sci.* **2000**, *85*, 1-33.

(2) Peppas, N. A.; Bures, P.; Leobandung, W.; Ichikawa, H. *Eur. J. Pharm. Biopharm.* **2000**, *50*, 27-46.

(3) Peppas, N. A.; Mikos, A. G. *Hydrogels in Medicine and Pharmacy*; CRC Press: Boca Raton, 1986; Vol. 1.

(4) Brannon-Peppas, L. *Absorbent Polymer Technology*; Elseiver: Amsterdam, 1990.

(5) Peppas, N. A.; Langer, R. *Science* **1994**, *263*, 1715-1720.

(6) Peppas, N. A. *Curr. Opin. Colloid Interface Sci.* **1997**, *2*, 531-537.

(7) Kim, J. J.; Park, K. *J. Controlled Release* **2001**, *77*, 39-47.

(8) Traitel, T.; Cohen, Y.; Kost, J. *Biomaterials* **2000**, *21*, 1679-1687.

(9) Yu, H.; Grainger, D. W. *J. Controlled Release* **1995**, *34*, 117-127.

(10) Dorkoosh, F. A.; Verhoef, J. C.; Ambagts, M. H. C.; Rafiee-Tehrani, M.; Borchard, G.; Junginger, H. E. *Eur. J. Pharm. Sci.* **2002**, *15*, 433-439.

(11) Park, T. G. *Biomaterials* **1999**, *20*, 517-521.

(12) Kagatani, S.; Shinoda, T.; Konno, Y.; Fukui, M.; Ohmura, T.; Osada, Y. *J. Pharm. Sci.* **1997**, *86*, 1273-1277.

(13) Decher, G.; Hong, J. D. *Berichte Der Bunsen-Gesellschaft-Physical Chemistry Chemical Physics* **1991**, *95*, 1430-1434.

(14) Decher, G.; Hong, J. D.; Schmitt, J. *Thin Solid Films* **1992**, *210*, 831-835.

(15) Shi, X.; Shen, M.; Mohwald, H. *Prog. Polym. Sci.* **2004**, *29*, 987-1019.

(16) Bertrand, P.; Jonas, A.; Laschewsky, A.; Legras, R. *Macromol. Rapid Commun.* **2000**, *21*, 319-348.

(17) Lvov, Y. M.; Price, R. R.; Selinger, J. V.; Singh, A.; Spector, M. S.; Schnur, J. M. *Langmuir* **2000**, *16*, 5932-5935.

(18) Sukhorukov, G.; Mohwald, H.; Decher, G.; Lvov, Y. *Thin Solid Films* **1996**, *285*, 220-223.

(19) Ai, H.; Fang, M.; Jones, S. A.; Lvov, Y. *Biomacromolecules* **2002**, *3*, 560-564.

(20) Lvov, Y.; Ariga, K.; Onda, M.; Ichinose, I.; Kunitake, T. *Langmuir* **1997**, *13*, 6195-6203.

(21) He, J. A.; Valluzzi, R.; Yang, K.; Dolukhayan, T.; Sung, C. M.; Kumar, J.; Tripathy, S. K.; Samuelson, L. B., L.; Tomalia, D. A. *Chem. Mater.* **1999**, *11*, 3268-3274.

(22) Heflin, J. R.; Figura, C.; Marciu, D.; Liu, Y.; Claus, R. O. *Appl. Phys. Lett.* **1999**, *74*, 495-497.

(23) Lenahan, K. M.; Wang, Y. X.; Liu, Y. J.; Claus, R. O.; Heflin, J. R.; Marciu, D.; Figura, C. *Adv. Mater.* **1998**, *10*, 853-855.

(24) Fulda, K. U.; al., e. *Thin Solid Films* **1998**, *329*, 752-757.

(25) Caruso, F.; Schuler, C.; Kurth, D. G. *Chem. Mater.* **1999**, *11*, 3394-3399.

(26) Rubner, M. F.; Chung, A. J. *Langmuir* **2002**, *18*, 1176-1183.

(27) Caruso, F.; Quinn, J. F. *Langmuir* **2004**, *20*, 20-22.

(28) Onda, M.; Ariga, K.; Kunitake, T. *J. Biosci. Bioeng.* **1999**, *87*, 69-75.

(29) Hoshi, T.; Saiki, H.; Anzai, J. *Biosens. Bioelectron.* **2000**, *15*, 623-628.

(30) Cassier, T.; Lowack, K.; Decher, G. *Supramol. Sci.* **1998**, *5*, 309-315.

(31) Anzai, J.-i.; Kobayashi, Y.; Nakamura, N.; Nishimura, M.; Hoshi, T. *Langmuir* **1999**, *15*, 221-226.

(32) Caruso, F.; Niikura, K.; Furlong, D. N.; Okahata, Y. *Langmuir* **1997**, *13*, 3427-3433.

(33) Anzai, J.-i.; Akase, S. *Macromol. Biosci.* **2002**, *2*, 361-364.

(34) Anzai, J.-i.; Kobayashi, Y. *Langmuir* **2000**, *16*, 2851-2856.

(35) Caruso, F.; Yang, W. J.; Trau, D.; Renneberg, R. *Langmuir* **2000**, *16*, 8932-8936.

(36) Caruso, F.; Trau, D.; Mohwald, H.; Renneberg, R. *Langmuir* **2000**, *16*, 1485-1488.

(37) Sukhorukov, G. B.; Antipov, A. A.; Voigt, A.; Donath, E.; Mohwald, H. *Macromol. Rapid Commun.* **2001**, *22*, 44-46.

(38) Tiourina, O. P.; Antipov, A. A.; Sukhorukov, G. B.; Larionova, N. I.; Lvov, Y.; Mohwald, H. *Macromol. Biosci.* **2001**, *1*, 209-214.

(39) Antipov, A. A.; Sukhorukov, G. B.; Leporatti, S.; Radtchenko, I. L.; Donath, E.; Mohwald, H. *Colloid Surf. A-Physicochem. Eng. Asp.* **2002**, *198-200*, 535-541.

(40) Fang, M.; Grant, P. S.; McShane, M. J.; Sukhorukov, G. B.; Golub, V. O.; Lvov, Y. M. *Langmuir* **2002**, *18*, 6338-6344.

(41) Caruso, F.; Mohwald, H. *Langmuir* **1999**, *15*, 8276-8281.

(42) Caruso, F.; Lichtenfeld, H.; Giersig, M.; Mohwald, H. *J. Am. Chem. Soc.* **1998**, *120*, 8523-8524.

(43) Carrara, M.; Kakkassery, J. J.; Abid, J.-P.; Fermin, D. J. *ChemPhysChem* **2004**, *5*, 571-575.

(44) Kotov, N. A.; Kekany, I.; Fendler, J. H. *J. Phys. Chem.* **1995**, *99*, 13065-13069.

(45) Serpe, M. J.; Jones, C. D.; Lyon, L. A. *Langmuir* **2003**, *19*, 8759-8764.

(46) Jones, C. D.; Lyon, L. A. *Macromolecules* **2000**, *33*, 8301-8306.

(47) Motonaga, T.; Shibayama, M. *Polymer* **2001**, *42*, 8925-8934.

(48) Philippova, O. E.; Hourdet, D.; Audebert, R.; Khokhlov, A. R. *Macromolecules* **1997**, *30*, 8278-8285.

(49) Diez-Pena, E.; Quijada-Garrido, I.; Barrales-Rienda, J. M. *Polymer* **2002**, *43*, 4341-4348.

(50) Chiu, H.-C.; Lin, Y.-F.; Hung, S.-H. *Macromolecules* **2002**, *35*, 5235-5242.

(51) Brange, J.; Langkjoer. In *Stability and Characterization of Protein and Peptide Drugs*; Wang, Y. J.; Pearlman, R., Eds.; Plenum Press: New York, 1993; pp 315-350.

(52) Kim, J. J.; Park, K. *Journal of Controlled Release* **2001**, *77*, 39-47.

(53) Hwang, S. H.; Maitani, Y.; Qi, X.-R.; Takayama, K.; Nagai, T. *Int. J. Pharm.* **1999**, *179*, 85-95.

(54) Harmon, M. E.; Kuckling, D.; Frank, C. W. *Macromolecules* **2003**, *36*, 162-172.

(55) Bae, Y. H.; Okano, T.; Kim, S. W. *J. Controlled Release* **1989**, *9*, 271-279.

CHAPTER 4

SYNTHESIS, CHARACTERIZATION AND APPLICATIONS OF POLY(ETHYLENE GLYCOL) (PEG) CROSS-LINKED PNIPAM MICROGELS

This chapter focuses on the fundamental synthesis and characterization of PEG cross-linked microgels. Thermoresponsive poly(*N*-isopropylacrylamide) (pNIPAm) microgels cross-linked with various concentrations of PEG diacrylates of three different PEG chain lengths were synthesized via free-radical precipitation polymerization in order to investigate the phase transition and protein adsorption behavior as the hydrophilicity of the network is increased. It also deals with macromolecule loading studies designed to elucidate future applications of such oligomerically cross-linked materials. Characterization through ^{1}H NMR, isopycnic centrifugation as well as protein adsorption studies provides some insight into the morphology of these porous systems as a function of temperature. Dynamic Light Scattering (DLS) reveals that as the concentration of PEG cross-linker incorporated into the microgels is increased, an increase in the temperature and breadth of the phase transition occurs. Qualitative differences in microgel density using isopycnic centrifugation confirm that higher PEG concentrations result in denser networks. Efficient incorporation of PEG cross-linker was confirmed with ^{1}H NMR, and variable temperature NMR studies suggest that in the deswollen state, the longer PEG cross-links are flexible enough to protrude from the dense globular microgel. This behavior apparently manifests itself as a decrease in non-specific protein adsorption with

increasing PEG length and content. These PEG modified particles also prove useful in hydrophilic macromolecule loading applications. Hence, these systems may show promise in drug delivery and/or biomedical applications.

4.1 Introduction

Efforts to incorporate biocompatible polymers within responsive hydrogel networks have been vigorously pursued in recent years. Addition of poly(ethylene glycol) (PEG), a hydrophilic, non-degradable polymer,[1] into bio-related materials has many advantages, including biocompatibility, non-toxicity, non-immunogenicity and water solubility.[2] Nanoparticles that are surface-modified with PEG have become increasingly investigated[3,4] due to the fact that PEG facilitates control of protein adsorption and minimizes nonspecific cell adhesion *in vitro*.[5-8] This also makes PEG-modified systems highly attractive for drug delivery applications.[9-12] For example, controlled delivery of macromolecules has been investigated using degradable PEG hydrogel networks[13,14] partly due to the fact that many materials made from hydrophilic polymers have also been shown to be relatively non-inflammatory.[2,15] Furthermore, PEG has been synthesized within semi-interpenetrating polymeric networks for drug release devices.[16,17]

Incorporation of PEG chains also allows tunability of the hydrophilic/hydrophobic balance of these hydrogel networks, thereby controlling their deswelling characteristics.[18] Much work has been done wherein PEG chains have been grafted to hydrogels, thereby greatly affecting their deswelling behavior.[19,20] Recently, our group has shown that by grafting PEG chains to the periphery of pNIPAm core/shell hydrogel nanoparticles, a reduction in bovine serum albumin (BSA) adsorption, as well

as an increased LCST and breadth of the phase transition, occurred.[3] Yet, little work has focused on using PEG chains as cross-linking units within discrete thermoresponsive microgel particles.

Herein, we describe results from studies performed to show that modulation of phase transition behavior and microgel surface energy can be accomplished by incorporating oligomeric cross-linkers of varying length. Characterization through ^{1}H NMR, isopycnic centrifugation as well as protein adsorption studies provide some insight into the morphology of these porous systems as a function of temperature. These particles also prove effective in hydrophilic macromolecule loading applications. Hence, these systems may show promise in drug delivery and/or biomedical applications.

4.2 Experimental Section

Materials

All chemicals were obtained from Sigma Aldrich unless otherwise noted. *N*-isopropylacrylamide (NIPAm) was recrystallized from hexane (J. T. Baker) prior to use. Sodium dodecyl sulfate (SDS), ammonium persulfate (APS), *N, N'*-Methylene(bisacrylamide) (BIS), fluorescein isothiocyanate labeled insulin (FITC-insulin) from bovine pancreas, FITC-dextran (4, 000, 70, 000 and 150, 000 MW), FITC labeled bovine serum albumin (FITC-BSA), deuterium oxide (D_2O), sucrose and poly(ethylene glycol) diacrylate (PEG) (PEG MW 200, 575 and 700, Polysciences, Inc.) were used as received. Phosphate buffered saline (PBS) solution (pH 7.4, 0.02 M) was prepared in house from NaCl (Fisher), Na_2HPO_4 (EM Science) and KH_2PO_4. Water used in all experiments was distilled and then purified using a Barnstead E-Pure system

operating at a resistance of 18 MΩ. A 0.2 μm filter was incorporated into this system to remove particulate matter.

Particle Synthesis

Thermoresponsive pNIPAm microgels, synthesized by precipitation polymerization via a method slightly modified from that previously described, were cross-linked with PEG diacrylate of MWs 200, 575 and 700 at concentrations of 0.2, 1, 2 and 5 mole %.[21] 2 mole % BIS cross-linked microgels were also synthesized for comparison. The total monomer concentration was 100 mM in all reactions. SDS was used as a surfactant and APS was used as the free radical initiator. The NIPAm monomer, cross-linker and surfactant (0.01 g) were dissolved in 200 mL of nanopure water, filtered through a 0.2 μm nylon membrane filter to remove any large particulate matter and then continuously stirred in a three-neck, 250 mL round-bottom flask. This solution was heated to 70 ºC while being purged with N_2 gas. Approximately one hour later, the temperature of the solution was stable at 70 ºC. Fifteen minutes later, the reaction was initiated by adding a hot (70 ºC) solution of APS (1 mM final concentration). The solution turned turbid within 10 minutes, indicating successful initiation. The reaction proceeded for 6 hours under a constant stream of nitrogen. Following synthesis, the microgels were filtered using a P2 Whatman filter paper and then dialyzed (using 10, 000 MWCO) for 2 weeks against nanopure water with a daily exchange of fresh water.

Dynamic Light Scattering (DLS)

Hydrodynamic radii and light scattering intensities were obtained by DLS (Protein Solutions, Inc.). Prior to analysis, the purified microgels were diluted in filtered nanopure (using 0.2 μm filters) water until a count rate of 250 kCt/sec was obtained. The

suspensions were then held at each temperature for 10 minutes to achieve thermal equilibration before measurements were taken. Longer equilibration times did not result in variations of particle radius, polydispersity or light scattering intensity. The data points presented herein are an average of 25 measurements with a 5 second acquisition time. Hydrodynamic radii were calculated from the measured diffusion coefficients using the Stokes-Einstein equation. All correlogram analyses were performed with manufacturer supplied software (Dynamics v.5.25.44, Protein Solutions, Inc.). The volume deswelling ratios (V_o/V) of the microgels were calculated via the relation $V_o/V = R_o^3/R^3$, where R_o and R are the DLS measured particle radii at 25 °C and the measured temperature, respectively.

Isopycnic Sucrose Density Gradient Centrifugation

Sucrose density gradient equilibrium centrifugation studies were carried out using a Beckman ultracentrifuge with 10 mL ultraclear centrifuge tubes. A sucrose density gradient was made by carefully layering 25 %, 20 %, 15 % and 10 % sucrose solutions (2.0 mL each) within the centrifuge tubes and then depositing 30 μL of the PEG cross-linked pNIPAm microgels on top. The samples were then centrifuged at 26 °C, 25,000 rpm for 4 hours to allow the particle bands to reach their equilibrium density zones. Actual densities of these particles were not calculated, but qualitative differences were obtained by comparing the distances traveled down the sucrose density gradient. Samples were prepared in triplicate and are presented as an average value ± one standard deviation.

^{1}H NMR

A Varian Unity 300 MHz NMR spectrometer was used to determine the chemical compositions of the PEG cross-linked microgels. Lyophilized microgels (1.0 mg) were redispersed in D_2O and the spectra were recorded at both 20 and 40 °C. Before taking measurements, the sample was thermally equilibrated for 15 minutes at each temperature. No changes in the signal intensities were observed if the equilibration time was prolonged.

Protein Adsorption

The amount of protein adsorbed to the PEG cross-linked microgels was previously determined using the dye-complexation based Bradford Assay.[3,22] For these experiments, fluorescein isothiocyanate labeled BSA (FITC-BSA) was used to eliminate the need for complexation and allow for more sensitive spectrofluorimetric measurements. The PEG cross-linked microgels (10 mg/mL) were mixed with FITC-BSA (1 mg/mL) in 0.02 M PBS, pH 7.4. These samples were incubated by shaking in a heat block on a shaker table at either 25 or 37 °C for three hours and then centrifuged at 14, 000 rpm for 60 minutes at either 25 or 37 °C. The amount of protein remaining in solution was determined by extracting 200 µL of supernatant and then diluting this with 3 mL of 0.02 M PBS, pH 7.4. The concentration of protein that did not adsorb to the particles was then determined by measuring the fluorescence intensity of the solution using λ_{ex} = 473 nm and λ_{em} = 512 nm, and correlating these intensity values to a calibration curve. The value for the amount of protein adsorbed to the microgels was finally calculated taking into account the dilution factor and the concentration of FITC-

BSA in a control sample that did not contain any microgels. Samples were prepared in triplicate and are presented as an average value ± one standard deviation.

Macromolecule Loading Studies

To determine the capability of these microgels to effectively load macromolecules, the PEG cross-linked microgels (10 mg/mL) were mixed with FITC-dextran (4, 000, 70, 000 or 150, 000 MW) or FITC-insulin (1 mg/mL) in 0.02 M PBS, pH 7.4 via shaking. After 24 hours of incubation, the amount of macromolecule remaining in solution (not loaded) was determined by first centrifuging at 14, 000 rpm at 26 °C for 60 minutes. Then 200 µL of supernatant was extracted and diluted with 3 mL of 0.02 M PBS, pH 7.4. The comparative amount of macromolecule that did not load into the particles was then determined by measuring the fluorescence intensity of the solution using λ_{ex} = 473 nm and λ_{em} = 512 nm. To quantitate the amount of macromolecule that loaded into the microgels, the sample supernatant fluorescence was compared to that of a control sample containing no microgels. Samples were prepared in triplicate and are represented as an average value ± one standard deviation.

4.3 Results and Discussion

Particle Synthesis and Characterization

In this work, thermoresponsive pNIPAm microgels were cross-linked with PEG diacrylate of MWs 200, 575 and 700 to investigate the effect of cross-linker chain length, as well as concentration, on the overall phase transition behavior of these particles. Table 4-1 illustrates the chain lengths and corresponding repeat units for these three cross-linkers, along with the chain length for BIS. PEG is more hydrophilic than the NIPAm

Table 4-1. Properties of cross-linkers used for microgel syntheses

Cross-linker	Chain length (Å)	Ethylene Glycol repeats
***N, N'*-Methylene(bisacrylamide)**	**12**	**N/A**
PEG 200 diacrylate	**28.6**	**4**
PEG 575 diacrylate	**63.5**	**13**
PEG 700 diacrylate	**78.6**	**16**

monomer. Thus, incorporation of these chains as cross-linking units should influence the hydrophilic balance and thereby alter the deswelling thermodynamics of the microgels. Increasing the PEG chain length from a relatively short chain (MW 200; four repeat units and a chain length of 29 Å) to a longer one of MW 700 (16 repeat units and a chain length of 79 Å) could dramatically affect the overall phase transition behavior and perhaps morphology of these loosely cross-linked networks.

Characterization of hydrodynamic radius as a function of temperature was performed using DLS. Figure 4-1 illustrates the volume phase transition behavior of these systems as a function of PEG chain length (Panels a, b, and c correspond to PEG 200, 575 and 700, respectively). In terms of PEG content, a subtle increase in the phase transition temperature can be observed for the PEG 200 samples upon increasing the concentration from 0.2 to 5 mole % (panel a1). For these systems, a slightly broadened phase transition can also be observed upon increasing the PEG content. For the intermediate chain length of PEG 575 samples, the same trend is observed (panel b1). For the longest PEG chain (PEG 700), the most pronounced difference in VPT behavior is exhibited upon increasing the cross-linker concentration (panel c1). To better visualize

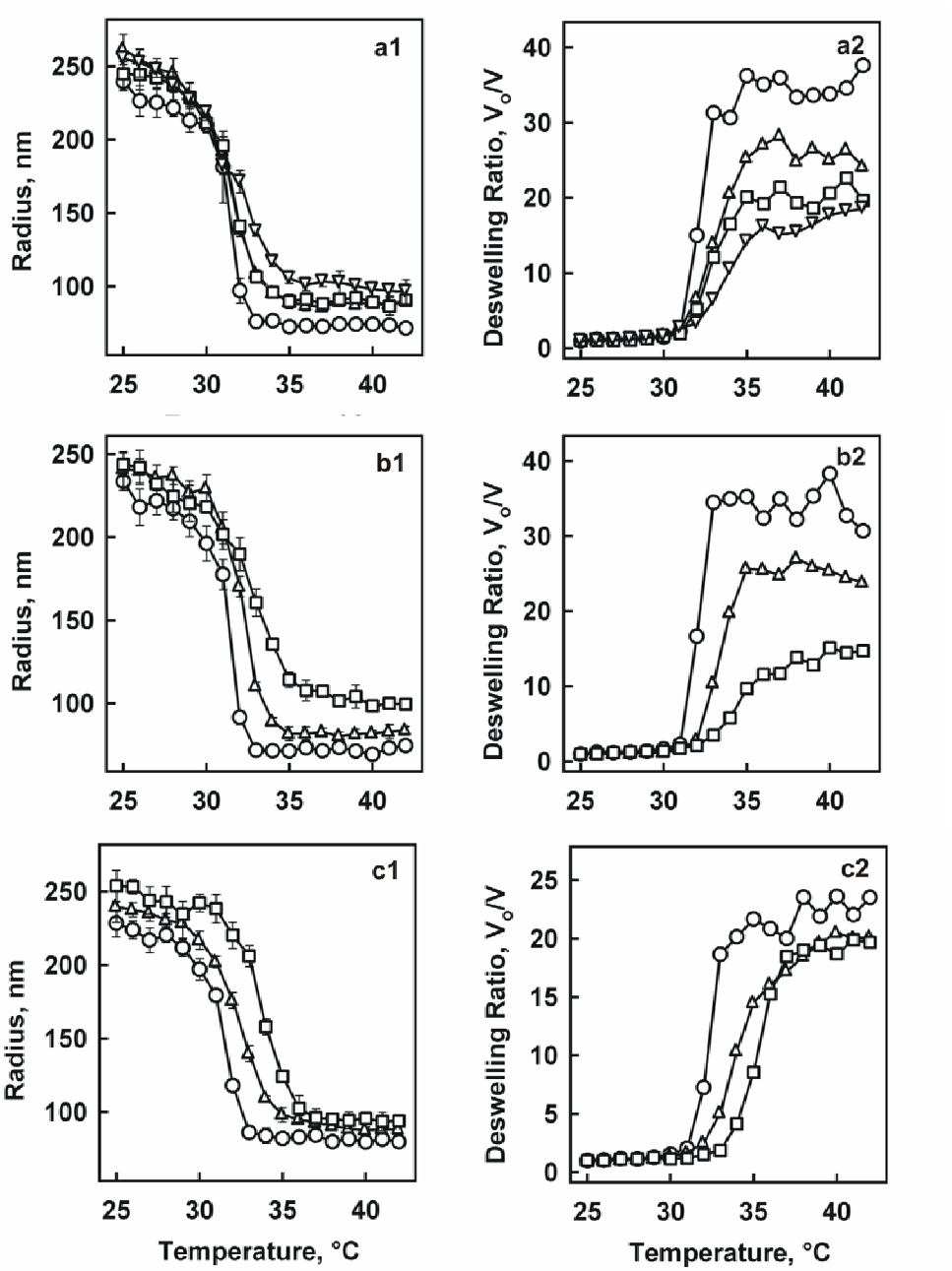

Figure 4-1. Temperature dependent DLS determined hydrodynamic radii (panel 1) and deswelling ratios (panel 2) of (a) PEG 200, (b) PEG 575 and (c) PEG 700 cross-linked pNIPAm microgels; 0.2 (circles), 1 (upward triangles), 2 (squares) and 5 (downward triangles) mole % cross-linker concentrations.

phase transition differences between particles of different radii, the size variations have been normalized to deswelling volume ratios as described in the experimental section. Panels a2, b2, and c2 represent the deswelling ratios for the corresponding microgels and also show an increase in VPT temperature as well as breadth with increased PEG content, especially for the longest chain length of PEG 700 (panel c2). In the case of PEG 200, it appears that the 5 mole % (panel a2) microgels deswell to the least extent (show the smallest change in deswelling ratio), while the 2, 1 and 0.2 mole % microgel systems show a steady increase in deswelling magnitude with a decrease in cross-linker content. These findings suggest that less elastic and denser networks are produced with higher PEG content. The same trend is observed for the PEG 575 samples where an increase in cross-linker content results in smaller deswelling magnitudes. For the PEG 700 systems, there is an observable decrease in the deswelling ratio for the more highly cross-linked microgels (1 and 2 mole %) over the 0.2 mole % system.

To illustrate the effects of cross-linker chain length on modulation of the phase transition behavior of these particles, Figure 4-2 shows the deswelling curves for 0.2 (panel a), 1 (panel b) and 2 (panel c) mole % PEG cross-linker. 2 mole % BIS cross-linked microgels are also included in panel c for comparison. At an extremely low concentration of PEG (0.2 mole %), increasing the chain length from PEG 200 to PEG 700 MW essentially does not alter the phase transition behavior of the nanoparticles (panel a1) where all three samples exhibit approximately the same sharp phase transition with an LCST at approximately 31-32 °C. The fact that quite sharp phase transitions resulted for all chain lengths could indicate a uniform distribution of sub-chain lengths within the microgels due to a constant cross-linker incorporation rate at these low PEG

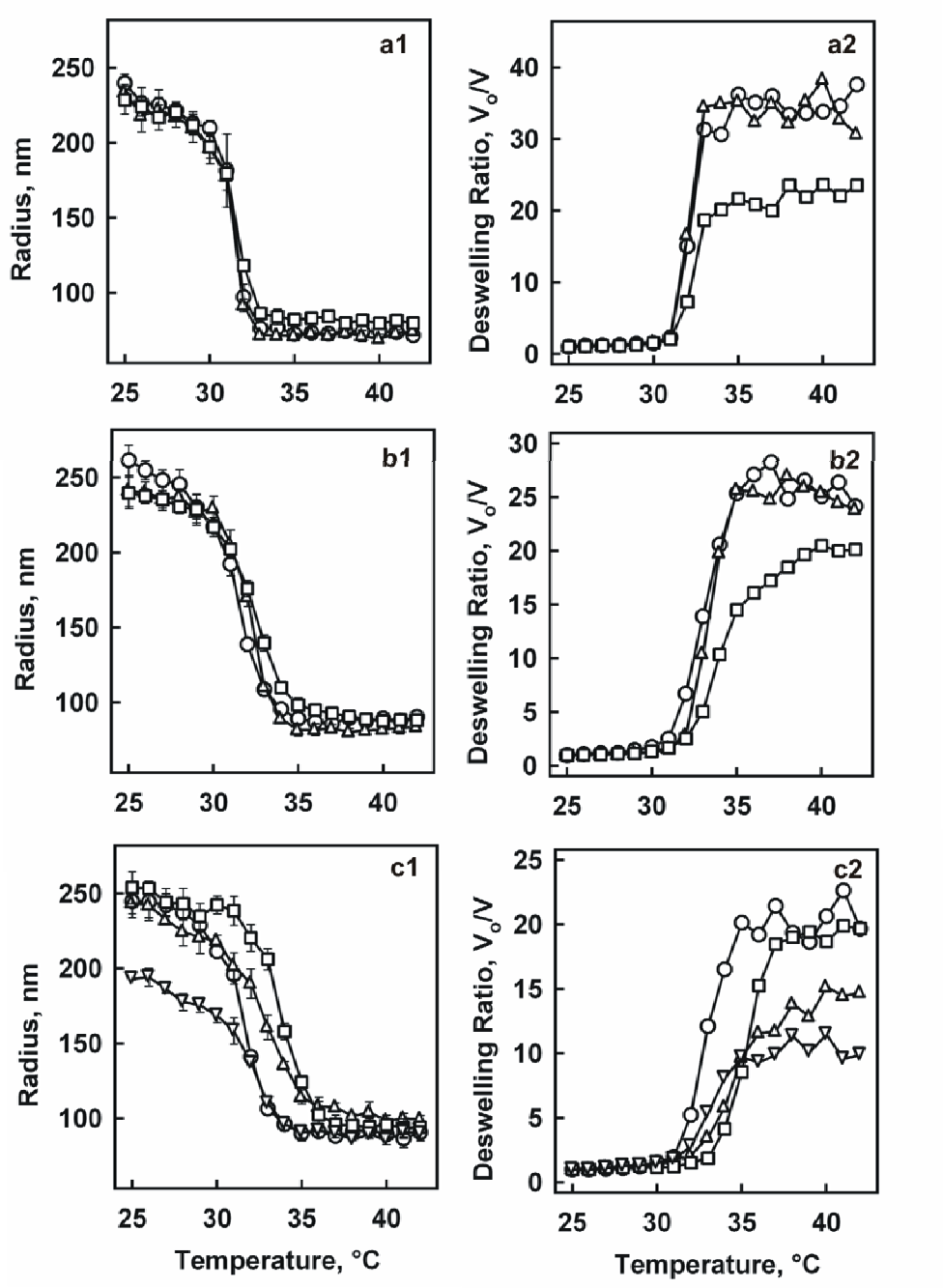

Figure 4-2. Temperature dependent DLS determined hydrodynamic radii (panel 1) and deswelling ratios (panel 2) of (a) 0.2, (b) 1.0 and (c) 2.0 mole % PEG cross-linked pNIPAm microgels; PEG 200 (circles), PEG 575 (upward triangles), PEG 700 (squares) and BIS (downward triangles).

concentrations. Inspection of the deswelling ratios (panel a2), however, shows that there is an observable decrease in deswelling magnitude as the chain length increases. At a slightly higher concentration of PEG (1 mole %), more distinct differences in the deswelling thermodynamics can be observed upon increasing the cross-linker chain length (panel b1), where a small elevation in breadth and LCST value occurs. Again, for these systems there is a diminished deswelling capacity observed as the cross-linker chain length increases. At 2 mole %, the effect of incorporating longer hydrophilic chains within these microgels can be clearly observed (panel c1). As the PEG MW increases from 200 to 575 to 700, the phase transition significantly shifts to a higher temperature due to an increased hydrophilic balance of the particles, which reduces the propensity for hydrophobic collapse of pNIPAm. Noted increased breadth of the phase transitions could be due to a more heterogeneous distribution of sub-chain lengths. The increased LCST values with increased incorporation of hydrophilic moieties has been observed before and has been attributed to increased gel hydration which restricts hydrophobic network aggregation.[23] Similar observations have also been made by Virtanen et al. who noted increased solubilization of pNIPAm by poly(ethylene oxide) (PEO) chains resulted in an increased LCST. They also noted broadening of the phase transitions as the content of PEO was increased.[20,24] By comparison, the 2 mole % BIS microgels displayed approximately the same PT temperature as the PEG 200 microgels with a significantly smaller deswelling magnitude. These findings suggest that the BIS cross-linker, being the shortest and also being more hydrophobic than PEG, results in a denser network with a decreased ability to swell in water. All of these results obtained by PCS suggest that these

types of syntheses are quite robust and result in well-behaved thermoresponsive microgels with predictable shifts in phase transition behavior.

Isopycnic Sucrose Density Gradient Centrifugation

Differences in microgel density were investigated using isopycnic density gradient centrifugation studies. Sucrose gradients were prepared by carefully layering 25, 20, 15 and 10 % sucrose solutions on top of each other and then placing the microgel samples (30 μL) on top of the entire gradient. Upon centrifugation at high speeds, the microgels traveled through the gradient until reaching the point where the microgels are perfectly buoyant (an equilibrium density zone was reached). This technique allowed for extremely tight microgel bands to be observed (approximately 3 mm in width) and therefore, qualitative comparisons between different sample densities could be made. The tabulated results are shown in Table 4-2. The samples with the highest concentration of PEG (2 mole %) and 5 mole % BIS traveled farthest down the sucrose gradient while the 0.2 mole % samples traveled the least, regardless of PEG chain length. These results confirm what one would predict for cross-linked networks; increasing the concentration of cross-linker causes denser particle networks to be formed. These findings correlate well with literature findings based on BIS cross-linked pNIPAm microgels where within 1 to 7 % cross-linker concentration, the higher the BIS content, the more dense the cross-linked network became.[25]

Table 4-2. Isopycnic sucrose density gradient centrifugation results for PEG and BIS cross-linked microgels

Mole %	Cross-linker	Avg. distance traveled, cm
0.2	**PEG 200**	**2.27 ± 0.02**
2.0	**PEG 200**	**2.64 ± 0.05**
0.2	**PEG 575**	**2.12 ± 0.03**
2.0	**PEG 575**	**2.65 ± 0.01**
0.2	**PEG 700**	**2.15 ± 0.01**
2.0	**PEG 700**	**2.59 ± 0.01**
2.0	**BIS**	**2.62 ± 0.02**
5.0	**BIS**	**2.99 ± 0.02**

^{1}H NMR

To further characterize these PEG cross-linked microgel systems, ^{1}H NMR spectra of all samples were recorded at both 20 and 40 °C to investigate the structure of the particles in both their swollen and deswollen states. To determine actual PEG incorporation into these systems, the ratio of the PEG peak (at 3.52 ppm, resulting from the methyl protons in the OCH_2CH_2 repeat units) to the main pNIPAm peak (at 1.1 ppm, resulting from the methyl protons of the isopropyl group) was calculated at room temperature. The proton assignments for the pNIPAm polymer are in agreement with its chemical structure and are illustrated in Figure 4-3.[26,27] The peak at 1.1 ppm can be attributed to the methyl protons of the *N*-isopropyl group (peak a). The resonance for the

methylene proton of the isopropyl group is observed at 3.8 to 4.0 ppm (peak b) while the resonances from 1.2 to 2.2 ppm (peaks c and d) are attributed to the protons on the polymer backbone. The entire ratio results are shown in Table 4-3 and confirm that the expected concentration of PEG was effectively incorporated. The value obtained for the 0.2 mole % PEG 200 microgels, however is higher than expected. This is most likely due to the fact that at this low concentration of such a short chain length, the PEG peak in ^{1}H NMR was extremely small and perhaps overestimation of the integrated peak area was made.

Shown in Table 4-3 are also the PEG/pNIPAm peak (e/a) ratios obtained for the microgels at temperatures both below and above their LCST values. For all samples, an increase in the ratios of PEG/pNIPAm peak areas is observed upon particle collapse. This may suggest that the PEG cross-links are mobile enough to partially protrude from the deswollen network during pNIPAm collapse, which has been observed previously for PEG-grafted pNIPAm microgels.[3] It should be noted that for the longer chain lengths of PEG 575 and PEG 700, the most notable increase in these ratios is observed while a statistically insignificant increase is observed for the PEG 200 samples. These findings suggest that the shortest cross-link chains are buried within the collapsed microgels while the longer chains may perhaps be flexible enough to protrude from the deswollen networks.

Table 4-3. ^{1}H NMR determined peak integrations at 20 °C and PEG/pNIPAm peak integration ratios at 20 and 40 °C for PEG cross-linked microgels

Sample	Mole % PEG	Mole % PEG detected	PEG peak/pNIPAm peak at 20 °C	PEG peak/pNIPAm peak at 40 °C
PEG 200	**0.2**	**0.33**	**0.01**	**not determined**
PEG 200	**1.0**	**0.94**	**0.02**	**0.03**
PEG 200	**2.0**	**1.94**	**0.06**	**0.10**
PEG 200	**5.0**	**3.88**	**0.10**	**0.13**
PEG 575	**0.2**	**0.16**	**0.01**	**0.34**
PEG 575	**1.0**	**0.98**	**0.06**	**0.11**
PEG 575	**2.0**	**2.00**	**0.16**	**0.38**
PEG 700	**0.2**	**0.20**	**0.04**	**0.19**
PEG 700	**1.0**	**0.98**	**0.11**	**0.31**
PEG 700	**2.0**	**1.97**	**0.20**	**0.48**

Figure 4-3 shows ^{1}H NMR spectra for 2 mole % PEG 700 pNIPAm microgels at both 20 and 40 °C. This figure clearly illustrates that upon raising the temperature above the LCST of these systems, the pNIPAm peak resonances become suppressed while the PEG peaks seem to increase in relation, thus supporting the earlier finding that the mobility of the long PEG chains is not strongly coupled to the more solid-like pNIPAm chains in their deswollen state. Virtanen et al. observed similar results where they noted that PEO grafts tended to turn outward into the aqueous phase at temperatures both below

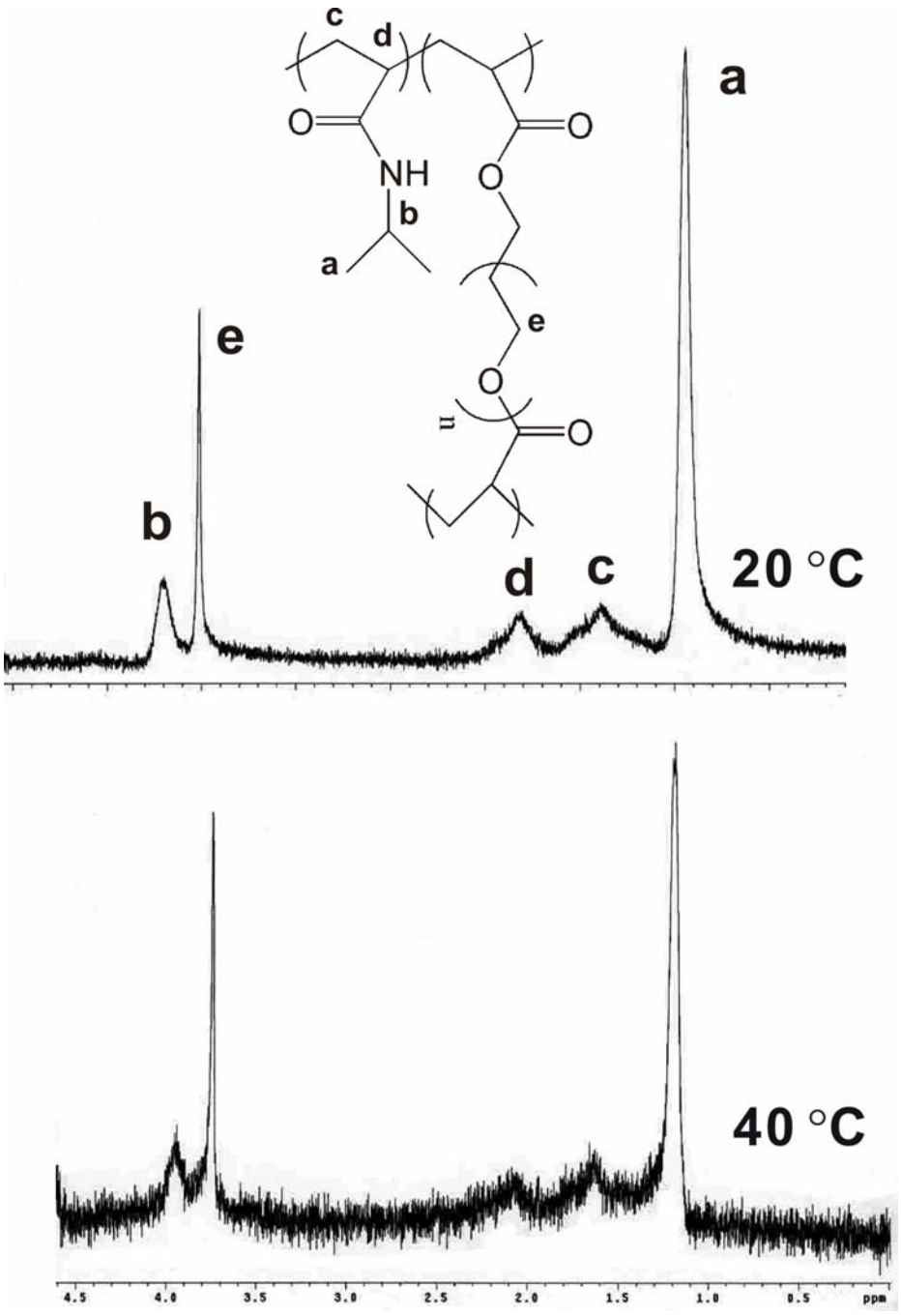

Figure 4-3. ^{1}H NMR spectra of 2 mole % PEG 700 cross-linked pNIPAm microgels in D_2O at 20 and 40 °C.

and above the LCST of pNIPAm.[24] Similar findings were also observed by Gan et al. for PEG modified pNIPAm core/shell nanoparticles.[3]

Protein Adsorption

Another probe to give us insight into the properties of these networks is the measure of non-specific protein adsorption, using FITC-BSA as the model protein. We hypothesized that the cross-linked PEG chains, presumably occupying mainly the interior of the particles, would significantly influence the protein adsorption properties of these microgels in their swollen and deswollen states. FITC-BSA protein adsorption studies were carried out at temperatures below and above the LCST of the microgels. The results for these studies are presented in Figure 4-4. At 25 °C (black bars), below the phase transition temperature, there is an observable decrease in the amount of FITC-BSA adsorbed to the PEG 200, PEG 575 and PEG 700 samples as the chain length and content increases. This presumably is a result of an increased hydrophilicity of these networks, causing a decrease in the hydrophobic protein adsorption properties of the microgels. These results are in agreement with previous findings where hydrogen bonded water to PEG resulted in a high degree of water solvation, thus preventing hydrophobic protein adsorption.[7] At 37 °C (grey bars), where the microgels are in their phase-separated state, there is only an observable decrease in the amount of protein adsorption for the longest chain systems (PEG 700). This result could be supportive of the earlier ^{1}H NMR findings that suggested these chains were long enough and flexible enough to protrude from the collapsed deswollen network. These findings imply that there is a critical cross-linker chain length needed to significantly modulate the surface energy of these particles in their deswollen state. The results for FITC-BSA adsorption under swollen (25 °C) versus

deswollen (37 °C) conditions show that, in all cases, an increase in the amount of protein adsorbed to the particles resulted when the microgels were in their collapsed states. It is apparent from these results, as others have reported previously,[3,28] that even though the flexible PEG chains may be extended to the outer aqueous environment of the collapsed dense globule in some cases, the propensity for protein adsorption is still stronger when the particles are hydrophobically collapsed. The 2 % BIS cross-linked systems resulted in the largest amount of FITC-BSA adsorption, which is attributable to the fact that these are the most hydrophobic systems compared to the hydrophilically modified, PEG containing microgels.

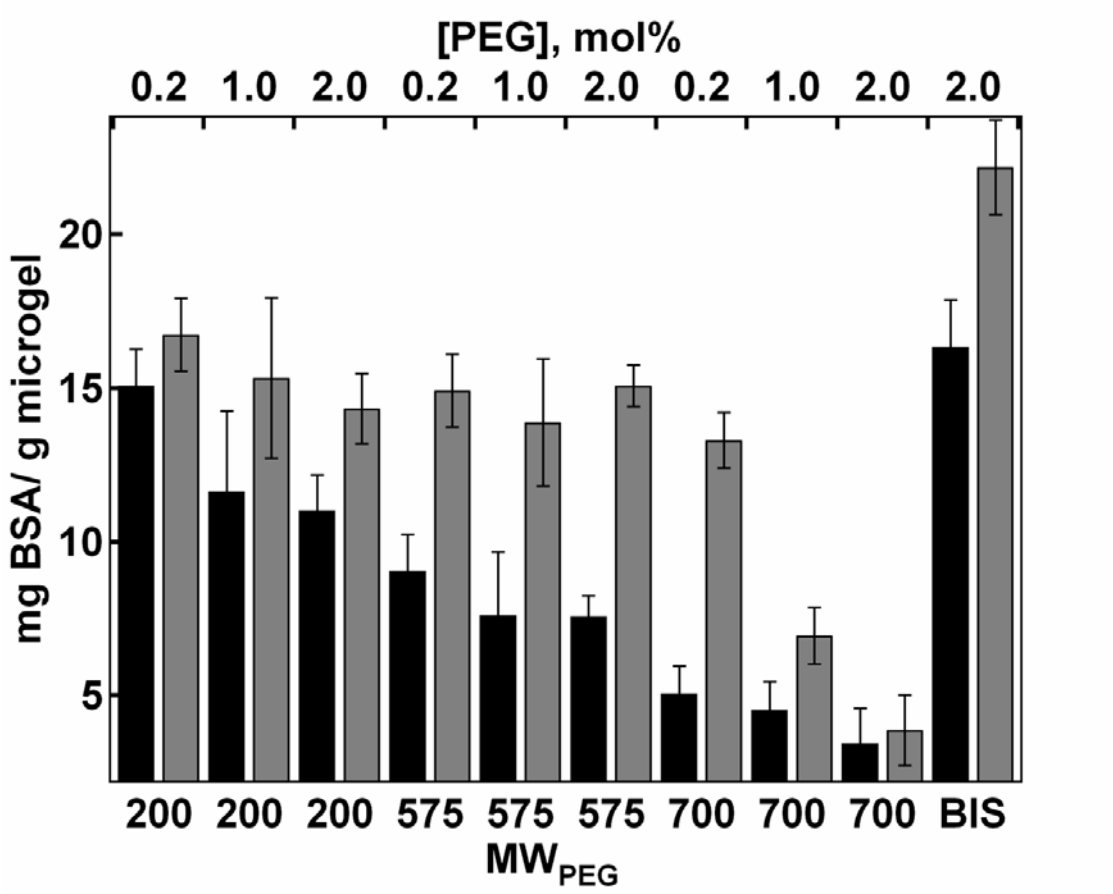

Figure 4-4. FITC-BSA protein adsorption results for PEG and BIS cross-linked microgels in 0.02 M PBS, pH 7.4; black (25 °C) and grey (37 °C). The PEG MW is indicated on the bottom axis, while the PEG concentrations in the microgels are indicated on the top axis.

Macromolecule Loading

To probe the efficacy of these types of systems for macromolecule drug delivery, loading studies using varying MW species were performed. To investigate microgel porosity, four different sized macromolecules were investigated (4, 000, 70, 000, and 150, 000 MW FITC-dextrans along with 5, 800 MW FITC-insulin). The first of these results are illustrated in Figure 4-5 and show that as the content of PEG 200 cross-linker

increases from 0.2 to 5 mole % an overall increase in the amount of 70, 000 (panel a) and 150, 000 (panel b) MW FITC-dextran loaded results (as indicated by less FITC-dextran remaining in the supernatant). These findings suggest that the most hydrophilic microgels yield the best loading results for these hydrophilic macromolecules. Thus, the two most hydrophilic samples, 5 mole % PEG 200 and 2 mole % PEG 700, were tested for loading efficacy of three different MW macromolecules as illustrated in Figure 4-6. These results show that in all cases, the 2 mole % PEG 700 loaded more of each macromolecule with the smallest MW species (4, 000 MW FITC-dextran) loading at the highest yield. These findings suggest that perhaps it is the most hydrophilic system that shows most promise in loading of hydrophilic macromolecules and perhaps microgel porosity plays a role.

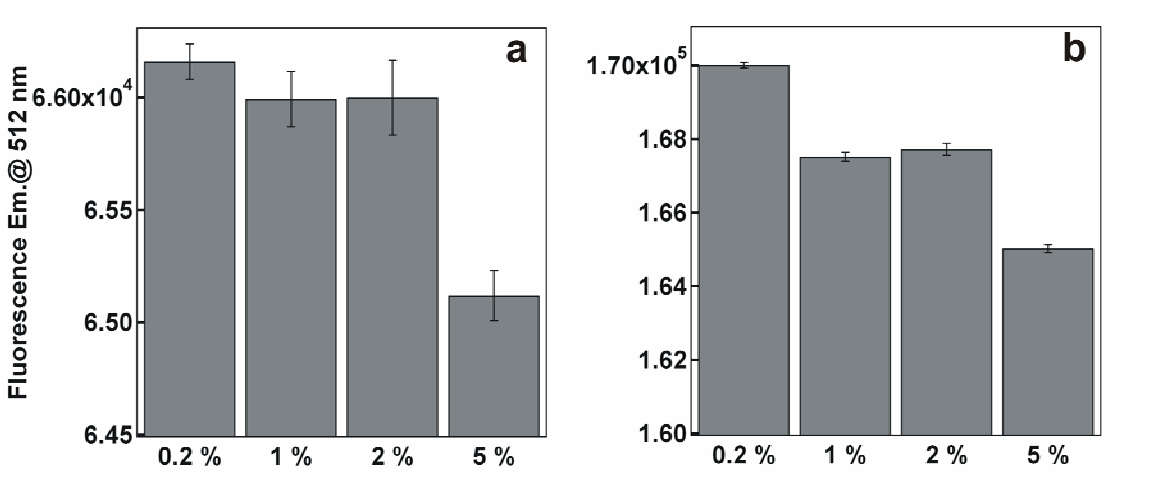

Figure 4-5. Macromolecule loading efficiency results for 0.2, 1, 2 and 5 mole % PEG 200 cross-linked pNIPAm microgels in 0.02 M PBS, pH 7.4 for (a) 70, 000 MW FITC-dextran and (b) 150, 000 MW FITC-dextran.

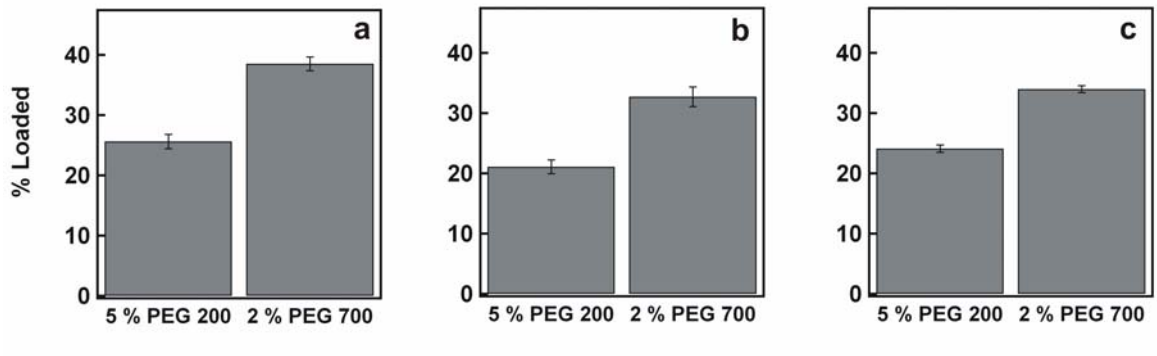

Figure 4-6. Macromolecule loading efficiency results for 5 mole % PEG 200 and 2 mole % PEG 700 cross-linked pNIPAm microgels in 0.02 M PBS, pH 7.4 for (a) 4, 000 MW FITC-dextran, (b) 70, 000 MW FITC-dextran and (c) 5, 800 MW FITC-insulin.

4.4 Conclusions

By incorporating hydrophilic, flexible oligomeric cross-linkers (PEG chains) within pNIPAm microgels, predictable modulation of the phase transition behavior as well as particle surface energy can be achieved. DLS studies reveal that as the concentration of PEG incorporated into the microgels was raised, an increase in the phase transition temperature, as well as breadth, was observed. Isopycnic centrifugation studies indicated that a higher PEG content resulted in denser cross-linked systems. Efficient incorporation of the PEG cross-linker was confirmed with ^{1}H NMR and variable temperature NMR studies are suggestive of a particle structure where the longest, most freely mobile cross-linking chains stretch outward from the collapsed globule. The protein adsorption studies showed that reduced protein sticking resulted when the concentration of PEG incorporated into the microgels increased. Above the LCST, the microgels containing the longest cross-link chains resulted in the least amount of FITC-BSA adsorption, and also suggest that these long chains are flexible enough to protrude from the collapsed microgel network. These oligomerically cross-linked systems also proved effective in hydrophilic macromolecule loading. Overall these PEG cross-linked microgels displayed highly predictable behavior that may serve useful for biomedical applications, such as protein drug delivery vehicles and/or bioengineering.

4.5 References

(1) Revzin, A.; Russell, R. J.; Yadavalli, V. K.; Koh, W.-G.; Deister, C.; Hile, D. D.; Mellott, M. B.; Pishko, M. V. *Langmuir* **2001**, *17*, 5440-5447.

(2) Harris, J. M. *Poly(Ethylene Glycol) Chemistry Biotechnical and Biomedical Applications*; Plenum: New York, 1992.

(3) Gan, D.; Lyon, L. A. *Macromolecules* **2002**, *35*, 9634-9639.

(4) Ahmad, H.; Tauer, K. *Macromolecules* **2003**, *36*, 648-653.

(5) Tziampazis, E.; Kohn, J.; Moghe, P. V. *Biomaterials* **2000**, *21*, 511-520.

(6) Shen, M.; Pan, Y. V.; Wagner, M. S.; Hauch, K. D.; Castner, D. G.; Ratner, B. D.; Horbett, T. A. *J. Biomater. Sci., Polym. Ed.* **2001**, *12*, 961-978.

(7) Zhang, M.; Desai, T.; Ferrari, M. *Biomaterials* **1998**, *19*, 953-960.

(8) Du, H.; Chandaroy, P.; Hui, S. W. *Biochim. Biophys. Acta* **1997**, *1326*, 236-248.

(9) Mellott, M. B.; Searcy, K.; Pishko, M. V. *Biomaterials* **2001**, *22*, 929-941.

(10) Vinogradov, S.; Batrakova, E.; Kabanov, A. *Colloids Surf. B* **1999**, *16*, 291-304.

(11) Govender, T.; Riley, T.; Ehtezazi, T.; Garnett, M. C.; Stolnik, S.; Illum, L.; Davis, S. S. *Int. J. Pharm.* **2000**, *199*, 95-110.

(12) Ward, J. H.; Peppas, N. A. *J. Controlled Release* **2001**, *71*, 183-192.

(13) Elbert, D. L.; Pratt, A. B.; Lutolf, M. P.; Halstenberg, S.; Hubbell, J. A. *J. Controlled Release* **2001**, *76*, 11-25.

(14) Zhao, X.; Harris, J. M. *J. Pharm. Sci.* **1998**, *87*, 1450-1458.

(15) Chowdhury, S. M.; Hubbell, J. A. *J. Surgical Research* **1996**, *61*, 58-64.

(16) Buonaguidi, M.; Carelli, V.; Di Colo, G.; Nannipieri, E.; Serafini, M. F. *Int. J. Pharm.* **1997**, *147*, 1-10.

(17) Cho, C.-S.; Han, S.-Y.; Ha, J.-H.; Kim, S.-H.; Lim, D.-Y. *Int. J. Pharm.* **1999**, *181*, 235-242.

(18) Scott, R. A.; Peppas, N. A. *Biomaterials* **1999**, *20*, 1371-1380.

(19) Kaneko, Y.; Nakamura, S.; Sakai, K.; Aoyagi, T.; Kikuchi, A.; Sakurai, Y.; Okano, T. *Macromolecules* **1998**, *31*, 6099-6105.

(20) Virtanen, J.; Baron, C.; Tenhu, H. *Macromolecules* **2000**, *33*, 336-341.

(21) Jones, C. D.; Lyon, L. A. *Macromolecules* **2000**, *33*, 8301-8306.

(22) Bradford, M. M. *Anal. Biochem.* **1976**, *72*, 248-254.

(23) Shibayama, M.; Mizutani, S.-y.; Nomura, S. *Macromolecules* **1996**, *29*, 2019-2024.

(24) Virtanen, J.; Tenhu, H. *Macromolecules* **2000**, *33*, 5970-5975.

(25) Guillermo, A.; Cohen Addad, J. P.; Bazile, J. P.; Duracher, D.; Elaissari, A.; Pichot, C. *J. Polym. Sci., Part B: Polym. Phys.* **2000**, *38*, 889-898.

(26) Larsson, A.; Kuckling, D.; Schonhoff, M. *Colloids Surf., A* **2001**, *190*, 185-192.

(27) Tokuhiro, T.; Amiya, T.; Mamada, A.; Tanaka, T. *Macromolecules* **1991**, *24*, 2936-2943.

(28) Kawaguchi, H.; Fujimoto, K.; Mizuhara, Y. *Colloid Polym. Sci.* **1992**, *270*, 53-57.

CHAPTER 5

SYNTHESIS, CHARACTERIZATION AND APPLICATIONS OF POLY(ETHYLENE GLYCOL) (PEG) CROSS-LINKED PNIPAM-*CO*-ACRYLIC ACID MICROGELS

This chapter focuses on the fundamental synthesis and characterization of PEG cross-linked pNIPAm-*co*-Acrylic acid (pNIPAm-*co*-AAc) (9:1) microgels. It also deals with cell adhesion studies designed to elucidate future applications of such oligomerically cross-linked dually responsive materials. Herein, we describe results from studies performed to show that modulation of phase transition behavior and microgel surface energy can be accomplished by incorporating oligomeric cross-linkers of varying length and content within pH sensitive microgels. Characterization through DLS provides some insight into the responsivity of these porous systems as a function of temperature and pH. These particles also prove to be effective for non-fouling and cell adhesion-resistant applications when longer chain lengths or increased content are utilized. Thus, these types of oligomerically cross-linked dually responsive microgels could prove useful in biomedical applications.

5.1 Introduction

As described earlier, efforts to enhance the overall biocompatibility of hydrogel networks by incorporation of poly(ethylene glycol) (PEG) moieties have been thoroughly made in recent years. PEG is a hydrophilic, non-degradable polymer,[1] and has many features that make it attractive for bio-related materials. These include biocompatibility, non-toxicity, non-immunogenicity and water solubility.[2] Nanoparticles that are surface-modified with PEG have become increasingly investigated[3,4] due to the fact that PEG facilitates control of protein adsorption and minimizes nonspecific cell adhesion *in vitro*.[5-8] Incorporation of PEG chains allows tunability of the hydrophilic/hydrophobic balance of these hydrogel networks, thereby modulating their deswelling characteristics.[9] Much work has been done wherein PEG chains have been grafted to hydrogels, thereby greatly affecting their phase transition behavior.[10,11]

Incorporation of functional moieties within hydrogel materials that yield them pH responsive has been another heavily explored avenue. Variations in solution pH induce modulation of network ionization that result in changes in swelling capacity.[12] For example, the effect of modulated pH on the swelling properties of acid modified pNIPAm based networks has been studied in great detail.[13-18] Use of dually responsive temperature and pH sensitive hydrogel materials for controlled drug delivery applications has also been increasingly investigated.[19-21] Studies on acid incorporated and PEG modified networks have also been performed[22] are highly attractive for drug delivery applications.[21,23] Yet, little work has focused on using PEG chains as cross-linking units within discrete thermo- and pH responsive microgel particles. Herein, we describe results from investigations that show modulation of phase transition behavior, swelling

capacities and cell adhesion properties can be achieved by incorporating oligomeric cross-linkers of varying length and/or content into both thermo- and pH sensitive microgels.

5.2 Experimental

Materials

All chemicals were obtained from Sigma Aldrich unless otherwise noted. *N*-isopropylacrylamide (NIPAm) was recrystallized from hexane (J. T. Baker) prior to use. Sodium dodecyl sulfate (SDS), ammonium persulfate (APS), *N, N'*-Methylene(bisacrylamide) (BIS), sodium hydroxide (NaOH), anhydrous acrylic acid (AAc; Fluka), formic acid (J. T. Baker), 95% ethanol, 200 proof anhydrous ethyl alcohol and poly(ethylene glycol) diacrylate (PEG) (PEG MW 200, 575 and 700, Polysciences, Inc.) were used as received. 3-Aminopropyltrimethoxysilane (APTMS) was obtained from United Chemical Technologies. Phosphate buffered saline solution (pH 7.4, 0.02 M) was prepared in house from NaCl (Fisher), Na_2HPO_4 (EM Science) and KH_2PO_4. 12-well tissue culture-treated polystyrene plates were from Corning Inc. Dulbecco's phosphate buffered saline and Modified Eagle medium were purchased from Invitrogen. Murine NIH-3T3 fibroblasts (CRL-1658) were from the American Type Culture Collection. Newborn calf serum was purchased from Hyclone, while all other cell culture reagents were obtained from Invitrogen. Glass microscope coverslips (22 x 22 mm) were purchased from Fisher Scientific. 0.2 μm nylon membrane disks and Spectra/Por 10, 000 MWCO dialysis membrane were purchased from VWR. Water used in all experiments

was distilled and then purified using a Barnstead E-Pure system operating at a resistance of 18 MΩ. A 0.2 μm filter was incorporated into this system to remove particulate matter.

Particle Synthesis

Thermoresponsive pNIPAm-*co*-AAc (9:1) microgels, synthesized by precipitation polymerization via a method slightly modified from that previously described,[24] were cross-linked with PEG diacrylate of MWs 200, 575 and 700 at concentrations of 0.2, 1, 2 and 5 mole %.[2428] 2 mole % BIS cross-linked pNIPAm-*co*-AAc (9:1) microgels were also synthesized for comparison in cell adhesion studies. The total monomer concentration was 100 mM in all reactions. SDS was used as a surfactant and APS was used as the free radical initiator. The NIPAm monomer, cross-linker and surfactant (0.01 g) were dissolved in 200 mL of nanopure water, filtered through a 0.2 μm nylon membrane filter to remove any large particulate matter and then continuously stirred in a three-neck, 250 mL round-bottom flask. This solution was heated to 70 ºC while being purged with N_2 gas. Approximately one hour later, the temperature of the solution was stable at 70 ºC. To this hot solution, the acrylic acid comonomer was added. Fifteen minutes later, the reaction was initiated by adding a hot (70 ºC) 35 mg/mL solution of APS (1 mM final concentration). The solution turned turbid within 10 min, indicating successful initiation. The reaction proceeded for 6 hours under a constant stream of nitrogen. Following synthesis, the microgels were filtered using a P2 Whatman filter paper and then dialyzed (using 10, 000 MWCO) for 2 weeks against nanopure water with a daily exchange of fresh water.

Dynamic Light Scattering (DLS)

Hydrodynamic radii and light scattering intensities were obtained by DLS (Protein Solutions, Inc.). The 20 mM solutions of pH 3.5 and 6.5 were first prepared using the appropriate buffer systems (formate and phosphate). Prior to analysis, the purified microgels were diluted in filtered media (using 0.2 μm filters) until a count rate of 250 kCt/s was obtained. The suspensions were then held at each temperature for 10 minutes to achieve thermal equilibration before measurements were taken. Longer equilibration times did not result in variations of particle radius, polydispersity, or light scattering intensity. The data points presented here are an average of 25 measurements with a 5 second acquisition time and a signal-to-noise ratio threshold of 2.5. Hydrodynamic radii were calculated from the measured diffusion coefficients using the Stokes–Einstein equation. All correlogram analyses were performed with manufacturer-supplied software (Dynamics v.5.25.44, Protein Solutions, Inc.).

Light Scattering

To monitor the phase transition behavior of one set of these microgels in high ionic strength cell-culture medium (pH 7.4), a light scattering profile was obtained using a steady state fluorescence spectrophotometer (Photon Technology International) equipped with a Model 814 PMT photon-counting detector. The slit widths were set to a bandwidth of 1.5 nm while the excitation and emission monochromators were each set to pass 600 nm light. The scattered light intensity of the solution was monitored at an angle of 90° as a function of time and temperature using a temperature ramp experiment. The temperature range was from 24 to 52 °C, the temperature ramp rate was set at 1 °C/minute, the integration time was set at 1 second and data was collected every 0.1 °C.

The temperature was controlled using a PE 60 temperature controller Peltier stage (Linkam Scientific Instruments Ltd., Surrey, UK). The cuvette was filled with 3.5 mL of cell culture medium and 50 μL of the microgel solution.

Potentiometric Titrations

To verify 10 mole % acrylic acid incorporation into these PEG cross-linked pNIPAm-*co*-AAc (9:1) microgels, potentiometric titrations were performed. The microgels were first lyophilized, then weighed out and resuspended in nanopure water to yield a final concentration of 5 mg/mL. This solution was titrated against standardized 10 mM NaOH using 150 μL aliquots. After each aliquot was added, the solution was allowed to stir for 1 minute and then left to sit for 5 minutes before equilibrated pH measurements were taken. Based on the theoretical concentration of acrylic acid incorporated into the microgels, the number of mmole of acid/gram of solid was calculated. Upon completion of a titration curve, the inflection point was used to determine the end point and hence, the volume of base needed to neutralize the acid groups. From this volume of base, the actual concentration of acrylic acid in the solution was calculated. This value was used in reference to the theoretical value and hence, the effective amount of acrylic acid incorporated into the microgels was calculated.

Cell Adhesion Studies

The actual cell adhesion studies were performed by Catherine D. Reyes, a graduate student in Dr. Andres J. Garcia's lab in The Woodruff School of Mechanical Engineering, Georgia Institute of Technology. Stock solutions (8 mg/mL) of the PEG or BIS cross-linked pNIPAm-*co*-AAc (9:1) microgels were first prepared by dissolving lyophilized microgels in 20 mM PBS. A spin-coating process was used to deposit one

layer of PEG cross-linked pNIPAm-*co*-AAc (9:1) microgels onto glass microscope cover slips. The glass substrates were first cleaned by placing in a hot plasma cleaner for 10 minutes. After this, the slides were rinsed with 200 proof anhydrous ethyl alcohol before functionalization. A 0.4 % APTMS solution in anhydrous ethanol was used to make the glass slides positively charged. The slides were left in this solution at room temperature for two hours and were then rinsed well with 95 % ethanol and finally stored in 95 % ethanol. Prior to spin coating, the positively functionalized slide was rinsed well with nanopure water and then gently dried with nitrogen gas. This slide was placed on the spin coater chuck and held in place via vacuum. The rotor speed was maintained at 3, 000 rpm. Deposition of one microgel layer consisted of depositing 5 drops of the PEG cross-linked pNIPAm-*co*-AAc (9:1) microgel solution (pH 7.4), waiting 20 seconds and then rinsing vigorously with nanopure water. 2 mole % BIS cross-linked pNIPAm-*co*-AAc (9:1) microgels were also used in these studies for comparison of cross-linker hydrophobicity. Microgel-coated glass coverslips were transferred to separate wells in a 12-well tissue culture-treated polystyrene plate. The coverslips were sterilized with 2 mL 70 % ethanol and then rinsed three times with Dulbecco's phosphate buffered saline. Murine NIH-3T3 fibroblasts (CRL-1658) were detached from tissue culture plates using trypsin/EDTA and resuspended in Dulbecco's Modified Eagle medium containing 10 % newborn calf serum and 1% penicillin-streptomycin. Cells were seeded onto the wells containing the microgel-coated coverslips at a density of 10,000 cells/cm^2 with 1 mL of growth media per well. The culture plates were maintained at 37 ºC in a humid environment supplemented with 5 % CO_2 from 1 hour to 3 days. Phase contrast images

were captured using a Nikon Eclipse E400 fluorescence microscope with 10x and 20x objectives and ImagePro Plus image acquisition software.

5.3 Results and Discussion

Particle Synthesis and Characterization

In this work, dually responsive pNIPAm-*co*-AAc (9:1) microgels were cross-linked with PEG diacrylate of MWs 200, 575 and 700 to investigate the effect of cross-linker chain length, as well as concentration, on the overall phase transition behavior of these networks as a function of both temperature and pH. As previously discussed, PEG is more hydrophilic than the NIPAm monomer. Thus, incorporation of these chains as cross-linking units should significantly affect their hydrophilic balance, and thereby, alter their deswelling behavior. Incorporation of a pH sensitive comonomer, as well as varying the hydrophilic oligomer chain length and/or content could dramatically alter the overall phase transition behavior and responsivity of these loosely cross-linked networks.

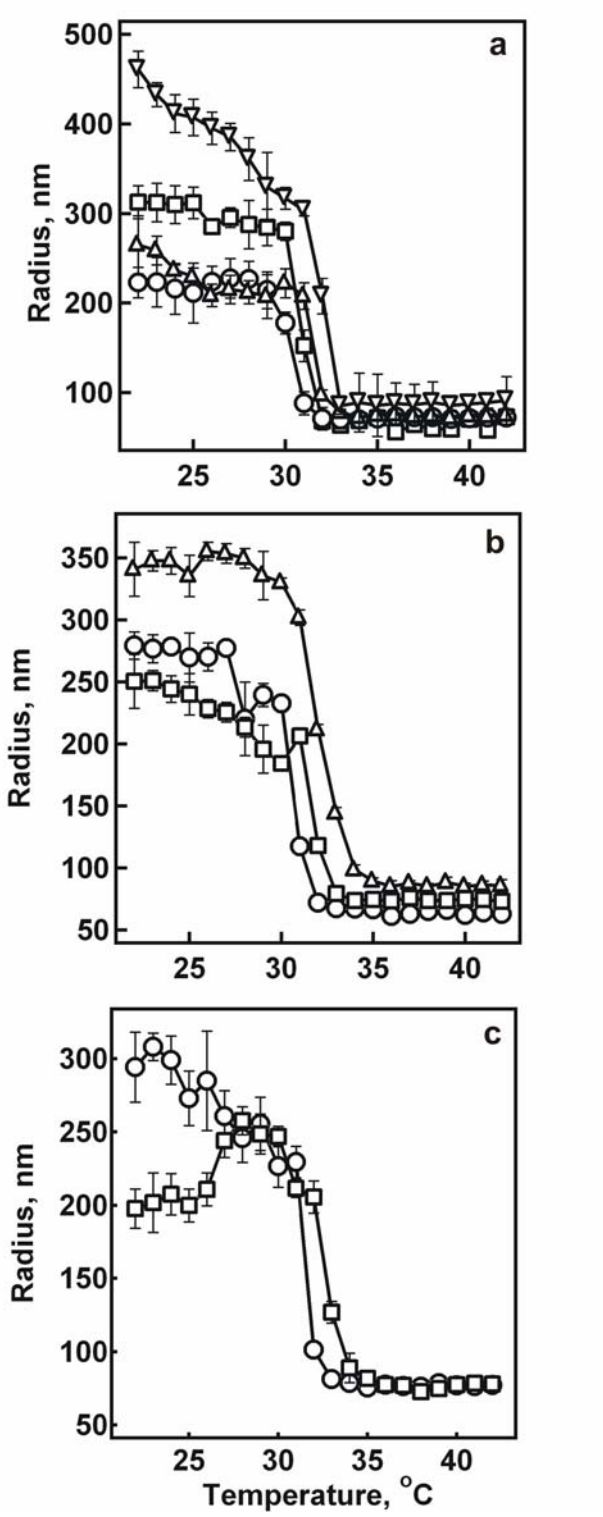

Figure 5-1. Temperature dependent DLS determined hydrodynamic radii of (a) PEG 200, (b), PEG 575 and (c) PEG 700 cross-linked pNIPAm-*co*-AAc (9:1) microgels at pH 3.5; 0.2 (circles), 1.0 (squares), 2.0 (upward triangles) and 5.0 (downward triangles) mole % cross-linker concentrations.

Characterization of hydrodynamic radius as a function of temperature was performed on these dually responsive networks using DLS. Figure 5-1 illustrates the volume phase transition behavior of these microgels as a function of PEG chain length at a constant pH of 3.5 (panels a, b and c correspond to PEG 200, 575 and 700, respectively). In terms of PEG content, an obvious increase in the phase transition temperature can be observed for the PEG 200 samples upon increasing the concentration from 0.2 to 5 mole % (panel a). For these systems, a trend of increasingly broadened phase transitions can also be observed upon increasing the PEG content with the sample of the highest cross-linker concentration of 5.0 mole % resulting in the broadest phase transition. Similar findings have been reported before by Virtanen et al. who noted increased solubilization of pNIPAm by poly(ethylene oxide) (PEO) chains resulted in anincreased LCST. They also noted broadening of the phase transitions as the content of PEO was increased.[11,25] For the intermediate chain length of PEG 575 samples, a more distinct increase in the phase transition temperature is noted upon increasing the cross-linker concentration from 0.2 to 1.0 to 2.0 mole %. The same trend of decreased PT sharpness is also observed with augmented cross-linker concentrations. For the longest PEG chain of MW 700, increased breadth of the PT can be observed even at only 1.0 mole %. It should be noted that for these types of syntheses, conditions of 2.0 mole % PEG 700 with 10 mole % acrylic acid did not result in robust synthetic conditions where phase separation was a significant problem. Furthermore, it was only for the shortest PEG cross-linker of 200 MW that 5.0 mole % was effectively incorporated.

To illustrate the effects of cross-linker chain length on modulation of the phase transition behavior of these particles, Figure 5-2 shows the deswelling curves for 0.2

(panel a), 1.0 (panel b) and 2.0 (panel c) mole % PEG cross-linker, again at a constant pH of 3.5. At an extremely low concentration of PEG (0.2 mole %), a subtle increase in the phase transition temperature is observed upon increasing the chain length from PEG 200 to PEG 700 MW (panel a). These findings are in contrast to previously reported results on PEG cross-linked networks without AAc comonomer (see Chapter 4). In these previous studies, essentially no difference in the phase transition temperature was observed when the chain length varied at this low mole %. We attribute modulation of the phase transition temperature however, in this case, to the overall increase in the hydrophilic balance of these networks considering 10.0 mole % acrylic acid was incorporated as a comonomer. At a slightly higher concentration of PEG (1.0 mole %), more distinct differences in the deswelling kinetics can be observed (panel b) upon increasing the cross-linker chain length, where a small elevation in breadth and LCST value occurs. At 2.0 mole %, the effect of incorporating longer hydrophilic chains within these AAc modified microgels can be clearly observed (panel c) by just increasing the MW from 200 to 575. Significant broadening of the phase transition occurs for the longer PEG 575 chain. In all cases, this shift of the phase transition out to higher temperatures can be attributed to the increased hydrophilic character of the particles, which reduces the propensity for hydrophobic collapse of the pNIPAm polymer backbone. Furthermore, increasing the PEG chain length within these already hydrophilically modified networks (with 10.0 mole % AAc comonomer) only augments the elevation of the hydrophilic balance of the network, thereby concurrently decreasing the propensity for structured water molecules to be expelled during microgel collapse. Again, these types of

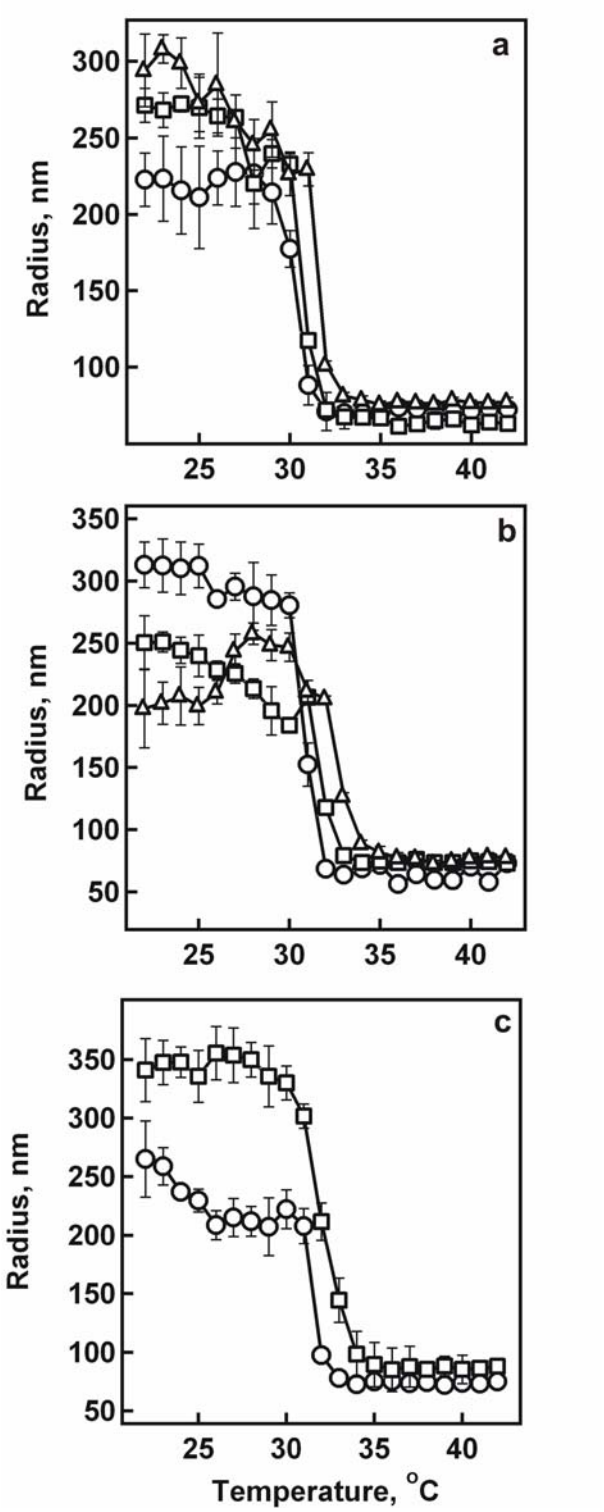

Figure 5-2. Volume phase transition curves for (a) 0.2, (b) 1.0 and (c) 2.0 mole % PEG cross-linked pNIPAm-*co*-AAc (9:1) microgels in pH 3.5 media. PEG 200 (circles), PEG 575 (squares) and PEG 700 (upward triangles).

observations have been made before by Virtanen et al. who noted an increased LCST and phase transition broadening as the concentration of PEO increased.[11,25]

To further consider the effect of PEG cross-linking on the structure of these pNIPAm-*co*-AAc (9:1) microgels, the sharpness and breadth of the transitions can be analyzed. The lowest mole % (0.2 mole %) samples resulted in sharper phase transitions for all chain lengths (panel a) in contrast to the higher concentrations of 1.0 (panel b) and 2.0 mole % (panel c). This could indicate a more heterogeneous distribution of sub-chain lengths for the higher concentration samples at 1.0 and 2.0 mole %. Higher LCST values with increased incorporation of hydrophilic moieties has been previously reported and has been attributed to increased gel hydration which restricts hydrophobic network aggregation.[30]

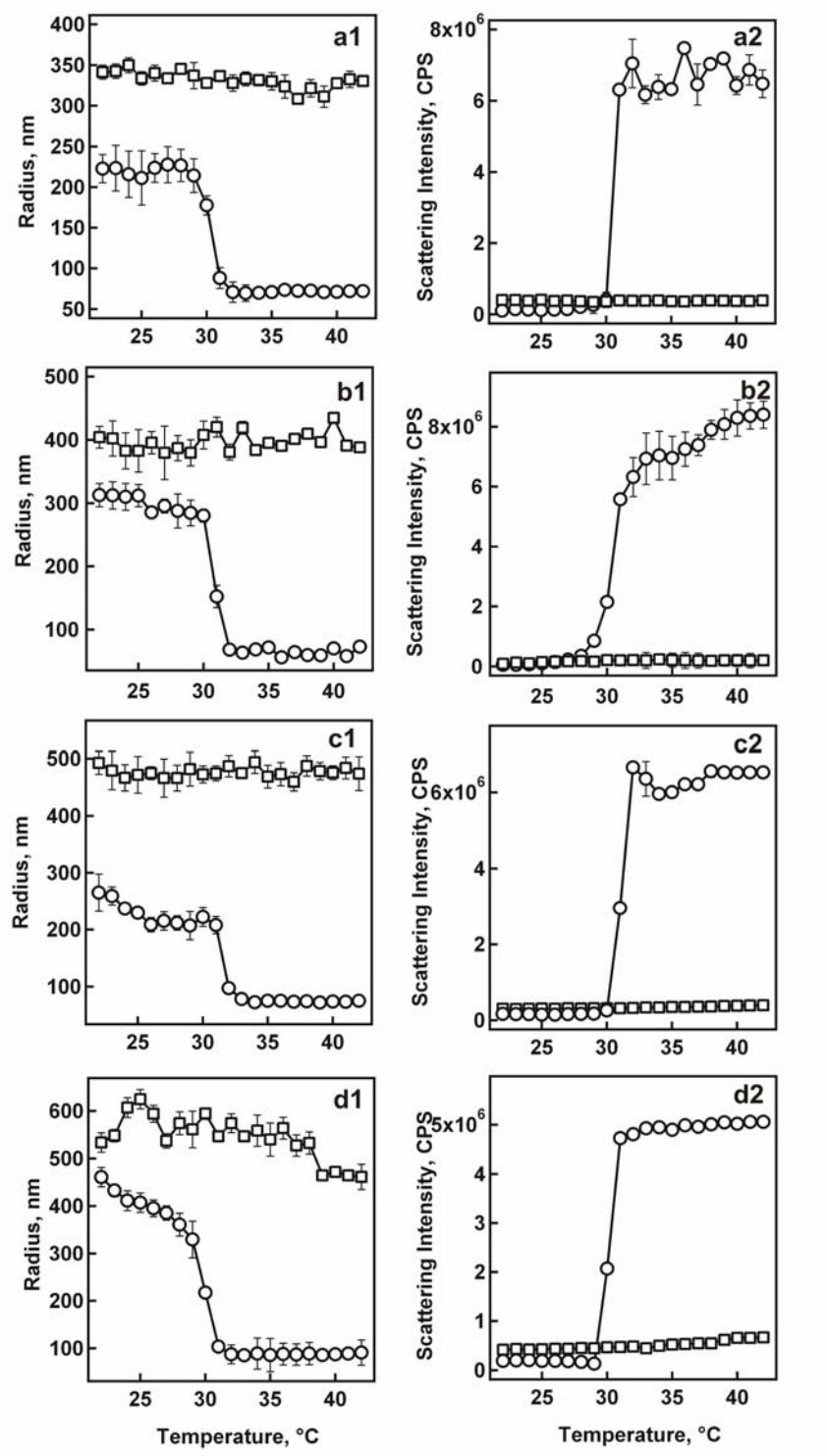

Figure 5-3. Volume phase transition curves (panels 1) for PEG 200 cross-linked pNIPAm-*co*-AAc (9:1) microgels in pH 3.5 (circles) and 6.5 (squares) media and corresponding light scattering profiles (panels 2). Panels a (0.2 mole %), panels b (1.0 mole %), panels c (2.0 mole %) and panels d (5.0 mole %).

To illustrate the pH responsivity of these PEG cross-linked AAc modified microgels, volume phase transition curves were obtained via DLS at pH 3.5 and 6.5. These pH values were chosen because they are below and above the p*K*a value of the acrylic acid groups incorporated at 10 mole % comonomer. As discussed previously in earlier chapters, this p*K*a value is approximately 4.26. Figure 5-3 illustrates the effects of varying pH on the PEG 200 cross-linked pNIPAm-*co*-AAc (9:1) hydrogel nanoparticles at 0.2 (panels a), 1.0 (panels b), 2.0 (panels c) and 5.0 (panels d) mole %. At all concentrations, under pH 3.5 conditions (circles), the microgels undergo a sharp volume phase transition at approximately 31-32 °C which corresponds well with the LCST of typical pNIPAm microgels.[26] At this pH value, the system is below the p*K*a of the acrylic acid groups and almost all of the acid groups within the microgels are protonated. When the pH of the system is increased to 6.5 (squares), however, the networks are well above the p*K*a value and the carboxylic acid groups are fully dissociated resulting in electrostatic repulsion between negatively charged acid groups which favors swelling. In addition to this, Donnan equilibrium guarantees a higher concentration of dissociated ions within the microgel interior, resulting in additional osmotic pressure that results in swelling.[13] This results in significant increases in the sizes of the microgels in all cases. This type of behavior, where greater swelling ratios result from increased hydrophilicity of the network, is common hydrogel behavior.[13,27-30] Furthermore, essentially no observable phase transition within the temperature range of 22–42 °C can be detected. Similar findings of diminishment of LCST behavior at high pH values for acrylic acid networks have been reported.[31] Panels 2 of Figure 5-3 illustrate the corresponding light scattering profiles of the same systems at the two pH values. Under both pH conditions,

the microgels in all cases show very little scattered light intensity at low temperatures below the corresponding LCST values. This is due to the fact that these porous microgel networks are highly solvated (approximately 95% water by volume) and are therefore, refractive index matched to their environment. When the microgels deswell into dense globules at temperatures above the LCST, however, the microgels display a higher scattering cross section, and therefore, a dramatic increase in scattered light intensity is detected from all suspensions above the LCST.

Figure 5-4 illustrates the pH sensitivity of the PEG 575 cross-linked pNIPAm-*co*-AAc (9:1) microgels at 0.2 (panels a), 1.0 (panels b) and 2.0 (panels c) mole %. Again, under low pH conditions of 3.5 (circles), the particles all display a typical volume phase transition at approximately 31-32 °C. At pH 6.5, however, all of the microgels display an increase in size due to osmotic swelling and Coulombic repulsion between the negatively charged AAc groups. This, once again, manifests itself as essentially no phase transition to be observed within the measured temperature range. The corresponding light scattering profiles for these networks, illustrated in panels 2 of Figure 5-4, once again illustrate the refractive index difference that occurs when the microgels are in their highly solvent swollen state (low temperatures) versus their collapsed deswollen state (high temperatures under low pH conditions). Figure 5-5 illustrates the pH effect on the responsivity of the PEG 700 cross-linked pNIPAm-*co*-AAc (9:1) microgels. The same trends of pH induced swelling and diminishment of volume phase transitions at high pH values can be observed.

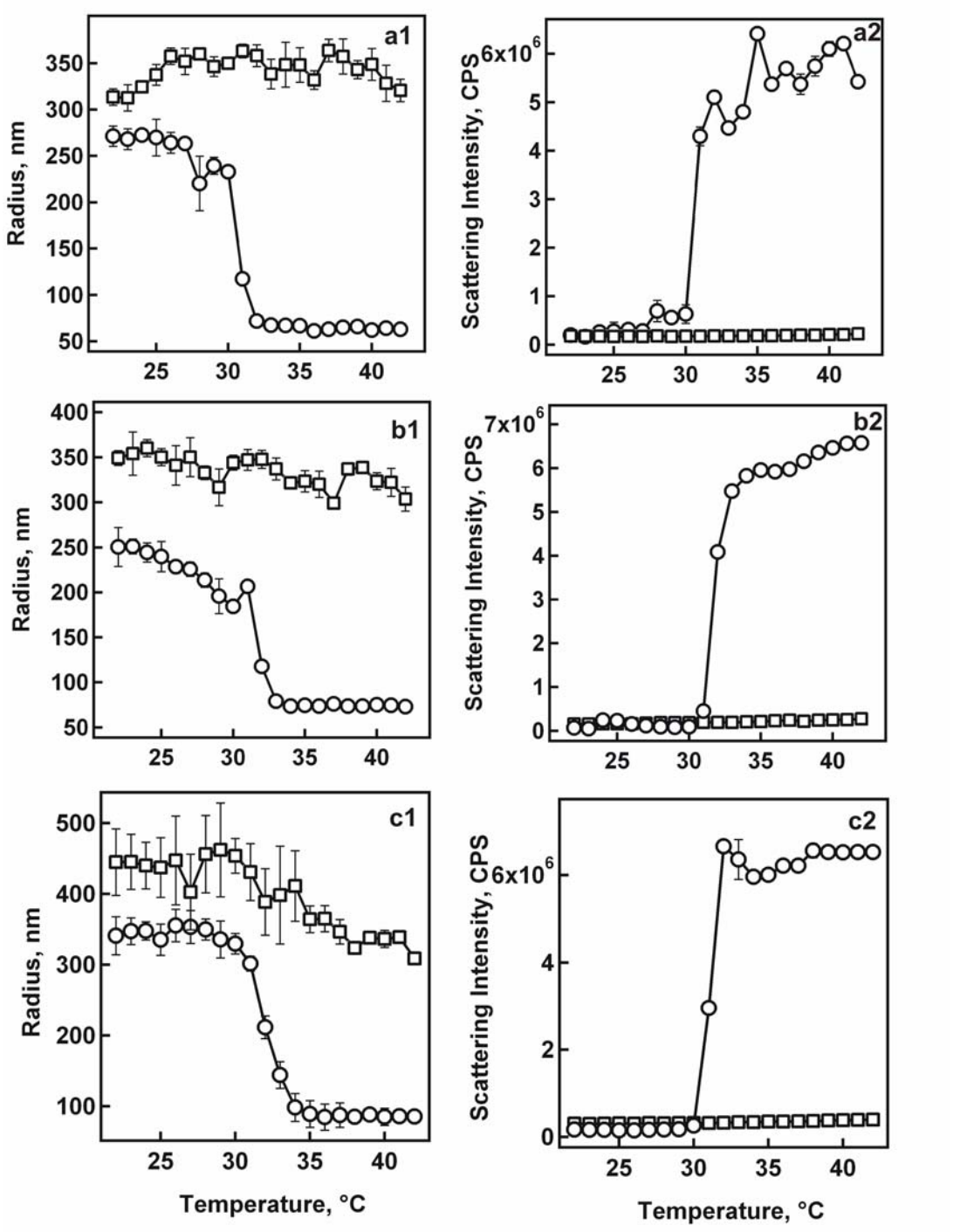

Figure 5-4. Volume phase transition curves (panels 1) for PEG 575 cross-linked pNIPAm-*co*-AAc (9:1) microgels in pH 3.5 (circles) and 6.5 (squares) media and corresponding light scattering profiles (panels 2). Panels a (0.2 mole %), panels b (1.0 mole %) and panels c (2.0 mole %).

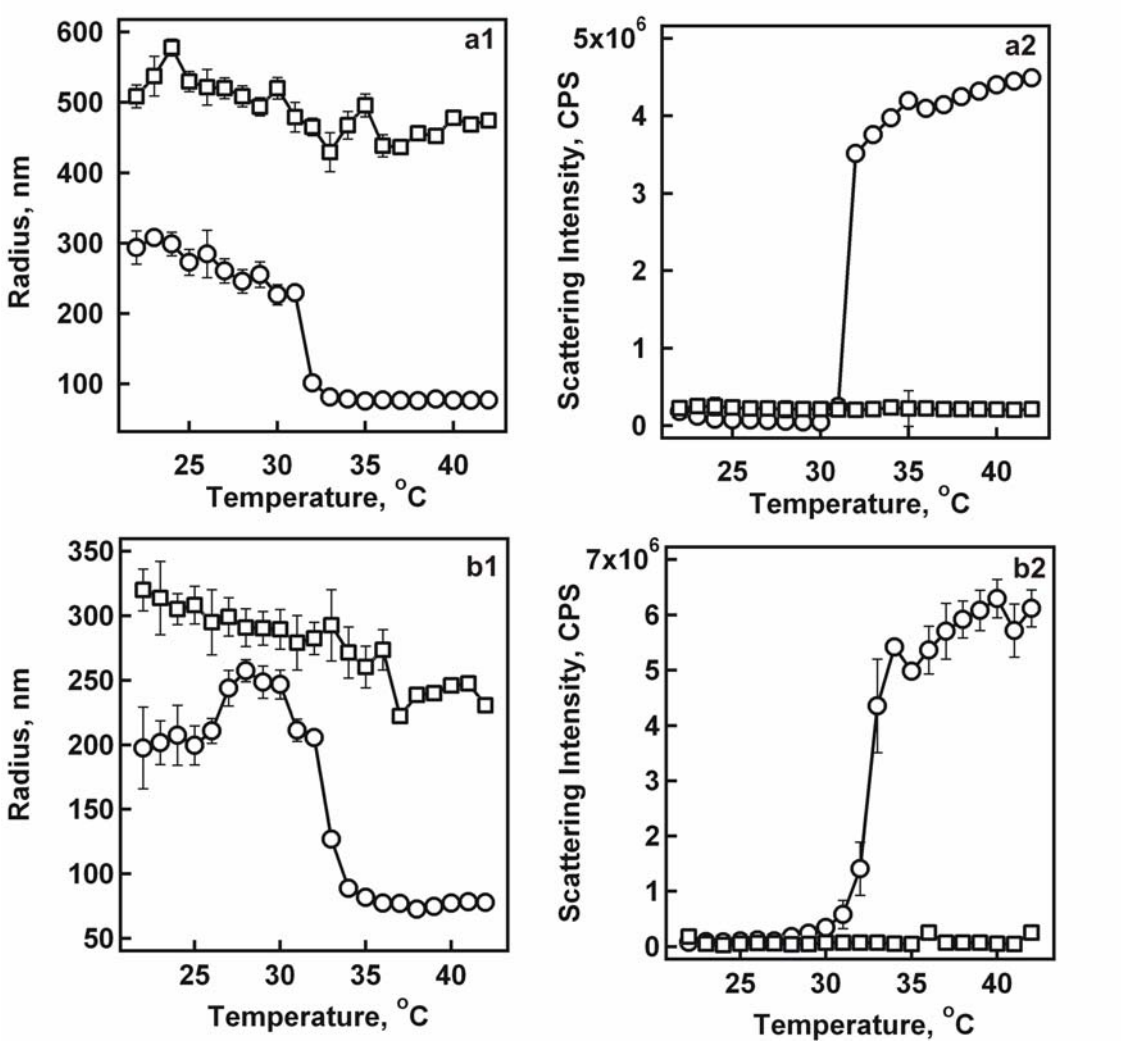

Figure 5-5. Volume phase transition curves (panels 1) for PEG 700 cross-linked pNIPAm-*co*-AAc (9:1) microgels in pH 3.5 (circles) and 6.5 (squares) media and corresponding light scattering profiles (panels 2). Panels a (0.2 mole %) and panels b (1.0 mole %).

Potentiometric Titrations

To verify 10.0 mole % acrylic acid incorporation, potentiometric titrations were performed on each microgel system using 10 mM sodium hydroxide as the base. The results are illustrated in Table 5-1.

Table 5-1. Potentiometric titration data obtained for PEG cross-linked pNIPAm-*co*-AAc (9:1) microgels

Sample	Mole % PEG	Mole % AAc calculated
PEG 200	**0.2**	**9.84**
PEG 200	**1.0**	**9.93**
PEG 200	**2.0**	**9.97**
PEG 200	**5.0**	**9.99**
PEG 575	**0.2**	**9.94**
PEG 575	**1.0**	**9.82**
PEG 575	**2.0**	**9.95**
PEG 700	**0.2**	**9.78**
PEG 700	**1.0**	**9.76**

These results verify that the acrylic acid comonomer was effectively incorporated into the PEG cross-linked pNIPAm-*co*-AAc microgels at values of at least 9.76 mole % or

greater. An example of an obtained potentiometric titration curve can be seen in Figure 5-6 for 2 mole % PEG 200 cross-linked pNIPAm-*co*-AAc (9:1) microgels.

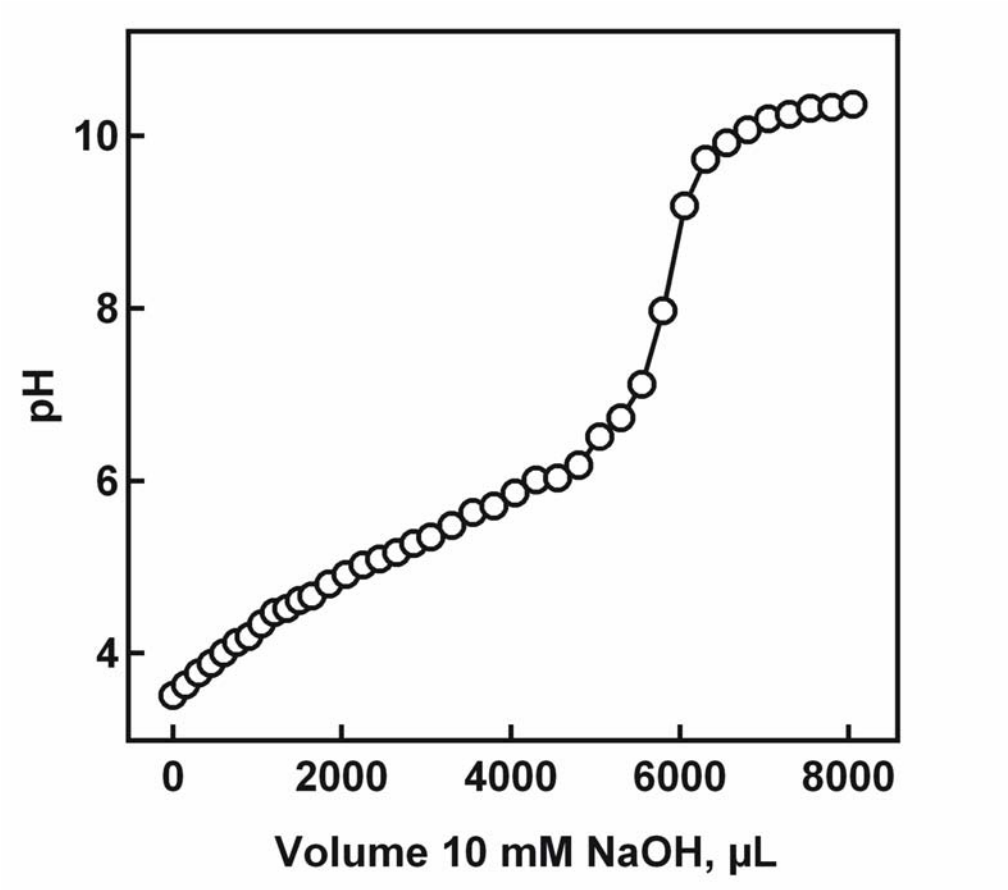

Figure 5-6. Potentiometric titration curve obtained for 2 mole % PEG 200 cross-linked pNIPAm-*co*-AAc (9:1) microgels.

Cell Adhesion Studies

It is generally acknowledged that reduction in adsorption of adhesive proteins from serum-containing solutions results in a reduction in cell adhesion and spreading. While protein adsorption studies were not performed on these PEG cross-linked pNIPAm-*co*-AAc (9:1) hydrogel nanoparticles, they have been performed on similarly prepared PEG cross-linked microgels not modified with AAc moieties that incorporated the same overall mole percentages of cross-linker as studied in this chapter (see Chapter 4). These previously discussed protein adsorption results showed that reduced protein sticking resulted when the concentration of PEG incorporated into the microgels increased. The previous findings also showed enhanced suppression of protein adsorption at elevated temperatures when the longest chain length of PEG 700 MW was used. Along this note, the efficacy of these PEG cross-linked pNIPAm-*co*-AAc (9:1) microgels for preventing cell adhesion when electrostatically attached to substrates in non-fouling applications was probed. As previously discussed in Chapter 3, incorporation of the acid groups in these microgels allows them to be electrostatically bound to positively functionalized glass substrates. An example of the thermoresponsivity of these microgels was tested in cell culture medium for 2 mole % PEG 200 cross-linked pNIPAm-*co*-AAc (9:1) particles and can be viewed in Figure 5-7. Due to the presence of AAc in the network the volume phase transition is shifted to higher temperatures and the curve becomes quite broad. However, these microgels are at least partially deswollen under cell culture conditions.

For the cell adhesion studies, stock solutions of the microgels were first prepared in 0.02 M PBS and then electrostatically attached to positively charged glass substrates

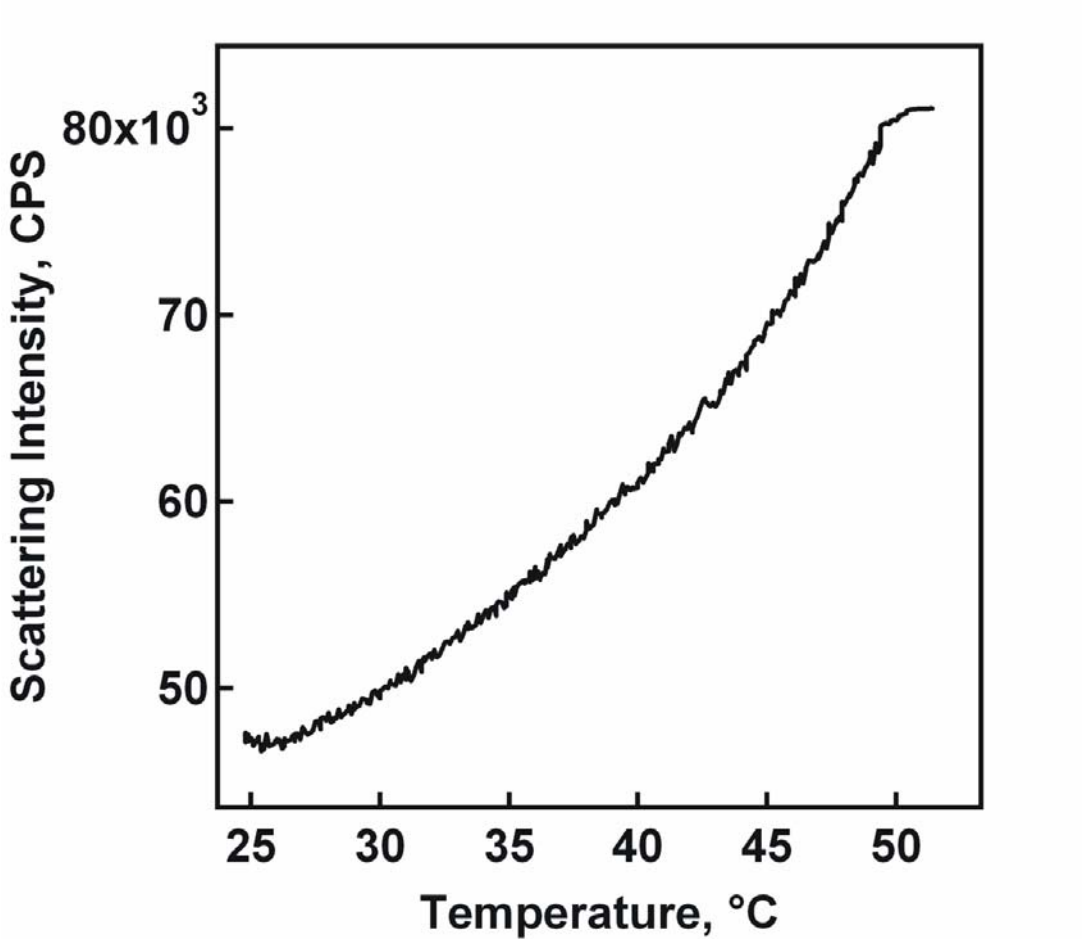

Figure 5-7. Phase transition curve obtained via light scattering for 2 mole % PEG cross-linked pNIPAm-*co*-AAc (9:1) microgels in cell culture medium.

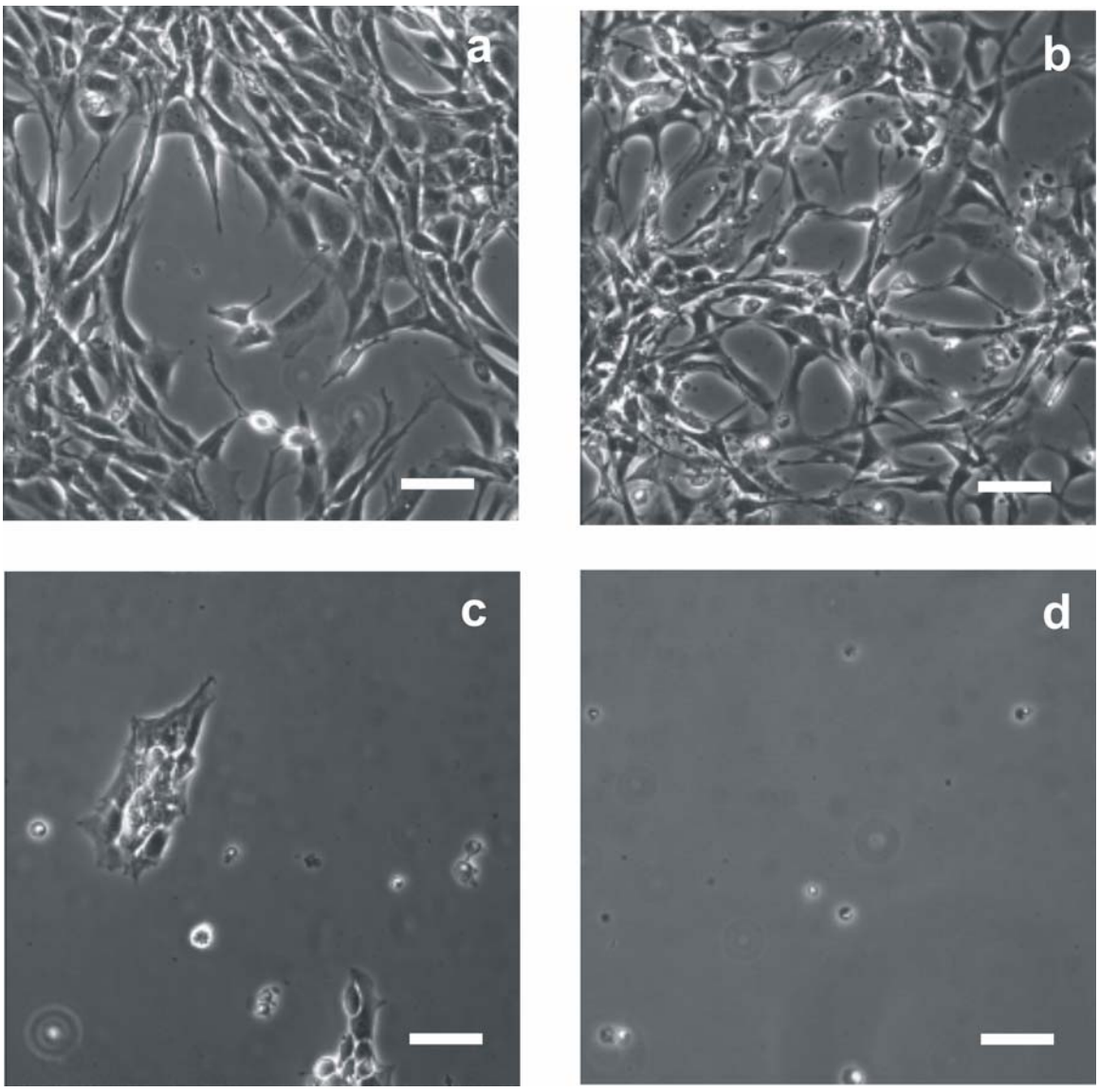

Figure 5-8. Optical micrographs (20 x magnification) of PEG 200 cross-linked pNIPAm-*co*-AAc (9:1) microgel functionalized substrates exposed to cell culture medium after three days at 37 °C; (a) 0.2, (b) 1.0, (c) 2.0 and (d) 5.0 mole % cross-linker concentrations. The scale-bar represents 20 μm.

via spin coating. These substrates were then exposed to fibroblasts in serum-containing cell culture medium at 37 °C for a set length of time to probe the non-fouling capabilities of these PEG microgel modified surfaces. The first of these results are illustrated in Figure 5-8 for the shortest cross-linker, PEG 200, at 0.2 (panel a), 1.0 (panel b), 2.0 (panel c) and 5.0 (panel d) mole %. There is a clear enhancement in the non-fouling capability of the substrates as the concentration of PEG cross-linker increases. Figure 5-9 represents the findings for PEG 575 cross-linked pNIPAm-*co*-AAc (9:1) systems at 0.2 (panel a), 1.0 (panel b) and 2.0 (panel c) mole %. These images portray the same trend in that as the PEG content increases, the surfaces display diminished cell adhesion after three days of incubation. For the PEG 700 microgels, Figure 5-10 illustrates that even at very low content (only 0.2 and 1 mole % for panel a and b, respectively), these longer cross-link chains are flexible enough to allow for enhanced non-fouling behavior. The concentration of PEG cross-links needed when using longer chains apparently decreases with an increase in PEG molecular weight, suggesting that a critical chain length is required to modify the surface energy of the deswollen particles. Similar findings have been reported by Du et al. for grafted PEG modified surfaces.[15]

The results obtained for the control samples are shown in Figure 5-11 and confirm that after three days, non-PEG modified surfaces result in significant cell adhesion and proliferation in culture. Overall, these cell adhesion results are in support of earlier discussed ^{1}H NMR and protein adsorption findings for PEG cross-linked microgels (see Chapter 4). The previously discussed results suggested that in their deswollen state, the structure of the microgels containing the longest chains was one where the PEG chains

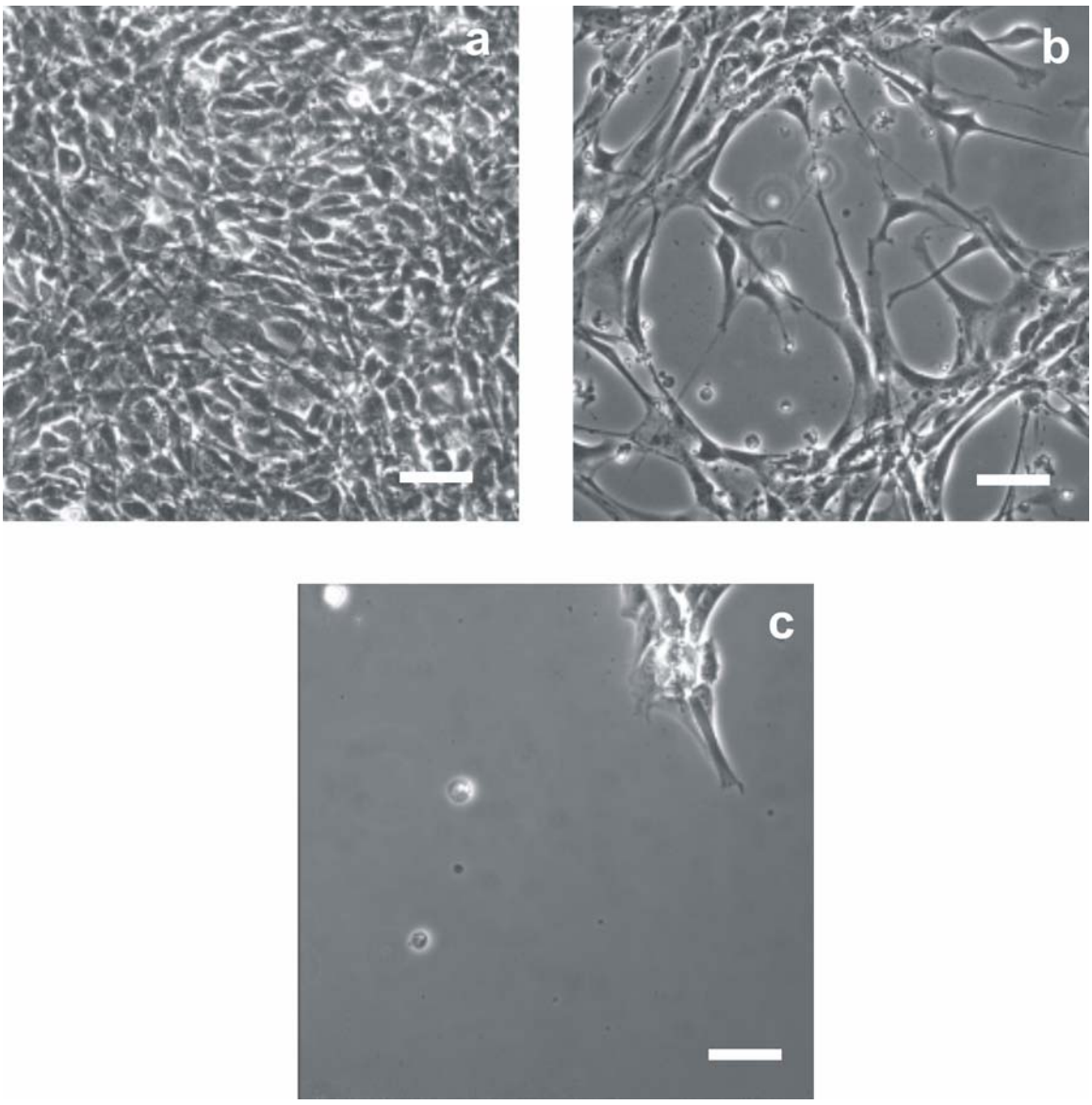

Figure 5-9. Optical micrographs (20 x magnification) of PEG 575 cross-linked pNIPAm-*co*-AAc (9:1) microgel functionalized substrates exposed to cell culture medium after three days at 37 °C; (a) 0.2 mole %, (b) 1.0 and (c) 2.0 mole % cross-linker concentrations. The scale-bar represents 20 μm.

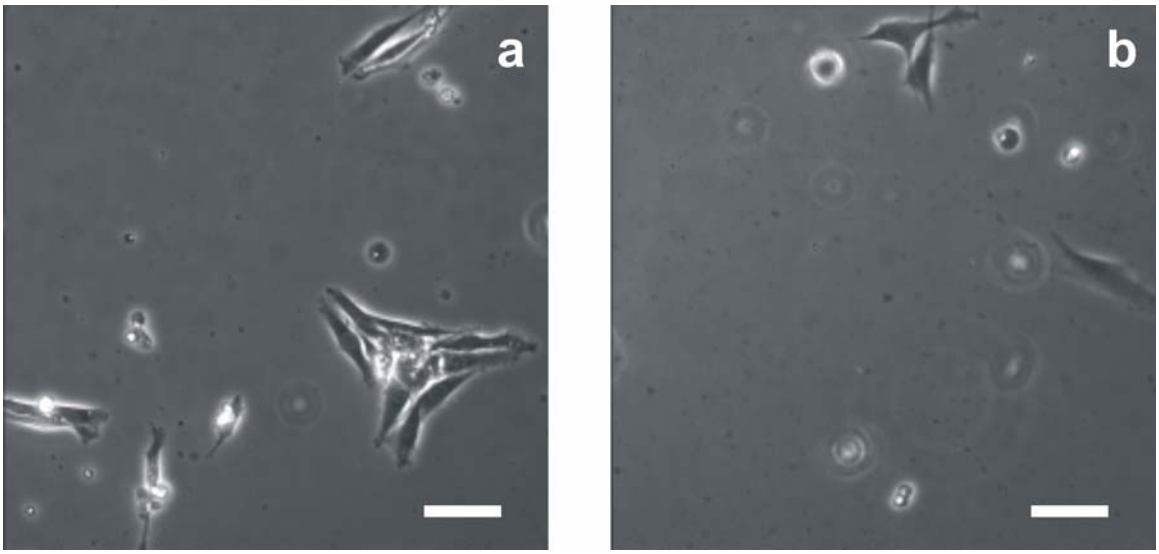

Figure 5-10. Optical micrographs (20 x magnification) of PEG 700 cross-linked pNIPAm-*co*-AAc (9:1) microgel functionalized substrates exposed to cell culture medium after three days at 37 °C; (a) 0.2 mole % and (b) 1.0 mole %. The scale-bar represents 20 μm.

were mobile enough to protrude from the hydrophobically collapsed network. Even though the experimental conditions have not been optimized with respect to surface coverage and/or PEG chain length, these studies are quite promising and illustrate that PEG cross-linked microgel functionalized surfaces can display tunable behavior in terms of cell adhesion by simply modifying the cross-linker content and/or chain length over a narrow range.

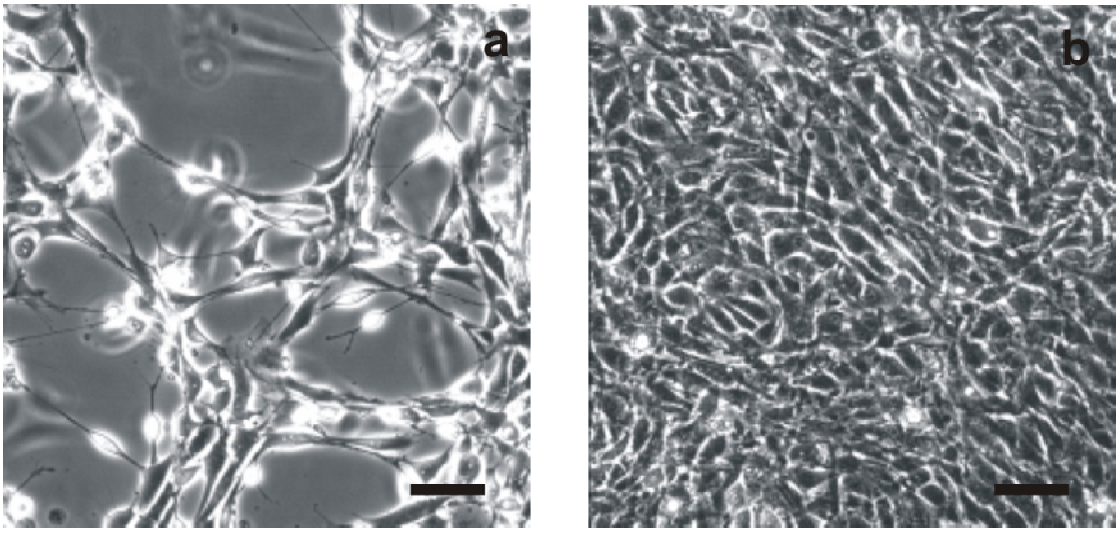

Figure 5-11. Optical micrographs (20 x magnification) of control samples exposed to cell culture medium after three days at 37 °C; (a) 2 mole % BIS cross-linked pNIPAm-*co*-AAc (9:1) microgels and (b) Tissue culture polystyrene. The scale-bar represents 20 μm.

5.4 Conclusions

By incorporating hydrophilic, flexible oligomeric cross-link chains (PEG chains) within dually responsive pNIPAm-*co*-AAc (9:1) microgels, added responsivity results in modulation of the phase transition behavior as well as swelling properties of the hydrogel particles. Results from DLS revealed that as the concentration of PEG incorporated into the microgels was augmented an increase in the phase transition temperature, as well as breadth, was observed. These acrylic acid modified microgels also exhibited pH induced swelling under pH 6.5 conditions. When electrostatically attached to a functionalized surface, these oligomerically cross-linked systems proved effective in non-fouling and cell adhesion control. These results support the earlier reported conclusions that in their

deswollen state, the oligomeric cross-links are mobile enough to protrude from the hydrophobic collapsed microgel interior (see Chapter 4). Such highly responsive networks may find applications in biomedical devices or controlled drug delivery devices.

5.5 References

(1) Revzin, A.; Russell, R. J.; Yadavalli, V. K.; Koh, W.-G.; Deister, C.; Hile, D. D.; Mellott, M. B.; Pishko, M. V. *Langmuir* **2001**, *17*, 5440-5447.

(2) Harris, J. M. *Poly(Ethylene Glycol) Chemistry Biotechnical and Biomedical Applications*; Plenum: New York, 1992.

(3) Gan, D.; Lyon, L. A. *Macromolecules* **2002**, *35*, 9634-9639.

(4) Ahmad, H.; Tauer, K. *Macromolecules* **2003**, *36*, 648-653.

(5) Tziampazis, E.; Kohn, J.; Moghe, P. V. *Biomaterials* **2000**, *21*, 511-520.

(6) Shen, M.; Pan, Y. V.; Wagner, M. S.; Hauch, K. D.; Castner, D. G.; Ratner, B. D.; Horbett, T. A. *J. Biomater. Sci., Polym. Ed.* **2001**, *12*, 961-978.

(7) Zhang, M.; Desai, T.; Ferrari, M. *Biomaterials* **1998**, *19*, 953-960.

(8) Du, H.; Chandaroy, P.; Hui, S. W. *Biochim. Biophys. Acta* **1997**, *1326*, 236-248.

(9) Scott, R. A.; Peppas, N. A. *Biomaterials* **1999**, *20*, 1371-1380.

(10) Kaneko, Y.; Nakamura, S.; Sakai, K.; Aoyagi, T.; Kikuchi, A.; Sakurai, Y.; Okano, T. *Macromolecules* **1998**, *31*, 6099-6105.

(11) Virtanen, J.; Baron, C.; Tenhu, H. *Macromolecules* **2000**, *33*, 336-341.

(12) Beltran, S.; Baker, J. P.; Hooper, H. H.; Blanch, H.; Prausnitz, J. M. *Macromolecules* **1991**, *24*, 549-551.

(13) Saunders, B. R.; Crowther, H. M.; Morris, G. E.; Mears, S. J.; Cosgrove, T.; Vincent, B. *Colloids Surf. A* **1999**, *149*, 57-64.

(14) Dowding, P. J.; Vincent, B.; Williams, E. *J. Colloid Interface Sci.* **2000**, *221*, 268-272.

(15) Aoyagi, T.; Ebara, M.; Sakai, K.; Sakurai, Y.; Okano, T. *J. Biomater. Sci., Polym. Ed.* **2000**, *11*, 101-110.

(16) Yoo, M. K.; Sung, Y. K.; Lee, Y. M.; Cho, C. S. *Polymer* **2000**, *41*, 5713-5719.

(17) Hirose, H.; Shibayama, M. *Macromolecules* **1998**, *31*, 5336-5342.

(18) Kishi, R.; Miura, T.; Kihara, H.; Asano, T.; Shibata, M.; Yosomiya, R. *J. Appl. Polym. Sci.* **2003**, *89*, 75-84.

(19) Gutowska, A.; Bark, J. S.; Kwon, I. C.; Bae, Y. H.; Cha, Y.; Kim, S. W. *J. Controlled Release* **1997**, *48*, 141-148.

(20) Kubota, N.; Matsubara, T.; Eguchi, Y. *J. Appl. Polym. Sci.* **1998**, *70*, 1027-1034.

(21) Bromberg, L.; Temchenko, M.; Hatton, T. A. *Langmuir* **2002**, *18*, 4944-4952.

(22) Lee, W.-F.; Chiu, R.-J. *J. Appl. Polym. Sci.* **2003**, *90*, 2214-2223.

(23) Torres-Lugo, M.; Peppas, N. A. *Macromolecules* **1999**, *32*, 6646-6651.

(24) Jones, C. D.; Lyon, L. A. *Macromolecules* **2000**, *33*, 8301-8306.

(25) Virtanen, J.; Tenhu, H. *Macromolecules* **2000**, *33*, 5970-5975.

(26) Pelton, R. H. *Adv. Colloid. Interface Sci.* **2000**, *85*, 1-33.

(27) Motonaga, T.; Shibayama, M. *Polymer* **2001**, *42*, 8925-8934.

(28) Philippova, O. E.; Hourdet, D.; Audebert, R.; Khokhlov, A. R. *Macromolecules* **1997**, *30*, 8278-8285.

(29) Diez-Pena, E.; Quijada-Garrido, I.; Barrales-Rienda, J. M. *Polymer* **2002**, *43*, 4341-4348.

(30) Chiu, H.-C.; Lin, Y.-F.; Hung, S.-H. *Macromolecules* **2002**, *35*, 5235-5242.

(31) Chen, G.; Hoffman, A. S. *Nature* **1995**, *373*, 49-52.

CHAPTER 6

OTHER MICROGEL LOADING STUDIES

This chapter focuses on fundamental loading studies of pNIPAm based microgel networks. It looks at macromolecule loading strategies for different cross-linked networks, as well as microgels with and without acrylic acid comonomer. It also differentiates between loading achieved via a breathing-in technique versus simple equilibrium partitioning. It is meant to elucidate general loading strategies that could be useful in future design of drug delivery devices using microgel based materials.

6.1 Introduction

As discussed in detail in previous chapters, due to the reversible deswelling nature of hydrogel networks, use of these materials in controlled drug release devices has been thoroughly pursued in recent years.[1-6] This squeezing phenomenon has been utilized as a mechanism to control both uptake and release of various model drug compounds using discrete microgel networks.[7-12] Due to the fact that proteins and peptides are inherently powerful therapeutic agents,[4] there have also been significant advances made in the design of controlled macromolecule release devices involving microgels.[10,13-16] Insulin has been of particular interest for controlled delivery from discrete microgel networks.[17-20] Along this note, and considering our initial success at insulin loading into our

microgels, we wanted to perform fundamental loading studies using larger bioactive species within our array of functionally modified microgel networks.

Herein, we describe results from studies designed to probe the effect of hydrophilic balance within microgel networks on impregnation of hydrophilic macromolecules. Hence, two different cross-linkers were studied, poly(ethylene glycol)-diacrylate versus *N,N'*-Methylenebis(acrylamide), and microgels both with and without acrylic acid comonomer were probed. In addition, the mechanism of loading was studied where equilibrium partitioning as well as loading via a breathing-in technique were compared. These studies could offer some insight into the design of future protein release devices using responsive microgel networks.

6.2 Experimental Section

Materials

All chemicals were obtained from Sigma Aldrich unless otherwise stated. *N*-Isopropylacrylamide (NIPAm) was recrystallized from hexane (J. T. Baker) prior to use. *N*, *N*′-Methylene(bisacrylamide) (BIS), ammonium persulfate (APS), anhydrous acrylic acid (AAc; Fluka), 95% ethanol, 200 proof anhydrous ethanol, fluorescein isothiocyanate labeled insulin (FITC-insulin) from bovine pancreas, formic acid, FITC-dextran (70, 000 MW), poly(ethylene glycol) diacrylate (PEG) (200 MW, Polysciences, Inc.) and FITC labeled bovine serum albumin (FITC-BSA; 68, 000 MW) were used as received. 3-Aminopropyltrimethoxysilane (APTMS) was obtained from United Chemical Technologies. Phosphate buffered saline solution (pH 7.4, 0.02 M) was prepared in house from NaCl (Fisher), Na_2HPO_4 (EM Science) and KH_2PO_4. Glass microscope coverslips

(22 × 22 mm) were purchased from Fisher Scientific. 0.2 μm nylon membrane disks and Spectra/Por 10, 000 MWCO dialysis membrane were purchased from VWR. Water used in all experiments was distilled and then purified using a Barnstead E-Pure system operating at a resistance of 18 MΩ. A 0.2 μm filter was incorporated into this system to remove particulate matter.

Particle Synthesis

The details of free-radical precipitation polymerization used in these studies have been discussed in previous chapters. In general, the following protocol was followed. Sodium dodecyl sulfate (SDS) was used as the stabilizing surfactant while ammonium persulfate (APS) was used as the free radical initiator. The NIPAm monomer, cross-linker (BIS or PEG diacrylate of 200 MW) and surfactant were dissolved in nanopure water and then filtered through a 0.2 μm nylon membrane filter to remove any large particulate matter that could act as unwanted nuclei in the reaction. This dissolved solution was continuously stirred in a three-neck, 250 mL round-bottom flask. This solution was heated to 70 ºC while being purged with N_2 gas. Approximately one hour later, the temperature of the solution was stable at 70 ºC. Fifteen minutes later, the reaction was initiated by adding a hot (70 ºC) solution of APS. The solution turned turbid within 10 minutes, indicating successful initiation. The reaction proceeded for approximately 6 hours under a constant stream of nitrogen gas. Following synthesis, the microgels were cooled and filtered using a P2 Whatman filter paper. They were then dialyzed (using 10, 000 MWCO) for 2 weeks against nanopure water with a daily exchange of fresh water. For the synthesis of pH sensitive microgels, acrylic acid was added approximately 15 minutes prior to the addition of the initiator.

For use of large microgels not containing acrylic acid comonomer, particles were borrowed from Ashlee St. John. To achieve large microgels without a charged comonomer, the total monomer concentration was kept at 140 mM and no surfactant was used. In short, 1.5 g NIPAm, 0.04 g BIS and 0.03 g APS were used in 100 mL nanopure water. The same synthesis procedure as cited above was followed otherwise.

Dynamic Light Scattering (DLS)

Characterization of the hydrodynamic radii and light scattering intensities of the microgels used in these studies has been discussed in detail in previous chapters. These results will not be discussed here.

Microgel Loading Strategies and Characterization of Loaded Microgels

For macromolecule loading studies, both equilibrium partitioning and swelling dried microgels in concentrated solution strategies were explored. Three model macromolecules studied were FITC-insulin, FITC-dextran (70, 000 MW) and FITC-bovine serum albumin (FITC-BSA; 68, 000 MW). For loading studies that involved the analysis of these FITC labeled probes in solution, the fluorescence emission was monitored using λ_{ex} = 473 nm and λ_{em} = 512 nm.

For initial macromolecule loading studies, microgels cross-linked with 2 mole % PEG 200 and 2 mole % BIS, both with and without acrylic acid comonomer, were investigated. The loading conditions in these experiments were kept at low pH (3.5) to probe the actual effect of hydrophilic content on loading and not just porosity of the networks that might be a factor under higher pH conditions. In these experiments, stock solutions of the microgels were prepared at 6 mg/0.9mL in 50 mM pH 3.5 formate buffer. To these already swollen solutions, 0.5 mL of 9.8 x 10^{-6} M 70, 000 MW FITC-dextran in

50 mM pH 3.5 formate buffer was added. These solutions were allowed to mix via shaking for 24 hours. They were then centrifuged at 14, 000 rpm for 90 minutes at 26 °C. 150 μL of supernatant was extracted from each sample and diluted with 4.0 mL of 0.02 M PBS. This dilution into PBS buffer was made so that the analyzed solutions would be at a suitable pH for fluorescence emission detection (FITC has poor emission properties at low pH). These solutions were then analyzed via fluorescence spectroscopy for qualitative differences in loading capacity.

For pH-induced loading, equilibrium partitioning was utilized where stock solutions of FITC-dextran and FITC-BSA were first prepared by dissolving approximately 3 mg of model drug in 1.5 mL of pH 3.5 formate buffer. This stock solution was then mixed with 10 mL of the 1 mole % BIS cross-linked pNIPAm-*co*-AAc (9:1) microgels, and the pH was adjusted to 7.4 by slow addition of 0.1 M NaOH. This solution was left to stir in the refrigerator overnight in the dark. This procedure mimics that used to load FITC-insulin into 1 mole % BIS cross-linked pNIPAm-*co*-AAc (9:1) microgels for the thermally modulated insulin release from microgel thin films (see Chapter 3).[21] The idea here is to ascertain if larger macromolecules than insulin could be effectively loaded into these dually responsive microgels via the same method. To ascertain effective macromolecule loading, the impregnated microgel dispersions were electrostatically deposited onto positively charged glass substrates via spin coating as a monolayer. It should be noted that the macromolecule loaded microgel solutions were at pH 7.4 and thus, should be negatively charged making them amenable for polyelectrolyte deposition.[21] Fluorescence microscopic images were then taken of these monolayers using an Olympus IX-70 inverted microscope equipped with a mercury arc lamp. Images

were captured using a color CCD camera (Pixel Fly, Cooke Corp.) and an Olympus 100x UplanFl 1.30 NA oil immersion objective.

To investigate the idea of loading microgels with macromolecules without the need for pH induced swelling, a simple breathing-in technique was explored where lyophilized 2 mole % BIS cross-linked microgels were allowed to swell in a concentrated solution of FITC-insulin for 24 hours. These microgels were synthesized by Ashlee St. John and were used because they were large enough in hydrodynamic radius to be observed using optical microscopy. FITC-insulin was first dissolved in pH 3.5 formate buffer to prepare the stock solution[22] and then the pH was increased by addition of NaOH until pH 7.4 was achieved. A final concentration of 3 mg/mL of insulin was achieved for the stock solution. 1 mL of this stock solution was added to 20 mg of lyophilized 2 mole % BIS pNIPAm microgels and the particles were allowed to swell in this solution, thereby imbibing the concentrated insulin, for 24 hours. To ascertain actual loading and not just adsorption, these FITC-insulin loaded microgels were cleaned via centrifugation at 14, 000 rpm for 30 minutes at 26 °C. After each centrifugation cycle, the supernatant was taken off and the FITC-insulin loaded microgel pellet was then redispersed in 20 mM PBS. The UV/vis absorbance of the supernatant solution was monitored for presence of FITC-insulin until negligible absorbance was seen. This occurred after two cleaning cycles. Again, to ascertain effective macromolecule loading of FITC-insulin into these 2 mole % BIS cross-linked pNIPAm microgels via a breathing-in technique, the loaded microgels were electrostatically deposited onto positively charged glass substrates via spin coating and then fluorescence microscopic images were taken.

6.3 Results and Discussion

Particle synthesis and characterization

The large 2 mole % BIS cross-linked pNIPAm microgels without acrylic acid comonomer were synthesized by Ashlee St. John. The obtained DLS results showed that they had an average hydrodynamic radius of 391.33 nm at 25 °C with an average polydispersity of 5.1 %. Hence, these microgels, once loaded and deposited onto a charged substrate should be visible for verification of effective FITC-insulin loading. As discussed in the experimental section, characterization of the other microgels used in these studies (2 mole % PEG and 2 mole % BIS cross-linked microgels both with and without 10.0 mole % acrylic acid comonomer) has been described in detail in previous chapters and will not be discussed here.

Microgel Loading Strategies and Characterization of Loaded Microgels

For these macromolecule loading studies, both equilibrium partitioning and swelling via a breathing-in technique were explored. The three model macromolecules studied were FITC-insulin, FITC-dextran (70, 000 MW) and FITC-bovine serum albumin (FITC-BSA).

Initial loading studies interrogated the impregnation of a large hydrophilic macromolecule (FITC-dextran of 70, 000 MW) into both PEG and BIS cross-linked microgels with and without AAc comonomer at 10.0 mole %. The idea here was to ascertain if any differences in the hydrophilic balance of the microgel networks played a significant role in their loading capacity. It is important to note that the loading conditions here were kept at pH 3.5 to directly probe the effect of hydrophilic balance and not porosity (which could be a factor under pH 7 conditions). The results for this

study are illustrated in Figure 6-1. For both 2 mole % PEG and BIS cross-linked samples, the microgels containing the acrylic acid comonomer at 10.0 mole % loaded more FITC-dextran than the corresponding microgels without AAc. This is indicated by decreased fluorescence emission observed in the supernatant, meaning more macromolecule loaded into the centrifuged microgel pellet. These results indicate that the overall hydrophilic balance does play a role in loading efficiency. Furthermore, the BIS cross-linked samples (the most hydrophobic networks) resulted in the lowest loading yields (as indicated by the highest fluorescence emission values). Again, these results indicate that the hydrophilic/hydrophobic balance of thermoresponsive microgels plays an important role in their ability to impregnate large hydrophilic macromolecules. These findings are in support of results discussed in Chapter 4 which showed that with higher PEG 200 content, enhanced loading of large FITC dextran molecules (both 70, 000 and 150, 000 MW) resulted.

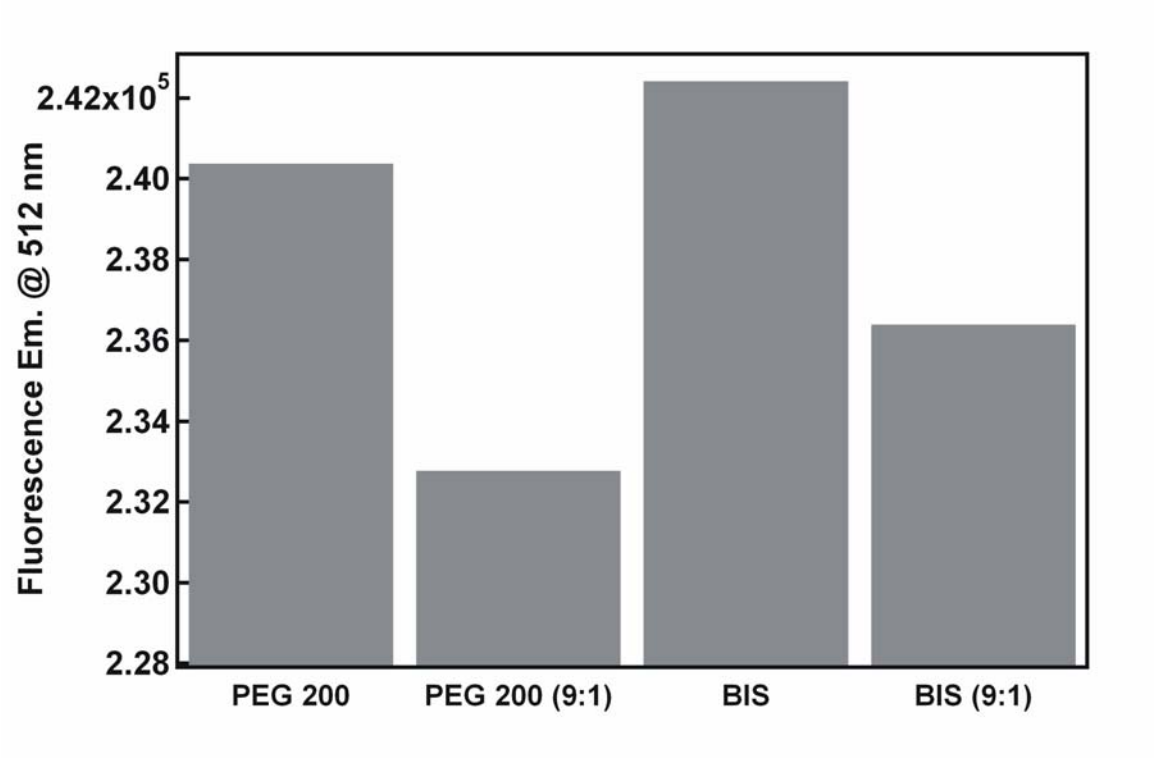

Figure 6-1. Plot of loading efficiency results obtained for FITC-dextran (70, 000 MW) loaded 2 mole % PEG and BIS cross-linked pNIPAm microgels both with and without 10.0 mole % acrylic acid comonomer.

This effect of enhanced hydrophilic macromolecule loading has been observed in preliminary studies. In these preliminary studies, after two weeks of initial loading and centrifugation, the drug loaded pellet for the 2 mole % BIS cross-linked pNIPAm-*co*-AAc (9:1) sample still appeared bright yellow versus the 2 mole % BIS and 5 mole % BIS cross-linked pNIPAm microgels. The sample pellets that did not contain acrylic acid comonomer were opaque and not yellow. Furthermore, it was obvious by eye that the supernatants for the networks without AAc were much brighter than the more effectively loaded AAc containing network. These results suggest that the more hydrophilic sample

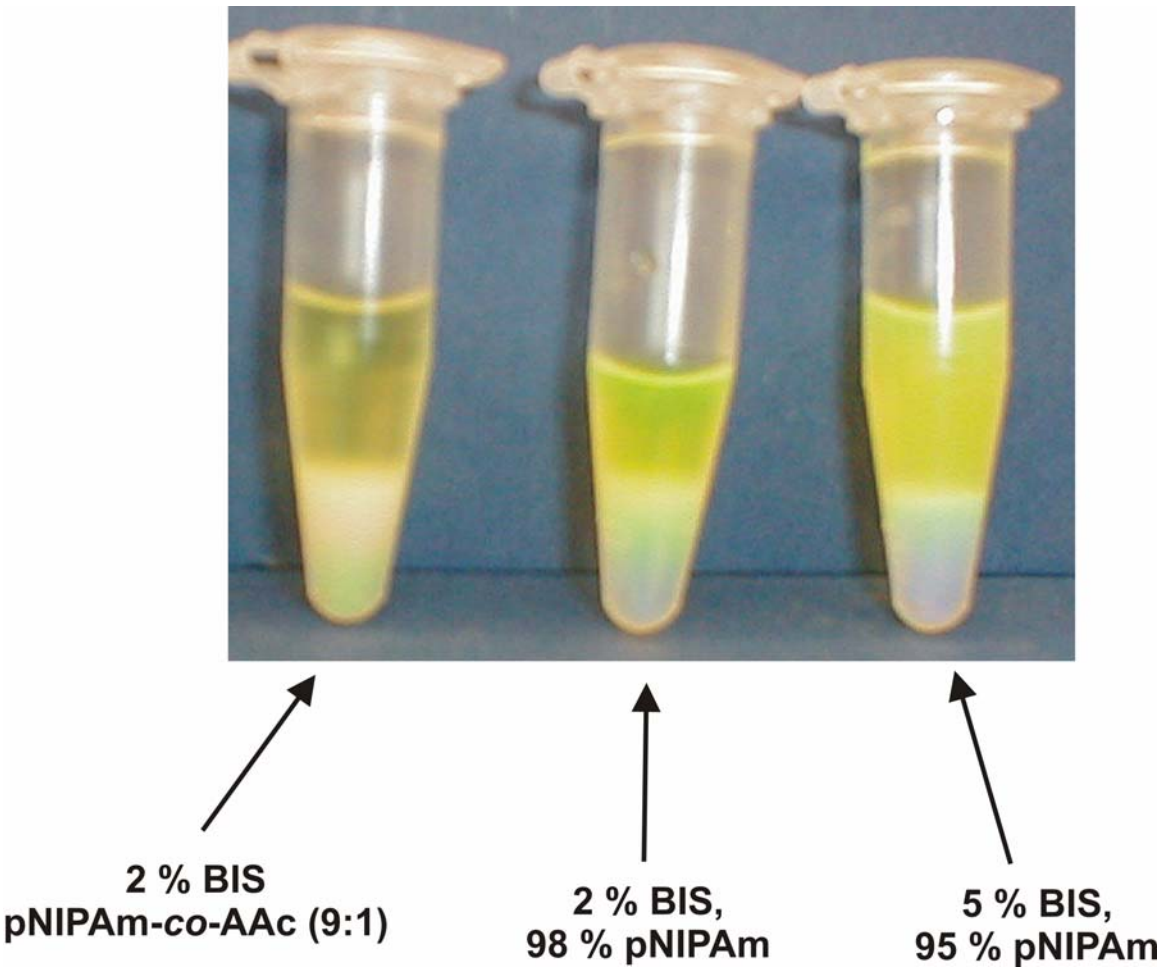

Figure 6-2. Photograph of FITC-dextran (70, 000 MW) loaded BIS cross-linked samples after two weeks of initial loading and centrifugation. The sample with 10.0 mole % AAc comonomer kept the macromolecule effectively loaded due to enhanced hydrophilic balance.

(that containing 10.0 mole % AAc) results in the most effective loading of the hydrophilic macromolecule.

Based on the positive results obtained for FITC-insulin loading into 1 mole % BIS cross-linked pNIPAm-*co*-AAc (9:1) microgels (see Chapter 3)[21] and the results discussed

above, we wanted to further prove the concept that acrylic acid modified BIS cross-linked microgels could effectively load larger macromolecules. We chose to load the identical 1 mole % BIS cross-linked pNIPAm-*co*-AAc (9:1) microgels using the same pH induced swelling protocol followed in the initial FITC-insulin loading studies (see Chapter 3). In these studies, we impregnated the microgels with both FITC-dextran (70, 000 MW) and FITC-BSA (68, 000 MW). After impregnation at pH 7.4, these loaded microgel solutions were electrostatically deposited onto positively functionalized glass substrates and then imaged via fluorescence microscopy. The first of these results are shown in Figure 6-3. As observed with the initial FITC-insulin pH induced loading studies, this fluorescence microscopic image indicates that the particles all appear highly fluorescent while there is little background fluorescence. This suggests that the large macromolecule was effectively impregnated into these microgels. Figure 6-4 shows a similar image obtained for FITC-BSA loaded microgels and again, suggests successful loading using this pH-induced swelling technique.

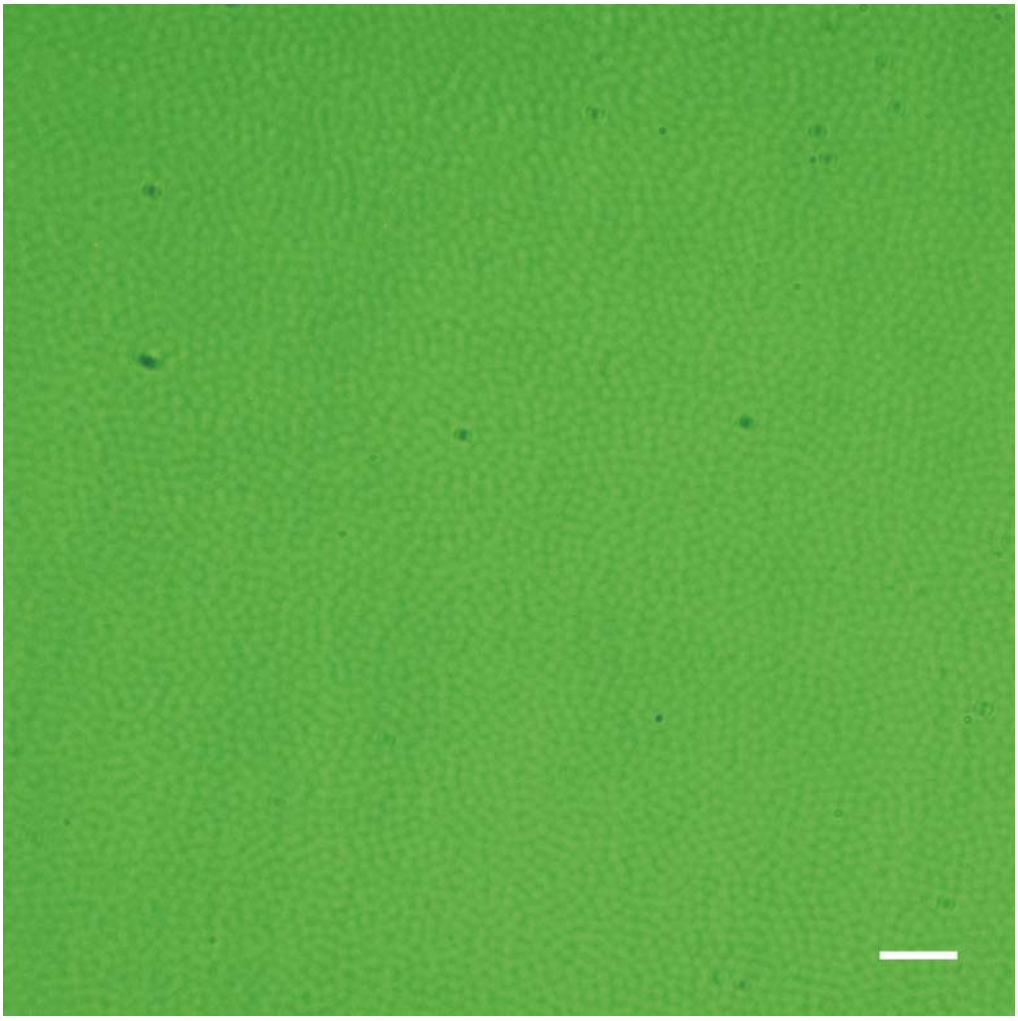

Figure 6-3. Fluorescence microscopic image of 1 layer of FITC-dextran (70, 000 MW) loaded 1 mole % BIS cross-linked pNIPAm-*co*-AAc (9:1) microgels via pH-induced swelling. Scale bar represents 20 μm.

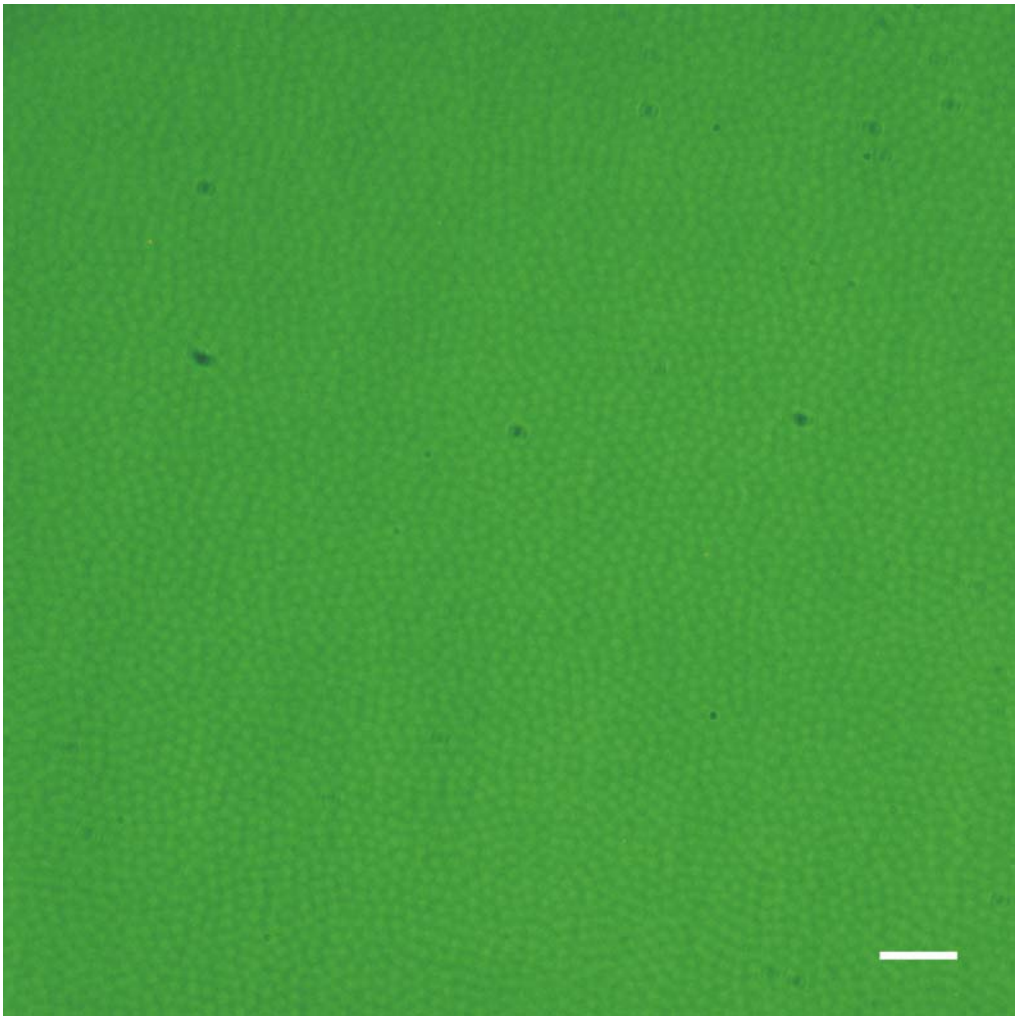

Figure 6-4. Fluorescence microscopic image of 1 layer of FITC-bovine serum albumin (68, 000 MW) loaded 1 mole % BIS cross-linked pNIPAm-*co*-AAc (9:1) microgels via pH-induced swelling. Scale bar represents 20 μm.

To investigate the idea of loading microgels with macromolecules without the need for pH-induced swelling, a simple breathing-in technique was explored where lyophilized 2 mole % BIS cross-linked microgels were allowed to swell in a concentrated solution of FITC-insulin for 24 hours. It should be noted that large microgels were borrowed from Ashlee St. John in this study so that optical microscopy could be used to probe loading. To ascertain actual loading and not just adsorption, these FITC-insulin loaded microgels were cleaned via centrifugation at 14, 000 rpm for thirty minutes at 26 °C. After each centrifugation cycle, the supernatant was taken off and the FITC-insulin loaded microgel pellet was then redispersed in 20 mM PBS. The UV/vis absorbance of the supernatant solution was monitored for presence of FITC-insulin until negligible absorbance was seen. This occurred after two cleaning cycles. The loaded microgel suspension was then deposited via spin coating onto a positively charged substrate and then imaged via fluorescence microscopy. Figure 6-5 shows this image and again, shows highly fluorescent microgels which suggest effective FITC-insulin loading with this breathing-in technique. In comparison to Figure 6-3 and 6-4, this image appears less fluorescent overall. But, this is to be expected considering the fact that these microgels were cleaned before deposition to remove any non-specifically adsorbed FITC-insulin. Even after thorough cleaning, though, this fluorescence microscopic image shows highly fluorescent microgels indicating that the FITC-insulin is effectively entrapped in the microgels.

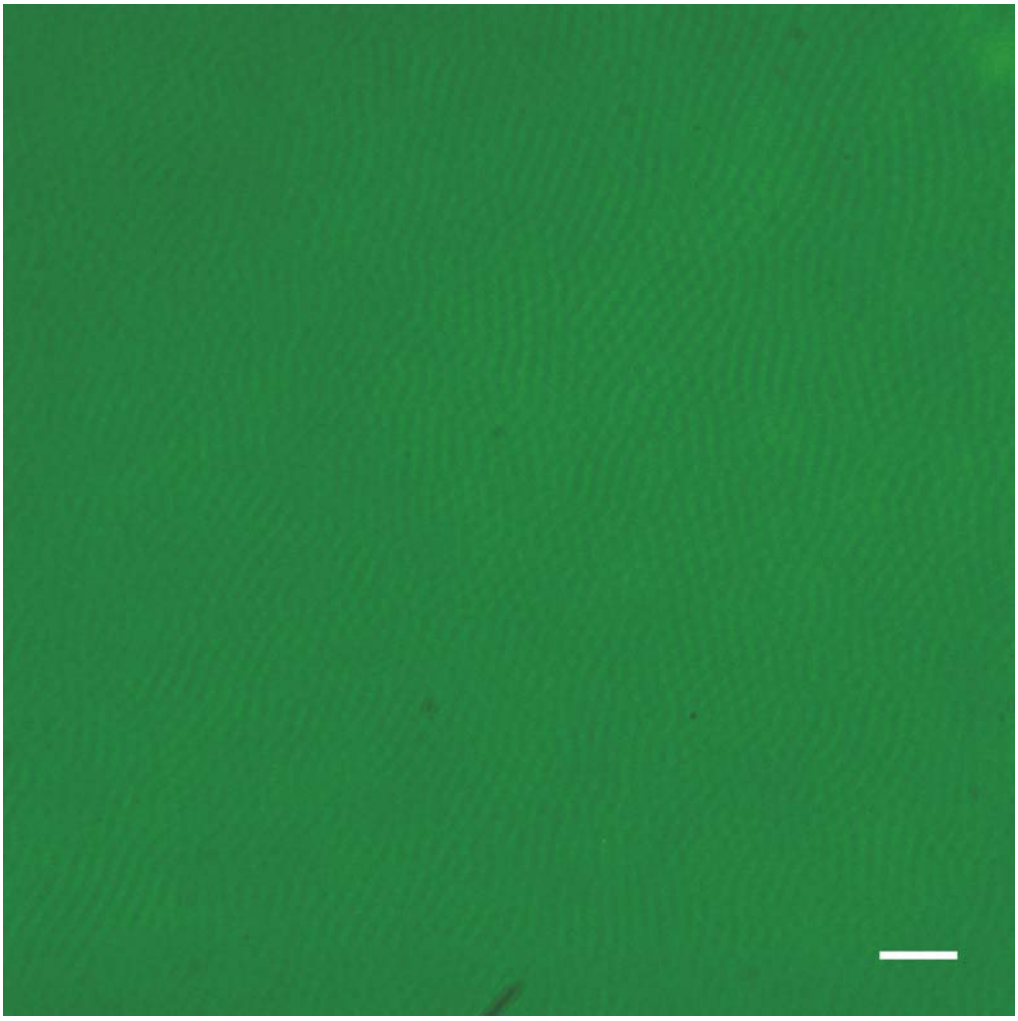

Figure 6-5. Fluorescence microscopic image of FITC-insulin loaded 2 mole % BIS cross-linked pNIPAm microgels via a breathing-in technique. Scale bar represents 20 μm.

6.4 Conclusions

These general loading strategies indicate that the hydrophilic balance of microgel networks does indeed significantly affect the corresponding loading capacities with respect to hydrophilic macromolecules. By simply changing the cross-linker chemistry to

utilize PEG versus BIS, enhanced loading can be achieved. Furthermore, incorporation of a pH sensitive comonomer, acrylic acid, can be advantageous for both pH induced loading as well as enhanced impregnation resulting from an overall increase in hydrophilicity. Beyond using a pH switch to imbibe macromolecules, these studies show that the inherent swelling behavior of microgels alone can be used as an effective loading tool of large bioactive species. These investigations could prove useful in the design of future protein release devices composed of stimuli-responsive hydrogel nanoparticles.

6.5 References

(1) Peppas, N. A.; Leobandung, W. *J. Biomat. Sci., Poly. Ed.* **2004**, *15*, 125-144.

(2) Siegel, R. A.; Ziaie, B. *Adv. Drug Delivery Rev.* **2004**, *56*, 121-123.

(3) Kikuchi, A.; Okano, T. *Adv. Drug Delivery Rev.* **2002**, *54*, 53-77.

(4) Hoffman, A. S. *Adv. Drug Delivery Rev.* **2002**, *54*, 3-12.

(5) Qiu, Y.; Park, K. *Adv. Drug Delivery Rev.* **2001**, *53*, 321-339.

(6) Kopecek, J.; Kopeckova, P.; Minko, T.; Lu, Z. R.; Peterson, C. M. *J. Controlled Release* **2001**, *74*, 147-153.

(7) Kiser, P. F.; Wilson, G.; Needham, D. *J. Controlled Release* **2000**, *68*, 9-22.

(8) Lynn, D. M.; Mansoor, M. A.; Langer, R. *Angew. Chem. Int. Ed.* **2001**, *40*, 1707-1710.

(9) Kim, I.-S.; Jeong, Y.-I.; Cho, C. S.; Kim, S.-H. *Int. J. Pharm.* **2000**, *211*, 1-8.

(10) Murthy, N.; Xu, M.; Schuck, S.; Kunisawa, J.; Shastri, N.; Frechet, J. M. J. *Proc. Natl. Acad. Sci.* **2003**, *100*, 4995-5000.

(11) Murthy, N.; Thng, Y. X.; Schuck, S.; Xu, M. C.; Frechet, J. M. J. *J. Am. Chem. Soc.* **2002**, *124*, 12398-12399.

(12) Goh, S. L.; Murthy, N.; Xu, M.; Frechet, J. M. J. *Bioconj. Chem.* **2004**, *15*, 467-474.

(13) Mellott, M. B.; Searcy, K.; Pishko, M. V. *Biomaterials* **2001**, *22*, 929-941.

(14) Wang, N.; Wu, X. S.; Li, J. K. *Pharm. Res.* **1999**, *16*, 1430-1435.

(15) Slager, J.; Domb, A. J. *Biomaterials* **2002**, *23*, 4389-4396.

(16) Hanes, J.; Chiba, M.; Langer, R. *Biomaterials* **1998**, *19*, 163-172.

(17) Kwong, A. K.; Chou, S.; Sefton, M. V. *J. Controlled Release* **1986**, *4*, 47-62.

(18) Soriano, I.; Evora, C.; Llabres, M. *Int. J. Pharm.* **1996**, *142*, 135-142.

(19) Leobandung, W.; Ichikawa, H.; Fukumori, Y.; Peppas, N. A. *J. Controlled Release* **2002**, *80*, 357-363.

(20) Damge, C.; Vranckx, H.; Balschmidt, P.; Couvreur, P. *J. Pharm. Sci.* **1997**, *86*, 1403-1409.

(21) Nolan, C. M.; Serpe, M. J.; Lyon, L. A. *Biomacromolecules* **2004**, *5*, 1940-1946.

(22) Dorkoosh, F. A.; Verhoef, J. C.; Ambagts, M. H. C.; Rafiee-Tehrani, M.; Borchard, G.; Junginger, H. E. *Eur. J. Pharm. Sci.* **2002**, *15*, 433-439.

CHAPTER 7

A ^{1}H NMR INVESTIGATION OF THERMALLY TRIGGERED INSULIN RELEASE FROM PNIPAM MICROGELS

We describe investigations of direct insulin release detection from thermoresponsive microgels using variable temperature ^{1}H NMR. pNIPAm microgels were imbibed with the peptide via a breathing-in technique which was compared to a simple equilibrium partitioning strategy. Dynamic light scattering results suggest that the phase transition of insulin-impregnated microgels is not perturbed as compared to the native particles. Variable temperature ^{1}H NMR studies, performed on both lyophilized microgels swollen in concentrated insulin versus simple mixing of solutions, suggests that the breathing-in methodology results in enhanced entrapment of the peptide. A centrifugation loading assay supports this finding and shows that the swelling technique results in more efficient impregnation. ^{1}H NMR temperature jump studies were also performed and suggest that the insulin release rate is partially decoupled from microgel collapse depending upon the temperature differential applied. These types of direct release investigations could prove as useful templates in the future design of controlled macromolecule drug delivery devices.

7.1 Introduction

As described previously, significant work has focused on using responsive hydrogels as carriers for peptide delivery in recent years.[1-5] Insulin is a therapeutic agent that is known to be endogenously released in a pulsatile manner[6-10] and hence, oscillatory insulin release from hydrogel systems has been heavily explored.[11] Work done by Siegel et al. has proposed a general strategy for pulsatile drug release[12] and these studies have been extended to self-regulated hormone release systems.[13,14] The use of discrete microgel particles for controlled insulin delivery has also found great precedence in the literature.[15-18]

We have previously reported results on thermally modulated insulin release from Layer-by-Layer (LbL) assembled microgel thin films (see Chapter 3).[19] The microgels utilized in this earlier discussed work contained pH sensitive acrylic acid groups. This pH responsivity allowed the microgels to swell under neutral pH conditions and this was what we hypothesized was the main driving force allowing for insulin imbibition into the particles. In this current study, we wanted to ascertain whether or not this pH swelling was necessary to effectively load our microgels with a macromolecularly sized therapeutic agent. Hence, microgels without acrylic acid comonomer were investigated. Two loading strategies were compared. One takes advantage of the inherent sponge-like ability of hydrogels to swell dramatically in solution, thereby allowing solute molecules to partition into the porous network. This technique was directly compared to a simple equilibrium partitioning strategy where an already swollen microgel solution was mixed with an insulin solution. In the previously mentioned work, a microgel thin film construct was utilized that resulted in relatively slow release rates from the films as compared to

the deswelling rate of the native microgels themselves in solution. Timed-release experiments on the seconds to minutes timescale that could detect direct insulin expulsion from microgels in solution could offer some insight into early release kinetics of these networks. To directly monitor insulin release into solution, we hypothesize that ^{1}H NMR can be used as a probe, considering the fact that similar release events have been previously studied in such a manner.[20] These types of studies could serve as model experiments to probe different particle release characteristics and may give us some insight into the possibility of ultimately tuning film release rates based on different particle properties in solution.

Herein, we describe results of optimized entrapment of a therapeutic agent, insulin, into thermoresponsive microgels. A rapid breathing-in technique results in efficient loading of the peptide. Direct insulin release from the microgels in solution was probed using a simple ^{1}H NMR technique. Temperature jump studies gave some insight into the correlation between microgel collapse and insulin release and suggested that the two were not directly correlated depending upon the temperature differential. These types of direct release studies that probe the interaction between entrapped and freely diffusing proteins and microgels could prove as model experiments in future design of macromolecule drug release from functionally modified thermoresponsive hydrogel networks. This could ultimately lead to the tailored design of peptide-loaded microgel thin films with tunable release rates.

7.2 Experimental

Materials

All chemicals were obtained from Sigma Aldrich unless otherwise stated. *N*-Isopropylacrylamide (NIPAm) was recrystallized from hexane (J. T. Baker) prior to use. *N, N′*-Methylene(bisacrylamide) (BIS), sodium dodecyl sulfate (SDS), ammonium persulfate (APS), deuterium oxide (D_2O), deuterated hydrochloric acid (DCl), deuterated sodium hydroxide (DOH), deuterated acetone and insulin (from bovine pancreas) were used as received. 0.2 μm nylon membrane disks and Spectra/Por 10, 000 MWCO dialysis membrane were purchased from VWR. Water used in all experiments was distilled and then purified using a Barnstead E-Pure system operating at a resistance of 18 MΩ. A 0.2 μm filter was incorporated into this system to remove particulate matter.

Particle Synthesis

2 mole % BIS cross-linked pNIPAm microgels were synthesized by precipitation polymerization via a method slightly modified from that previously described.[21] The total monomer concentration was 100 mM in all reactions. SDS was used as a surfactant and APS was used as the free radical initiator. The NIPAm monomer, cross-linker and surfactant (0.01 g) were dissolved in 200 mL of nanopure water, filtered through a 0.2 μm nylon membrane filter to remove any large particulate matter and then continuously stirred in a three-neck, 250 mL round-bottom flask. This solution was heated to 70 ºC while being purged with N_2 gas. Approximately one hour later, the temperature of the solution was stable at 70 ºC. Fifteen minutes later, the reaction was initiated by adding a hot (70 ºC) solution of APS (1 mM final concentration). The solution turned turbid within 10 minutes, indicating successful initiation. The reaction proceeded for 6 hours under a

constant stream of nitrogen. Following synthesis, the microgels were filtered using a P2 Whatman filter paper and then dialyzed (using 10, 000 MWCO) for 2 weeks against nanopure water with a daily exchange of fresh water.

Dynamic Light Scattering (DLS)

Hydrodynamic radii and light scattering intensities were obtained by DLS (Protein Solutions, Inc.). Prior to analysis, the purified microgels were diluted in filtered nanopure water (using 0.2 μm filters) until a count rate of 350 kCt/s was obtained. The suspensions were then held at each temperature for 15 minutes to achieve thermal equilibration before measurements were taken. Longer equilibration times did not result in variations of particle radius, polydispersity, or light scattering intensity. The data points presented here are an average of 5 measurements with a 60 s acquisition time and a signal-to-noise ratio threshold of 2.5. Hydrodynamic radii were calculated from the measured diffusion coefficients using the Stokes–Einstein equation. All correlogram analyses were performed with manufacturer-supplied software (Dynamics v.5.25.44, Protein Solutions, Inc.).

Impregnation of Microgels with Insulin

Two loading strategies were compared. The first was to swell lyophilized microgels in a concentrated solution of insulin for 24 hours. Insulin is sparingly soluble at neutral pH values but is quite soluble under acidic conditions.[22] Thus, it was first dissolved in deuterated HCl to prepare the stock solution[22] and then the pH was increased by addition of deuterated NaOH until pH 7.4 was achieved. A final concentration of 31 mg/mL of insulin was achieved. A known volume of diluted stock solution was then added to a known mass of lyophilized microgels (15.2 mg) and the particles were allowed

to swell in this solution, thereby imbibing the concentrated insulin, for 24 hours. The overall concentration of insulin in the final solution was 15 mg/mL. For the physical mixture, the same mass of lyophilized microgels was weighed out (15.2 mg) and dissolved in D_2O. This already swollen mixture of microgels was then physically mixed with a known volume of diluted insulin stock solution to yield the same overall concentration of insulin as the previously mentioned sample.

^{1}H NMR

A Bruker Digital Avance DRX 500 MHz NMR spectrometer was used for the insulin release investigations and experiments were run by Dr. Leslie Gelbaum. Lyophilized microgels (1.0 mg) and insulin (8.0 mg) were dissolved in 1 mL of D_2O and the spectra of each were recorded at 25 °C. Spectra of insulin loaded microgels (both swollen and mixed solutions) were also recorded at 25 °C. For the variable temperature studies, spectra of loaded microgels (both swollen and mixed solutions) were taken at 25, 28, 31, 34 and 37 °C. For these studies, before taking measurements, the samples were thermally equilibrated for 15 minutes at each temperature. No changes in the signal intensities were observed if the equilibration time was prolonged. For the temperature jump studies, the NMR spectrometer probe was set at either 34, 37 or 40 °C and a cool (25 °C) insulin impregnated sample (via swelling) was inserted into the spectrometer. Spectra were immediately recorded every 7.5 seconds and a total of 39 spectra were taken. For all variable temperature studies, an external deuterated acetone standard was used where the acetone solution was inserted into a microcapillary and was then sealed. This standard was then directly inserted into the center of the NMR tube containing the insulin loaded microgel solutions. The integrated ratios of the main pNIPAm peak at 1.1

ppm and the insulin peaks from 6.6 to 7.4 ppm were normalized with respect to the acetone standard. The main pNIPAm peak was chosen for integration due to its strong signal while the insulin peaks from 6.6 to 7.4 ppm were chosen due to non-spectral overlap.

Centrifugation Loading Assay

Following ^{1}H NMR analyses, both samples of the insulin loaded microgels (swollen and mixture) were transferred to 2 mL eppendorf tubes and centrifuged at 14, 000 rpm at 26 °C for 20 minutes. 250 μL of supernatant was extracted from each sample and then diluted with 4 mL of 20 mM PBS. The absorption spectra of these samples were analyzed via UV/vis spectroscopy, along with a control sample containing the same overall concentration of insulin as the loaded samples without any microgels present. The percent of insulin loaded was then calculated with respect to the control sample.

7.3 Results and Discussion

Particle synthesis and characterization

As described previously, 2 mole % BIS cross-linked pNIPAm microgels were chosen for these insulin loading and release investigations. We have previously reported results on insulin-impregnated microgels that contained pH sensitive acrylic acid groups (see Chapter 3).[19] This pH responsivity allowed the microgels to swell under neutral pH conditions and this was what we hypothesized was the main driving force allowing for insulin imbibition into the particles. In this study, we wanted to ascertain whether or not this pH swelling was necessary to effectively load our microgels with a macromolecularly sized therapeutic agent. Hence, microgels without acrylic acid

comonomer were investigated. Two loading strategies were compared. The first was to swell lyophilized microgels in a concentrated solution of insulin for 24 hours. Insulin is sparingly soluble at neutral pH values but is quite soluble under acidic conditions.[22] Thus, it was first dissolved in deuterated HCl to prepare the stock solution and then the pH was increased by addition of deuterated NaOH until neutral pH was achieved. This stock solution was then added to a known mass of dried microgels and the particles were allowed to swell in this solution, thereby imbibing the concentrated insulin, for 24 hours. The other method for comparison entailed a simple equilibrium partitioning technique whereby an already swollen microgel solution was physically mixed with an insulin solution. Both strategies utilized the same mass of dried microgels to start with and used the same overall concentration of insulin so they could be directly compared to one another.

To probe the effect that insulin impregnation has on the phase transition behavior of 2 mole % BIS cross-linked microgels, characterization of hydrodynamic radius as a function of temperature was performed on both insulin loaded microgels (via the swelling technique) and unloaded microgels using DLS. Panel a of Figure 7-1 illustrates the volume phase transition behavior of these two systems where the open circles represent the loaded sample and the open squares represent the unloaded sample. At low temperatures both sets of particles display approximately the same average hydrodynamic radius of 190 nm. The loaded and unloaded microgel networks both undergo a sharp volume phase transition at approximately 32 °C after which they deswell to a minimum hydrodynamic radius of approximately 90 nm. The LCST for both sets of particles corresponds well with the LCST of typical pNIPAm microgels.[23] Figure 7-1, panel b

shows the corresponding light scattering profiles of the same systems. Both sets of particles display very little scattered light intensity at low temperatures below the corresponding LCST values. This is because these porous microgel networks are highly solvent swollen (approximately 95% water by volume) and are therefore, nearly index matched to their environment. When the microgels collapse into dense globules at temperatures above the LCST, however, the microgels display a higher scattering cross section, and therefore, a dramatic increase in scattered light intensity is observed from the suspensions above the LCST. These results suggest that impregnation of the microgels with insulin does not perturb their deswelling capabilities and/or phase transition temperature to any significant extent.

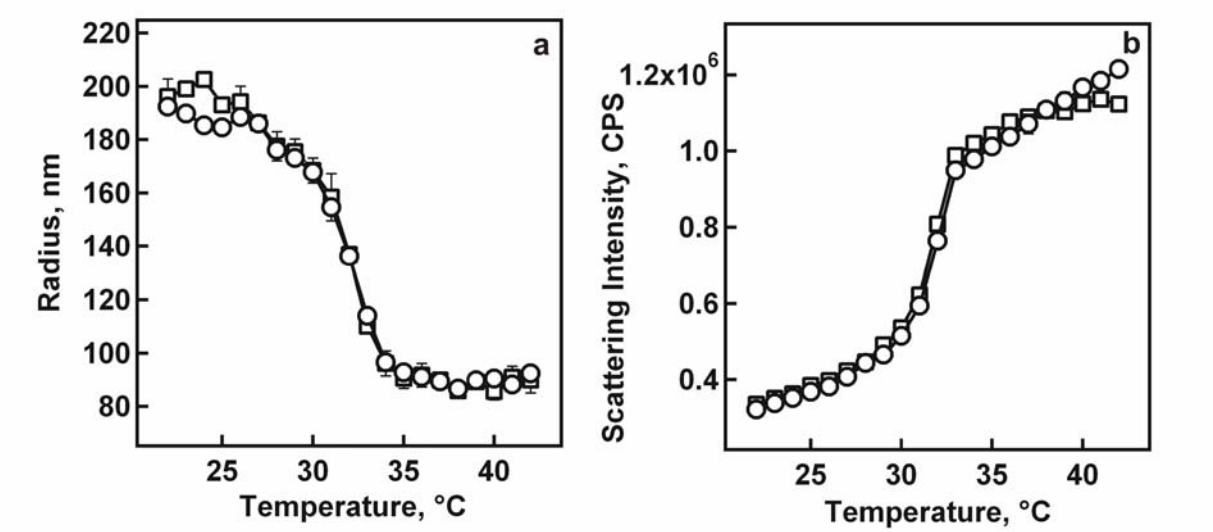

Figure 7-1. (a) Volume phase transition curves (in nanopure water) for 2 mole % BIS cross-linked pNIPAm microgels loaded via swelling (open circles) and not loaded (open squares) with insulin; (b) corresponding light scattering profiles for 2 mole % BIS cross-linked pNIPAm microgels loaded via swelling (open circles) and not loaded (open squares) with insulin.

^{1}H NMR

To design these direct release experiments, ^{1}H NMR spectra of insulin in D_2O (pH 7.4) and the 2 mole % BIS cross-linked microgels were first taken at 25 °C to determine if spectral resolution could be achieved. The spectra for insulin is illustrated in panel a of Figure 7-2. The proton assignments for the insulin resonances are in agreement with its chemical structure at this neutral pH value.[24] The peaks from approximately 0.6 to 1.1 ppm arise from isoleucine, leucine and valine residues while the peak at 1.4 ppm can be attributed to isoleucine, threonine, alanine and lysine moieties. The resonance at about 1.7 ppm arises from arginine, leucine and lysine residues while the peak at 1.8 ppm is attributed to arginine and lysine residues. The peak at 2.0 ppm results from proline,

isoleucine and glutamine residues while the peak at approximately 2.3 ppm is attributed to valine, glutamine, proline and glutamine residues. The resonance at 2.9 ppm is attributed to asparagine, tyrosine, lysine and cysteine residues. The peaks from 3.1 to 4.3 ppm are assigned to tyrosine, phenylalanine, histidine, arginine, proline, glycine, threonine, valine, isoleucine, leucine, lysine, alanine, serine, cysteine and asparagine residues. The peaks in the region of approximately 6.6 to 7.4 ppm arise from the thirty-five aromatic protons of the two histidines, three phenylalanines and four tyrosine residues. Panel b of Figure 7-2 shows the spectra obtained for the 2 mole % BIS cross-linked microgels and the proton assignments for the pNIPAm polymer also suitably correspond to its chemical structure.[33,34] The peak at 1.1 ppm can be attributed to the methyl protons of the *N*-isopropyl group. The resonance for the methylene proton of the isopropyl group is observed at 3.8 to 4.0 ppm while the resonances from 1.2 to 2.2 ppm are attributed to the protons on the polymer backbone. In all ^{1}H NMR spectra, the peak at approximately 4.7 ppm is the suppressed solvent water peak. While there is some spectral overlap within the region of 0.0 to 4.0 ppm, the most intense peak from the pNIPAm polymer at approximately 1.0 ppm is somewhat spectrally resolved. Furthermore, there is no spectral overlap for the down shifted insulin peaks from 6.6 to 7.4 ppm. It is these two peak signals that will be interrogated as a function of temperature to try and probe direct insulin expulsion from impregnated particles.

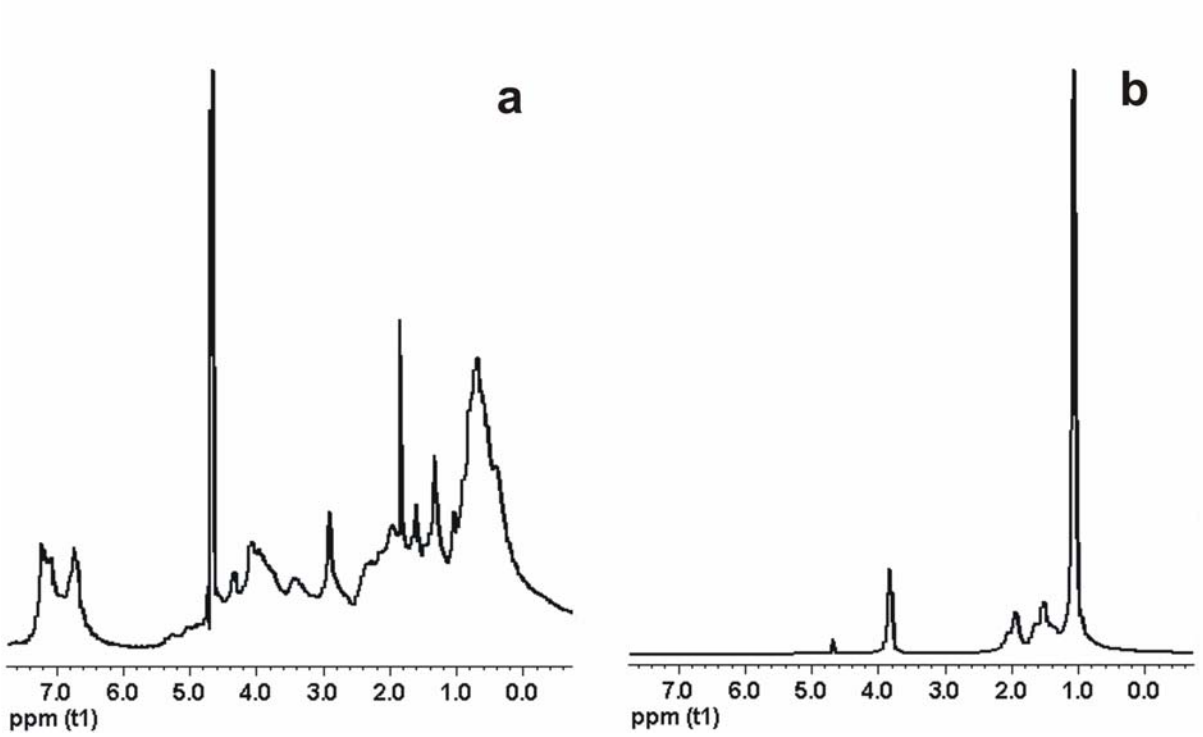

Figure 7-2. ^{1}H NMR spectra of (a) insulin in D_2O (pH adjusted to 7.4) and (b) 2 mole % BIS cross-linked microgels in D_2O at 25 °C.

To first investigate feasibility of detecting an increase in insulin signal due to expulsion from the microgels using this NMR technique, spectra of insulin loaded 2 mole % BIS cross-linked microgel samples (both swollen and mixed) were recorded at temperatures both below and above the phase transition temperatures of the particles. These results are shown in Figure 7-3. Panels a and b represent the spectra for insulin loaded microgels via the breathing-in technique at 25 °C and 37 °C, respectively. In these spectra, as mentioned in the experimental section, an external deuterated acetone standard

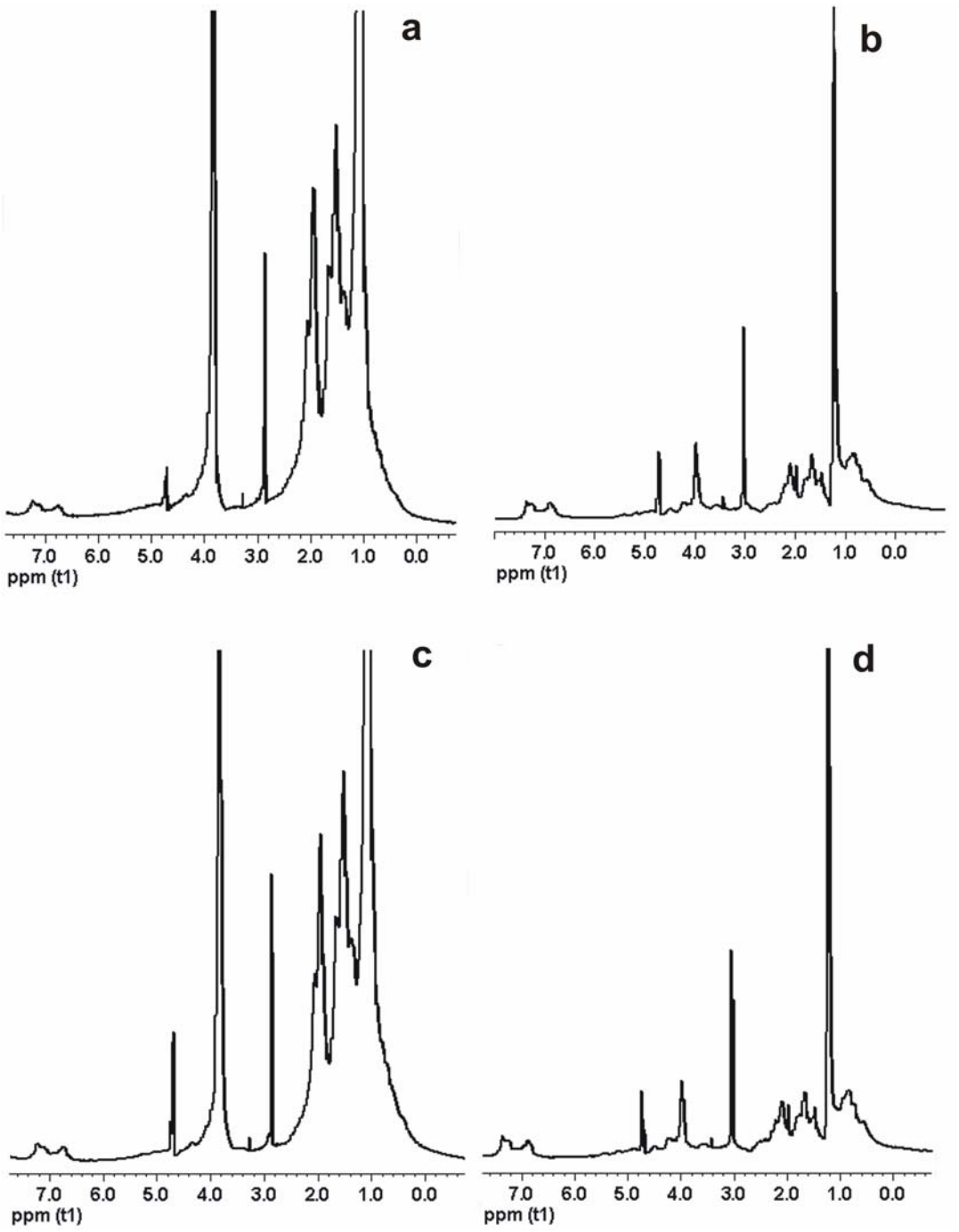

Figure 7-3. ^{1}H NMR spectra of insulin loaded 2 mole % BIS cross-linked microgels at temperatures below and above the volume phase transition temperature (overall pH 7.4); (a) insulin loaded microgels via breathing-in technique at 25 °C, (b) insulin loaded microgels via breathing-in technique at 37 °C, (c) insulin loaded microgels via mixing at 25 °C and (d) insulin loaded microgels via mixing at 37 °C.

was used for normalization and its resonance is observed at approximately 2.9 ppm. This resonance is somewhat shifted from what is expected since the water peak at 4.7 ppm was used as a reference. Panels c and d correspond to the insulin loaded microgel sample via simple equilibrium partitioning at temperatures below and above the LCST, respectively. For both sets of particles, at 25 °C the pNIPAm resonances dominate the spectra and only relatively small insulin peaks are observable in the far end of the spectra. Under these cold conditions, it is presumed that predominantly most of the insulin is impregnated within the microgel interior. Hence, the signal due to insulin is diminished due to lack of free rotation in the network. When the temperature is raised above the LCST to 37 °C, however, the particles deswell and release insulin into surrounding solution resulting in an increase in the insulin signal with respect to the acetone standard. It is clearly evident that for both loaded samples (swollen and mixed) a relative increase in the ratios of insulin/acetone occurs upon elevation in temperature from 25 to 37 °C while a concomitant decrease in the pNIPAm/acetone ratios results upon particle collapse. At elevated temperatures, the pNIPAm resonances become significantly depressed due to the fact that as the microgel hydrophobically collapses it becomes denser and more solid-like.[25-27] These results suggest that microgel deswelling results in osmotically driven insulin expulsion from the network as the free volume in the microgel interior decreases.

To probe this release event in more detail, ^{1}H NMR spectra of each loaded solution were obtained at equilibrated temperatures ranging from 25 to 37 °C every three degrees. The results for these experiments are shown in Figure 7-4. Panel a shows the normalized pNIPAm/acetone peak ratios as a function of temperature for the loaded

microgels via swelling (open circles) and via equilibrium partitioning (open squares). This plot illustrates that the temperature at which both sets of loaded microgels deswell suitably corresponds with their well-known phase transition temperature of 32 °C.[23] These profiles also correlate well with the LCST curves obtained for the loaded and unloaded solutions shown in panel a of Figure 7-1. Panel b of Figure 7-4 shows the peak ratios of insulin/acetone as a function of temperature for both loaded samples. A distinct difference in the release profiles is illustrated here where the normalized insulin signal for the physical mixture is consistently higher than that for the swollen sample at all temperatures. This indicates that perhaps, the swelling technique results in enhanced entrapment of the peptide versus simple mixing and hence, not as much insulin is free in solution to be detected. The slopes of the two profiles are also definitively different. The sample loaded with the breathing-in technique (open circles) does not display a significant increase in normalized insulin signal until 34 and 37 °C while the sample loaded via equilibrium partitioning shows a steady increase within the entire temperature range. These findings again suggest more efficient insulin loading for the swollen sample. The microgels loaded via mixing are perhaps leaky and hence, more insulin is in solution to be detected regardless of particle collapse. The sample impregnated via the breathing-in technique, however, effectively entraps insulin in the particle interior and it is not until the microgel partially or fully deswells that entrapped species are expelled into solution.

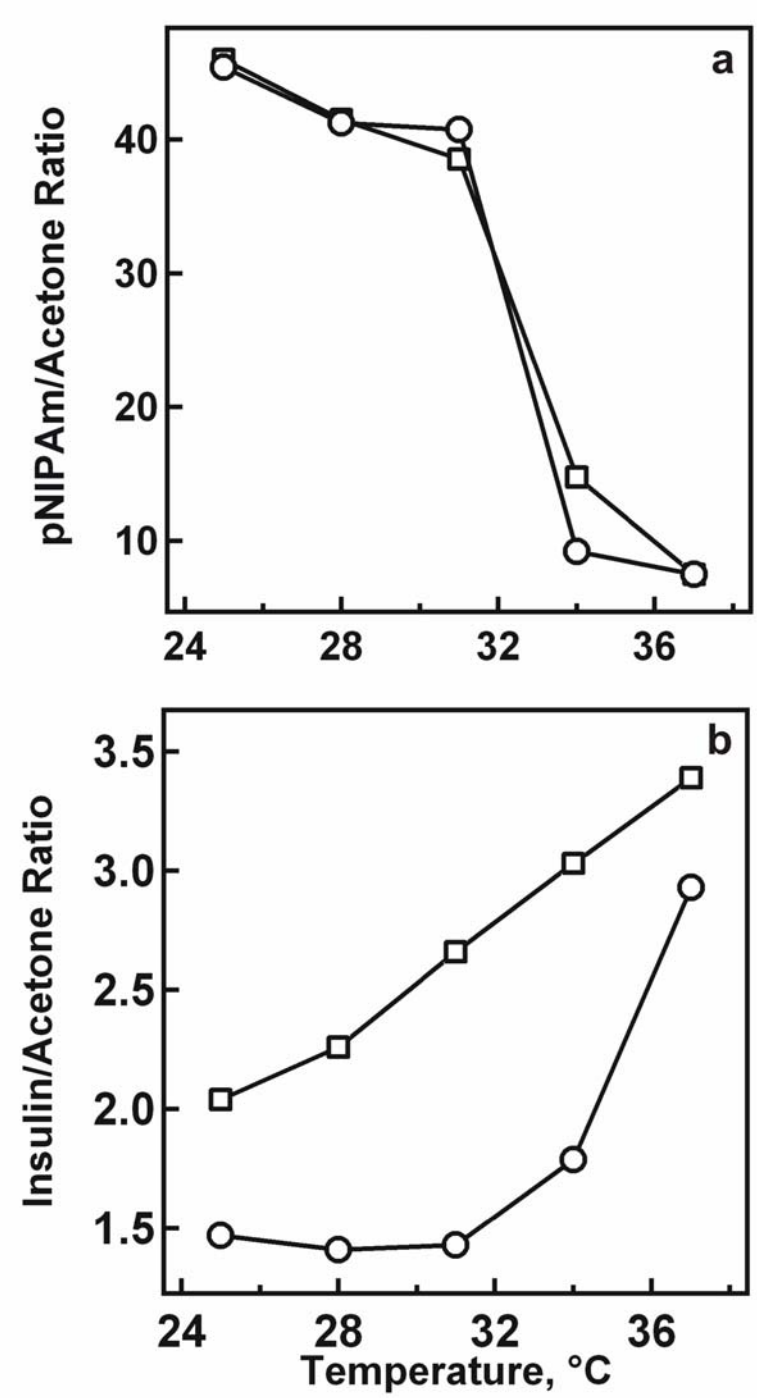

Figure 7-4. Plots of the normalized ratios of (a) pNIPAm/acetone standard and (b) insulin/acetone standard as a function of equilibrated temperature. Open circles represent insulin loaded microgels via the breathing-in technique; open squares represent insulin loaded microgels via equilibrium partitioning.

To try and probe the early stages of insulin release from 2 mole % BIS cross-linked microgels, ^{1}H NMR temperature jump investigations were conducted. In these investigations, an insulin-impregnated sample (via swelling) held at 25 °C was quickly inserted into the NMR spectrometer that was equilibrated at either 34, 37 or 40 °C. Upon insertion, the sample was immediately exposed to the elevated temperature and spectra were collected every 7.5 seconds. The results for this experiment are illustrated in Figure 7-5. Panel a shows the profiles for microgel collapse as a function of time and temperature. It is clear that differences in microgel deswelling rates occur depending upon the temperature differential used, with the 40 °C temperature jump resulting in fastest collapse. The magnitudes of deswelling are also distinctly different depending upon the temperature pulse applied. Panel b illustrates the corresponding insulin release profiles for each temperature jump. The 34 °C experiment shows that some insulin release occurs within the first 110 seconds and then this profile plateaus. This is most likely due to the fact that the microgels at this temperature are not fully deswollen and most of the insulin remains embedded within the microgel interior after an initial burst of release. The 37 °C temperature jump shows a somewhat different profile. Some release occurs within the first 60 seconds corresponding to the time course of the deswelling event at this temperature. This release, however, levels off after this up until approximately 220 seconds where slightly more insulin expulsion occurs. The 40 °C temperature jump experiment shows higher insulin/acetone ratios at all times, thus indicating a significant amount of insulin gets immediately released once the sample is injected. This release profile gradually increases with time suggesting gradual insulin partitioning out of the network. These NMR experiments are simple, quick and direct and

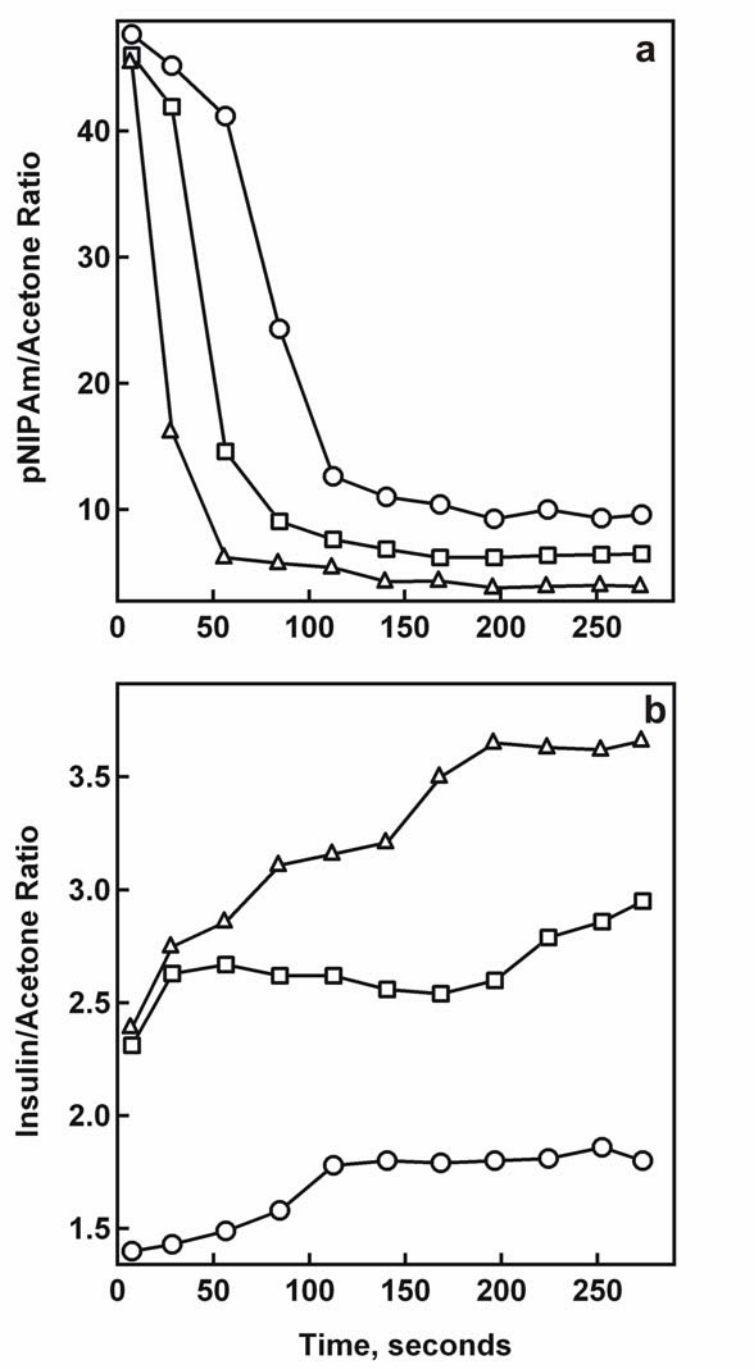

Figure 7-5. Plots of (a) 2 mole % BIS cross-linked microgel deswelling and (b) insulin release kinetics for an insulin loaded microgel sample (via swelling) subjected to a temperature jump from 25 °C to 34 (circles), 37 (squares) and 40 °C (triangles).

show promise in elucidation of differences in release kinetics between various functionalized particles.

Centrifugation Loading Assay

To ascertain how efficient each loading strategy actually was, a centrifugation loading assay was performed following NMR analyses. The loaded samples were allowed to reswell at 4 °C overnight and were then centrifuged and analyzed as described in the experimental section. The results for these experiments are shown in Table 7-1 along with a summary of the normalized pNIPAm and insulin ratios obtained in the ^{1}H NMR release studies. These results confirm all of the previously mentioned conclusions that the breathing-in technique does result in enhanced loading of the therapeutic agent, insulin at 40 %. The fact that the normalized insulin signal at 25 °C is higher for the mixture versus the sample swollen in concentrated insulin again reaffirms these differences and suggests effective peptide entrapment with the breathing-in technique. It is interesting to note that even after a release event occurred, both samples were able to reswell and reload the expelled peptide. This only reinforces the great promise that these type of microgel particles possess in pulsatile drug delivery applications.

Table 7-1. Insulin loading results for 2 mole % BIS cross-linked microgels and ^{1}H NMR normalized ratios of pNIPAm and Insulin at 25 °C

	Obtained via UV/vis	Obtained via ^{1}H NMR at 25 °C	
Insulin loaded microgel sample	**% Loaded Insulin**	**PNIPAm/Acetone Ratio**	**Insulin/Acetone Ratio**
Swollen	**40.2**	**45.45**	**1.47**
Mixture	**22.7**	**45.96**	**2.04**

7.4 Conclusions

A macromoleculary sized therapeutic agent, insulin, was rapidly and effectively impregnated into thermoresponsive pNIPAm microgels via a breathing-in technique that proved superior over simple equilibrium partitioning. Thermally induced release was directly monitored using ^{1}H NMR and again suggested that the swelling strategy results in entrapment of the peptide to some extent. A ^{1}H NMR temperature jump study was also performed and suggests that the rate at which insulin is released from the loaded network is partially decoupled from its collapse depending upon the thermal pulse used. These types of direct release experiments could prove as useful templates in the future design of controlled macromolecule release devices utilizing functionally modified thermoresponsive particles.

7.5 References

(1) Mellott, M. B.; Searcy, K.; Pishko, M. V. *Biomaterials* **2001**, *22*, 929-941.

(2) Murthy, N.; Xu, M.; Schuck, S.; Kunisawa, J.; Shastri, N.; Frechet, J. M. J. *Proc. Natl. Acad. Sci.* **2003**, *100*, 4995-5000.

(3) Wang, N.; Wu, X. S.; Li, J. K. *Pharm. Res.* **1999**, *16*, 1430-1435.

(4) Slager, J.; Domb, A. J. *Biomaterials* **2002**, *23*, 4389-4396.

(5) Hanes, J.; Chiba, M.; Langer, R. *Biomaterials* **1998**, *19*, 163-172.

(6) Chou, H. F.; Ipp, E. *Diabetes* **1990**, *39*, 112-117.

(7) Goodner, C. J.; Walike, B. C.; Koerker, D. J.; Ensinck, J. W.; Brown, A. C.; Chideckel, E. W.; Palmer, J.; Kalnasy, L. *Science* **1977**, *195*, 177-179.

(8) Hansen, B. C.; Jen, K. C.; Belbez, P. S.; Wolfe, R. A. *J. Clin. Endocrinol. Metab.* **1982**, *54*, 785-792.

(9) Lang, D. A.; Matthews, D. R.; Burnett, M.; Turner, R. C. *Diabetes* **1981**, *30*, 435-439.

(10) Porksen, N.; Munn, S.; Steers, J.; Vore, S.; Veldhuis, J.; Butler, P. *Am. J. Physiol.* **1995**, *269*, E478-E488.

(11) Moriyama, K.; Tooru, O.; Nobuhiko, Y. *J. Biomater. Sci., Polym. Ed.* **1999**, *10*, 1251-1264.

(12) Siegel, R. A.; Colin, G. P. *J. Controlled Release* **1995**, *33*, 173-188.

(13) Misra, G. P.; Siegel, R. A. *J. Controlled Release* **2002**, *81*, 1-6.

(14) Siegel, R. A.; Gu, Y.; Bladi, A.; Ziaie, B. *Macromol. Symp.* **2004**, *207*, 249-256.

(15) Kwong, A. K.; Chou, S.; Sefton, M. V. *J. Controlled Release* **1986**, *4*, 47-62.

(16) Soriano, I.; Evora, C.; Llabres, M. *Int. J. Pharm.* **1996**, *142*, 135-142.

(17) Leobandung, W.; Ichikawa, H.; Fukumori, Y.; Peppas, N. A. *J. Controlled Release* **2002**, *80*, 357-363.

(18) Damge, C.; Vranckx, H.; Balschmidt, P.; Couvreur, P. *J. Pharm. Sci.* **1997**, *86*, 1403-1409.

(19) Nolan, C. M.; Serpe, M. J.; Lyon, L. A. *Biomacromolecules* **2004**, *5*, 1940-1946.

(20) Sass, H.-J.; Musco, G.; Stahl, S. J.; Wingfield, P. T.; Grzesiek, S. *J. Biomolecular NMR* **2000**, *18*, 303-309.

(21) Jones, C. D.; Lyon, L. A. *Macromolecules* **2000**, *33*, 8301-8306.

(22) Dorkoosh, F. A.; Verhoef, J. C.; Ambagts, M. H. C.; Rafiee-Tehrani, M.; Borchard, G.; Junginger, H. E. *Eur. J. Pharm. Sci.* **2002**, *15*, 433-439.

(23) Pelton, R. H. *Adv. Colloid. Interface Sci.* **2000**, *85*, 1-33.

(24) Williamson, K. L.; Williams, R. J. P. *Biochemistry* **1979**, *18*, 5966-5972.

(25) Gan, D.; Lyon, L. A. *Macromolecules* **2002**, *35*, 9634-9639.

(26) Schoenhoff, M.; Schwarz, B.; Larsson, A.; Kuckling, D. *Prog. Colloid Polym. Sci.* **2002**, *121*, 80-87.

(27) Schoenhoff, M.; Larsson, A.; Welzel, P. B.; Kuckling, D. *J. Phys. Chem. B* **2002**, *106*, 7800-7808.

CHAPTER 8

FUTURE OUTLOOK

Given the initial progress made and encouraging results obtained with this thesis work on regulated macromolecule release from microgel materials, some future directions are described hereafter. Chapter 3 illustrated very promising results of tightly controlled pulsatile insulin release from extremely stable microgel thin film constructs. To explore this work even further, one could investigate many parameters in the actual construction of these macromolecule impregnated microgel thin films. These include exploration of spin coating deposition speed, concentration of polyions deposited, type of polyelectrolytes used (beyond PAH), varying charge density of these polyions (based on solution pH) and microgels (based on incorporated comonomer concentration), use of both positively charged (by addition of an amine comonomer) and negatively charged (by incorporation of other acid comonomers such as lactic acid) microgels, use of highly functional core/shell microgels and impregnation of microgels with various macromolecules (range of MWs and charge). The idea in varying all of these parameters would be to develop highly functional macromolecule impregnated microgel thin films with tunable release rates. Incoporation of microgels with higher LCST values (based on use of *N*-isopropylmethacrylamide as the main monomer) could also be very promising in that these constructs could potentially stay swollen *in vivo* and only deswell when an external thermal pulse was applied. Chapters 4 and 5 focused on fundamental synthesis of

more biocompatible PEG cross-linked microgels both with and without a pH sensitive comonomer. Incorporation of these types of microgels into macromolecule loaded microgel thin films could also be explored given the promising results that when these materials are deposited onto substrates, they display diminished cell adhesion properties. Exploration of these types of microgels within a core/shell motif may also prove fruitful. Chapter 6 concentrated on loading strategies using microgels of different hydrophilic balance, i.e. microgels with and without PEG and acrylic acid moieties. Further studies on loading macromolecules of different hydrophobicities into microgels of varying hydrophobic balance (use of butyl methacrylate based comonomers) could also be pursued. Furthermore, exploration of loading various macromolecules (with different hydrophobic balance, charge density and size) by both the pH induced loading strategy as well as the breathing-in technique into an array of functionally modified microgels could prove useful. Chapter 7 illustrated promising results on simple, quick and direct ^{1}H NMR experiments that could give some insight into early release events of macromolecules from microgels in solution. These types of model experiments could be utilized to probe release kinetics of various bioactive species loaded into an array of functionally modified microgel motifs. Furthermore, these studies could be extended where instead of just probing peptide loaded microgel solutions, effective cross-linked gels could be made by simple addition of polyelectrolytes. Hence, interrogation of protein release from a similar construct as that obtained with multi-layer thin films could be probed and perhaps would prove more useful.